Harnessing trabecular meshwork cells for the molecular profiling of primary open-angle glaucoma.

by

Qinyi Lu

Menzies Institute of Medical Research

Submitted in fulfilment of the requirements for the degree of Doctor of Philosophy

University of Tasmania

November 2020

Declaration

I certify that this thesis contains no material that has been accepted for any other degree or diploma at any other university, college or institution. To the best of my knowledge, this thesis does not contain material previously published by another person, except for where reference has been made.

This thesis may be made available for loan. Copying and communication of any part of this thesis is prohibited for one year from the date this statement was signed; after that time limited copying and communication is permitted in accordance with the Copyright Act 1968.

For projects involving harvesting human primary trabecular meshwork cells and Tasmanian Ophthalmic Biobank, the research presented and reported in this thesis was conducted by the Australian Health Ethics Committee (AHEC) of national health and medical research council (NHMRC). The proposed research study received human research ethics approval from the Royal Victorian Eye and Ear Hospital Ethics Committee, approval number 13-1151H, and by the human research ethics committee of the University of Tasmania, approval number H0012902.

Qinyi Lu

University of Tasmania

18th November 2020

ACKNOWLEDGEMENTS:

First and foremost I would like to thank my supervisor, Professor Alex Hewitt, without whom I cannot imagine where I am now. Alex fully supported my journey in scientific research and his encouragement always provided me the power to continue my study. I never thought I could learn so many skills in natural science, some of which I never heard, and some I only know from the media before I came to Menzies. I believe the skills I have learned will benefit me for the rest of my life.

I would also like to thank my co-supervisor, Associated Professor Tony Cook, who led me into the laboratory. I do appreciate your patients in helping me design the experiments and troubleshooting.

I would especially like to thank Dr. Rick Liu and Dr. Jana Talbot for your technical support and the expertise in the laboratory work, and thank Dr. Sandy Hung and Dr. Helena Liang for your support in harvesting the cells and generating the virus.

I would like to thank my team members, Jacqui Walker, Connor Greatbatch, Mohd Khairul Nizam, Peter Tran, Qi Wang, Vikrant Singh, Sueanne Chear, Kirsten FairFax, David Stellon, Abadh Chaurasia, Jacqueline Townley.

I would especially thank Jacqui and Connor for helping me edit my thesis, especially thank Nizam for giving me so much support on the lentivirus work from sequencing validation to the generation. I will remember the nights we made the lentivirus together with Peter Tran.

To my friends and families, many thanks for your understanding and support. I do have a wonderful period during my Ph.D. years.

ABSTRACT

Background:

Primary open-angle glaucoma (POAG) is the leading cause of irreversible blindness worldwide. Intraocular pressure (IOP) the only known modifiable risk factor for this disease. In POAG, elevated IOP leads to progressive loss of retinal ganglion cells, with IOP being primarily modulated by trabecular meshwork cells (TMCs) in the iridocorneal angle. The precise molecular drivers for the differentiation or dysfunction of TMCs is poorly understood. A number of transcription factors have been implicated in development of the ocular anterior segment, and recently a large genome-wide association study identified 53 loci associated with variation in IOP.

Aim:

The overriding aims of this thesis were:

1. To determine whether dental pulp-Mesenchymal stem cells (DP-MSCs) could be induced to exhibit the phenotypic properties of human TMCs through the exposure to growth factors involved in development of the anterior segment;
2. To investigate the morphological and transcriptome profiles created by Cell Painting and scRNA-seq in TMCs, where genes implicated in IOP variation have been knocked out by CRISPR.

Methods:

DP-MSCs were treated with retinoic acid (RA), TGF-β super-family members transforming growth factor-β2 (TGF-β2) and bone morphogenetic protein 4 (BMP4) for 5 days. The expressions of TMCs markers were investigated by qRT-PCR, functional TM cell characteristics were profiled by a collagen contraction assay, dexamethasone-induced myocilin secretion and through phagocytosis assessment.

To investigate genes associated with IOP, a clustered regularly interspaced short palindromic repeats (CRISPR) knockout screen was performed by transfecting the TMCs with lentivirus carrying the single-guide RNAs (sgRNAs) targeting 62 genes across 53 loci, together with 5 human non-targeting controls, in arrayed format. Cells were then seeded to the image plates

by flow cytometry for high-throughput morphological profiling assay, or pooled for single-cell RNA sequencing (scRNA-seq).

Results:

After 5 days of treatment with the combination of the three transcription factors, RA, TGF-β2 and BMP4 in the DP-MSCs, the TMCs marker *MYOC* were significantly upregulated, and the secreted myocilin was also upregulated determined by ELISA; however, the expression of *MYOC* was not increased or induced following dexamethasone exposure and the contractility of collagen gel was also not observed.

A total of 210, 234 cells were individually segmented and image-based profiling performed for CRISPR/Cas edited TM cells. A total of 910 morphological features were extracted for each of the gene knockout perturbations. Cells clustered into 2 major groups via unstructured hierarchical clustering. Significant features of the clusters were extracted related to the granularity of the golgi apparatus and mitochondrial. For transcriptional profiling a total of 25,879 single cells were demultiplexed and had their corresponding sgRNA identified. A total of 240 differentially expressed genes (DEGs) were identified and expression profiles with these genes. The profiles were also clustered into 2 groups via hierarchical clustering, the DEGs related to the difference of the 2 clusters are involved in the interferon alpha/beta signaling.

Conclusion:

Although DP-MSCs express markers of trabecular meshwork cells following the exposure of a combination of transcription factors, they were found not to acquire morphological profiles characteristic of trabecular meshwork function. High throughput analysis of cellular structure and function through cellpainting and scRNA-seq assays enabled the direct study of genetic perturbations at the single cell resolution. This work provides a framework for investigating the role of genes involved in the pathogenesis of glaucoma in both genetic and morphology.

1. INTRODUCTION

1.1 Prevalence of glaucoma

Glaucoma is a heterogeneous group of diseases defined by characteristic optic damage and vision loss. The glaucomas are categorized by the iridocorneal angle into open-angle glaucoma, angle-closure glaucoma, or developmental (congenital) glaucoma, with a further classification of primary and secondary types [1,2]. As the leading cause of irreversible blindness in the world, more than 60 million people were affected by this disease in 2010, and this number was estimated to increase to 80 million by 2020, and of these, approximately three out of four people would have open-angle glaucoma [2]. The potential glaucoma patients in Australia were 382 950 in 2012, which accounts for nearly 3.7% of people over 40 years old [3]. As the population ages, the prevalence of glaucoma is expected to rise even higher [3]. Furthermore, the cost of glaucoma is a significant economic burden to the Australian healthcare system, which is estimated to increase to $AU784 million by 2025 [4].

1.2 The pathology of primary open-angle glaucoma

Primary open-angle glaucoma (POAG) is the most common glaucoma subtype. Several risk factors are attributed to the progression of POAG. These include older age, family glaucoma history, some ethinic groups, use of corticosteroids, and high intraocular pressure (IOP) [5]. Normal IOP ranges from 12mmHg to 22 mmHg and it is the only known modifiable risk factor of POAG. Previous studies show that elevated IOP above 22mHg is strongly related to optic nerve damage, thought to be triggered by a series of cellular events leading to the death of retinal ganglion cells (RGCs). Under the presence of the elevated IOP, the retrograde delivery of trophic factors such as brain-derived neurotrophic factor is interrupted and reactive oxygen species (ROS) accumulate in the retina which results in glial cell activation. This especially occurs in the lamina cribrosa where the sclera is perforated by the passing of the optic nerve fibers [6–9]. Studies in mouse models show that activated glial cells (astrocytes) secrete tumor necrosis factor α (TNF-α), which leads to the loss of RGC axons and then the death of the whole cell [10]. Due to the structural changes of the optic nerve head, the cup

becomes larger and deeper with the loss of the prelaminar tissue. This can be observed through fundus examination and plays a critical role in the diagnosis of glaucoma (Fig. 1). Glaucomatous optic damage is also observed in the normal-tension glaucoma (NTG) patients whose IOP is in the 12mmHg to 22mmHg range. In NTG patients, the low cerebrospinal fluid pressure or intracranial pressure resulting in a relatively higher IOP is supposed to play a role in the development of glaucoma [11–13] .

Figure 1: *Elevated intraocular pressure leads to progressive damage of the optic nerve. A) Normal intraocular pressure; B) High intraocular pressure. Figure created with Biorender.com*

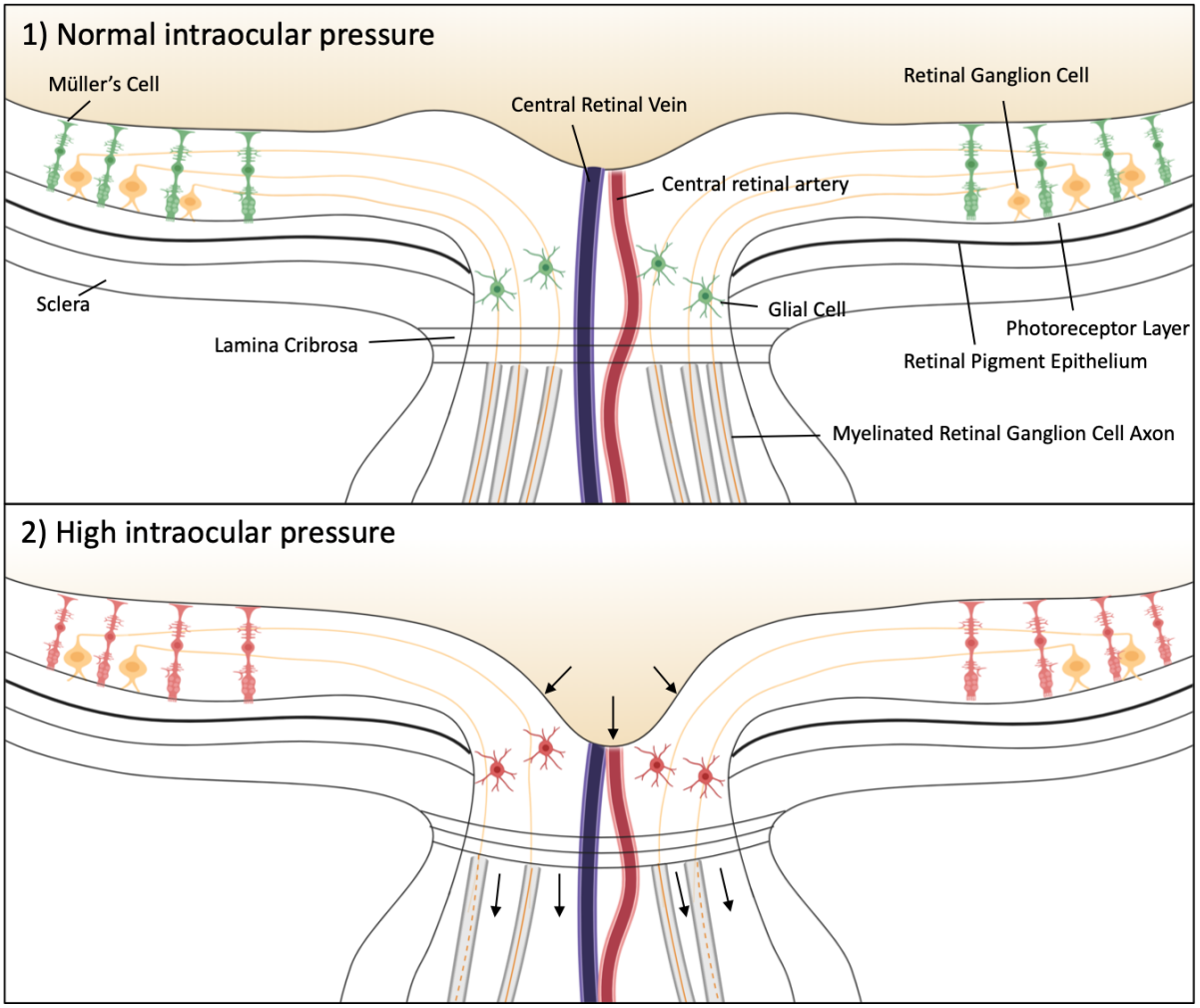

1.3 Genetics of primary open-angle glaucoma

POAG is considered to be a disease resulting from the interaction between multiple genes and environmental factors. Through genetic linkage analysis, three genes associated with POAG have been identified, myocilin (*MYOC*), optineurin (*OPTN*), and TANK-binding kinase (*TBK1*) [14–16].

Many studies have shown the *MYOC* variants cause dysfunction of trabecular meshwork cells (TMCs), leading to an elevated IOP (discussed in detail in later paragraphs) [1,17,18]. *OPTN* and *TBK1* share a common pathway in NTG, and both of these gene variants are also related to amyotrophic lateral sclerosis, a disease of the central nervous system [18,19]. Recently, an advanced technique of genome-wide association studies (GWAS) was applied to investigate the genetic associations for POAG. GWAS, based on the next generation, high-throughput DNA sequencing, can identify positive single nucleotide polymorphisms (SNPs) via analyzing hundreds of thousands of SNPs from individuals in case and control groups [20]. Many POAG associated loci have been found, which include Caveolin 1 and 2 (*CAV1/CAV2*), transmembrane and coiled-coiled-coil domains 1 (*TMCO1*), cyclin-dependent kinase inhibitor 2B antisense RNA 1 (*CDKN2B-AS1*), SIX homeobox 6 (*SIX6*), ATB binding cassette subfamily A member 1 (*ABCA1*), actin filament associated protein 1 (*AFAP1*), GDP-mannose 4,6-dehydratase (*GMDS*), Forkhead Box C1 (*FOXC1*), thioredoxin reductase 2 (*TXNRD2*), Ataxin 2 (*ATXN2*) [21–24]. Although the mechanistic role of these gene variants in POAG remains to be investigated, their potential affected site can be predicted by current studies (Table 1) [18].

Table 1: *POAG-associated genomic regions identified by GWAS*

Nearest Gene	Potential affected site
CAV1/CAV2	IOP [25]
CDKN2B-AS1	RGC [26]
SIX6	RNFL and IOP [27,28]
TMCO1	IOP [22]
AFAP1	retina, optic nerve, and TMCs [23]
ABCA1	Retina and TMCs [18,23,29]
TXNRD2	RGC [24,30]
FOXC1/GMDS	Eye development [23,31]
ATXN2	RGC[32]

A recent GWAS meta-analysis identified 85 novel SNPs associated with IOP using data from the UK Biobank, the International Glaucoma Genetic Consortium and the Australian & New Zealand Registry of Advanced Glaucoma Cohort [33]. Novel gene variants associated with POAG and IOP were discovered, including *ANGPT1, ANKH, MECOM and ETS1,* which may play an important role in the maintenance of IOP. Interestingly, this study also identified SNPs associated with corneal parameters, such as *ADAMTS6* (central corneal thickness), *MYOF, ANAPC1, GLIS3*, and *FNDC3B* (corneal hysteresis) [33]. Thus, GWAS has provided us the gene candidates related to POAG, but their roles in the pathogenesis of POAG remains to be investigated.

1.4 Anatomy of the trabecular meshwork

1.4.1 Circulatory system in the anterior segment of the eye

IOP is maintained by the circulatory system in the anterior segment of the eye. Aqueous humor is produced by the ciliary body, and then passes through the pupil from posterior chamber to anterior chamber to nourish the non vascularized tissue structures, i.e., the lens, cornea, and the trabecular meshwork (TM). Finally, Aqueous humor drains through the TM to Schlemm's canal in the iridocorneal angle, then flows back to the episcleral blood vessels

(Fig. 2). Elevated IOP generally results from reduced aqueous outflow in both open-angle glaucoma and angle-closure glaucoma, while TM plays a significant role in the elevated IOP in open-angle glaucoma [1,34].

Figure 2: *The generation and flow of aqueous humor flow in the anterior segment of the eye. Figure created with Biorender.com.*

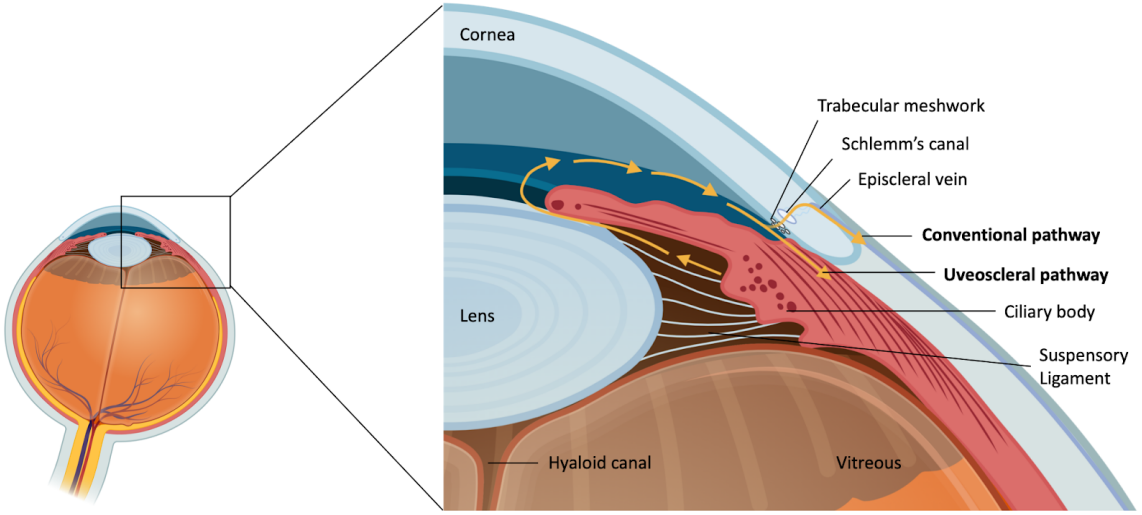

1.4.2 Anatomy of the trabecular meshwork

The human TM is a three-sided prismatic tissue located in the angle of the anterior chamber of the eye (Fig. 2). The unique location indicates that the TM plays a major role in the maintenance of aqueous humor. Approximately 80% of total aqueous humor outflow is carried by the TM and the remaining aqueous humor outflow is carried by uveoscleral outflow [5,35,36]. The spongy TM tissue allows aqueous humor to flow from the anterior chamber into Schlemm's canal. Histologically, the TM is divided into three parts: the inner uveal trabecular meshwork, which is from the anterior chamber to Schemm's canal, the corneoscleral trabecular meshwork, and the endothelial meshwork, also known as juxtacanalicular tissue (JCT) [37]. The uveal meshwork consists of one to two layers of TMCs which form long, narrow beams, covered by elliptical nuclei endothelial cells, with large, irregular spaces between beams. The corneoscleral meshwork consists of 8 to 14 layers and beams are broad and flat with the spaces between them becoming smaller [37]. The JCT meshwork, which is adherent to the endothelium of Schlemm's canal, does not form lamellae

or connective tissue beams, instead, it consists of 2 to 5 layers of scattered cells in connective tissue, with the cells embedded in a loosely arranged tissue extracellular matrix [38]. Thus, the intertrabecular spaces in each of the three parts become smaller, which means the resistance of the aqueous humor is increased from the inner uveal meshwork to JCT. As such, when IOP is increased, the outermost part of TM takes most of the outflow resistance [39](Fig. 3).

Figure 3: *Light micrograph of a meridional section through the trabecular meshwork [38]. TM: Trabecular meshwork; SS: Scleral spur; CM: Ciliary muscle; AC: Anterior chamber; JCT: Juxtacanalicular tissue, 2-5 layers of scattered cells; CTM: Corneoscleral trabecular meshwork, 8-14 layers of broad and flat beams; UTM: Uveal trabecular meshwork, 1-2 layers of beams with large and irregular spaces. Scale bars: 20 µm (A), 5 µm (B).*

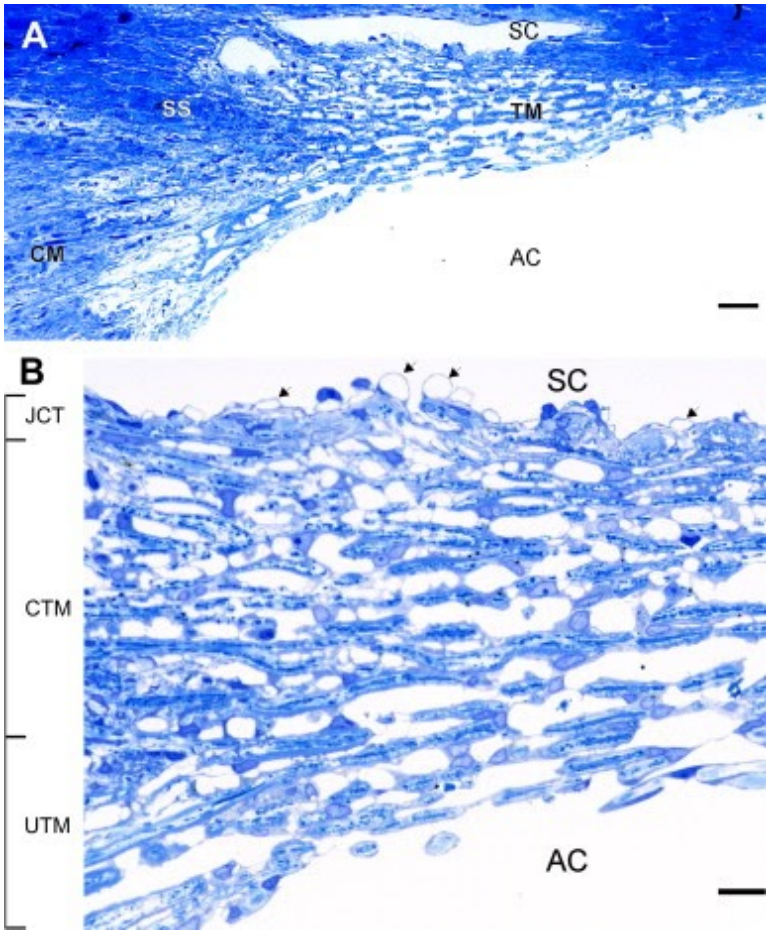

1.4.3 The role of trabecular meshwork in primary open-angle glaucoma

In POAG patients, structural alterations can be observed in the TM which are considered to increase the outflow resistance [1,40–42]. Decreased cellularity of the TM is common in POAG.This can result from the migration, phagocytosis, and the apoptosis of the TMCs, with cell apoptosis potentially caused by oxidative stress, mechanical stress, or trabecular hypoperfusion [43]. Another structural change common to PAOG-affected trabecular tissue is increased extracellular matrix (ECM) components. This may result from the increased concentration of transforming growth factor β (TGF-β2) in aqueous humor [44]. Studies have shown when mouse and human TM cells were treated with TGF-β2, the production of connective tissue growth factor would increase, which results in actin polymerization and ECM production. Also, TGF-β2 could upregulate the production and secretion of fibronectin, which contributes to the increased ECM deposition to reduce the outflow facility [45,46]. Thus, the status of TMCs plays an important role in the structural alteration in TM tissue, and TGF-β2 signaling is a contributor to pathogenesis.

1.4.4 The role of MYOC mutations in trabecular meshwork

MYOC was the first reported gene associated with glaucoma through genetic linkage analysis. *MYOC* mutations account for about 4% of adult POAG cases and more than 10% of juvenile-onset cases [1,14], and approximately 90% of the carriers of *MYOC* mutations would develop glaucoma phenotypes. To date, 282 variants have been documented in the *MYOC* gene, 85.1% of which are missense mutations and 40% result in POAG [47] (http://www.myocilin.com/, accessed March 2020). Moreover, myocilin allele−specific glaucoma patients typically have high levels of IOP [48,49]. The mechanisms of myocilin allele-specific glaucoma remain unclear. Overexpression or downregulation of myocilin does not generate glaucoma in mice models [50,51]. However, glaucoma-related *MYOC* mutations could change the structure of myocilin, altering the properties of the protein. An early study found the solubility of mutant myocilin was reduced in Triton-X 100 [52]. Study of the crystal structure has shown myocilin contains an olfactomedin domain, which is a five-bladed β-propeller structure involved in protein-protein interaction. Several glaucoma-associated *MYOC* mutations are located within or near this binding site [53,54]. The alteration of the protein binding properties may result in the aggregation of mutant myocilin, which is toxic to TMCs (Fig. 4) [55]. Myocilin aggregates could initiate a series of events such as endoplasmic

reticulum (ER) stress, the increase of ROS, and the impairment of mitochondrial function, which would finally result in the dysfunction of TMCs [5,55,56].

Previous research demonstrates how the structure of the TM facilitates the outflow of fluid from the eye and maintains a healthy IOP. When this structure is perturbed due to cell death or dysfunction from *MYOC* mutations, oxidative or mechanical stress, hypoperfusion, excess ECM or unknown causes, the TM function is compromised and glaucoma can develop.

Figure 4: *Schematic representation of the retention of mutant myocilin in trabecular meshwork cells, figure created with Biorender.com.*

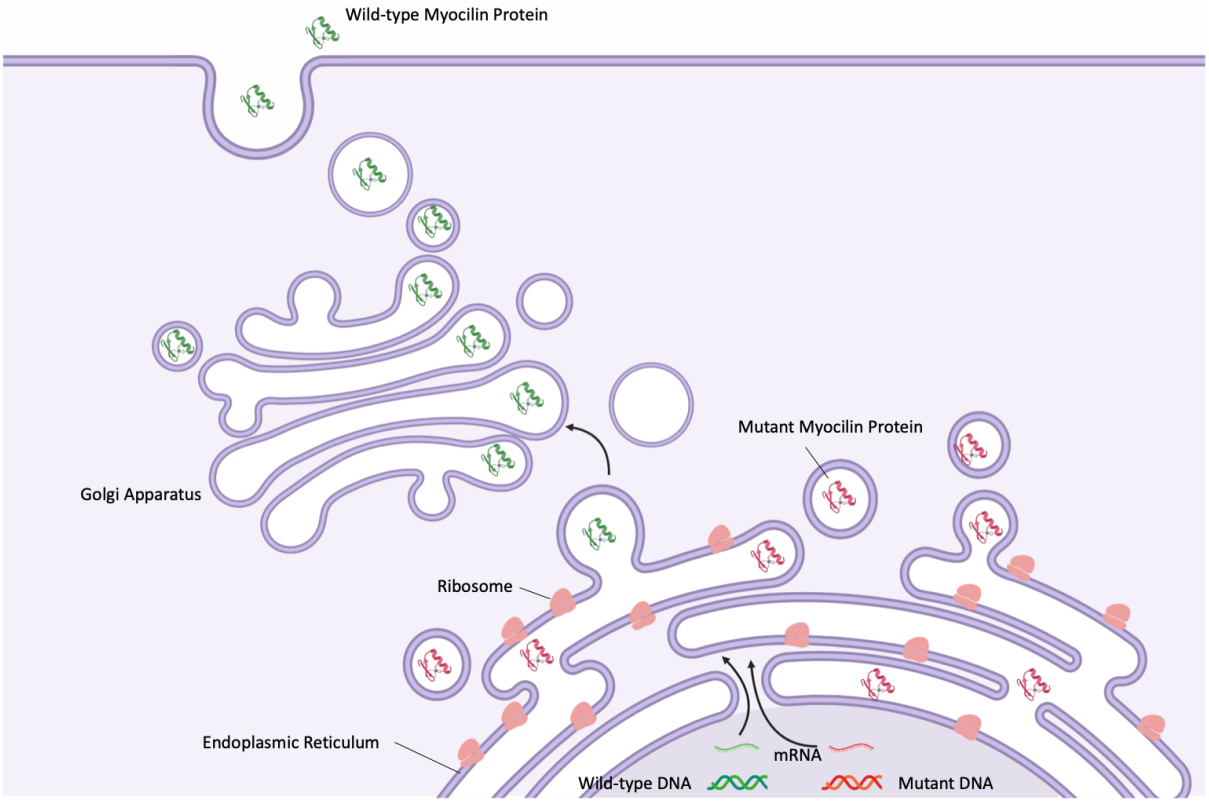

1.5 Treatments for open angle glaucoma

1.5.1 Currently available treatments

The only proven treatment for glaucoma is to decrease the IOP [57]. Currently, medication for lowering IOP mainly focuses on reducing the production of aqueous humor, such as β-adrenergic blockers, or increasing the uveoscleral outflow, such as prostaglandin [58]. IOP should be lowered toward a target level, which is usually 20% to 50% reduction in the initial pressure [5]. When medical treatment cannot achieve the target, laser trabeculoplasty or trabeculectomy may be necessary.

1.5.2 Emerging new drugs for glaucoma

Although not many medications targeting the TM for glaucoma have been approved yet, considering the TM tissue carries about 80% outflow of the aqueous humor, this is a promising area for research. Rho kinase (ROCK) inhibitors can lower IOP by acting on the TM [59]. The Rho family is a group of G-proteins including Rho, Rac, and CDC42. When bound to guanosine triphosphate, the protein effector molecules, Rho kinases, stimulate the polymerization of actin stress fibers and focal adhesions formation. These events enhance the tissue contraction by binding cells to the ECM. Thus, ROCK inhibitors can weaken the cell binding to its ECM, leading to wider spaces in the TM and reduced flow resistance. Furthermore, ROCK inhibitors can slow the progression of corticosteroid-induced glaucoma by suppressing ECM production [36,41]. To date, only two ROCK inhibitors are approved for clinical use, compound 28 (fasudil) and compound 165 (ripasudil). As the first ROCK inhibitor for glaucoma treatment, ripasudil shows a significant effect on IOP, which could lead to a decrease of 3.4 mmHg compared to baseline (0.4% eye drops, twice daily) [59]. However, conjunctival hyperemia is commonly observed in clinical trials, and ripasudil could reduce the bioavailability of timolol (β-adrenergic blockers) [59,60]. These side effects prevent ripasudil from being the first choice for glaucoma management, but there are still other ROCK inhibitors in clinical trials such as AR-13324 and AMA0076.[59]

Other candidates target the oxidative stress, since TM is the most sensitive tissue to oxidative damage in the anterior ocular segment [61]. A number of antioxidants could be potentially applied to suppress the production of ROS. Luna, et al. (2009) found that when primary porcine TM cells were treated with resveratrol (25μM) for 15 days, the production of ROS

and associated inflammatory markers including IL 1α, IL6, and IL8 are effectively prevented and that cell proliferation was not influenced by resveratrol [62]. Fatty acid omega-3 also has preventive effects against oxidative stress induced by H_2O_2 in primary human TMCs, and has been suggested for glaucoma prevention[63]. Other substances such as vitamins C and E, creatine, α-lipoic acid, nicotinamide, and catechins also have antioxidant effects, but their effect on TM is unknown. [64]

Another approach is using sodium 4-phenylbutyrate (PBA) for myocilin related glaucoma. This small chemical chaperone is able to correct protein folding abnormalities and restore the function of mutant cystic fibrosis transmembrane conductance regulator protein on the cell surface [65]. Zode et al. (2011, 2012) reported that PBA could help the secretion of mutant myocilin in TMCs of mice and reduce the ER stress induced by tunicamycin [66,67]. Ultimately full understanding of the pathogenesis of the disease can contribute to finding new drugs for glaucoma treatment, in addition to those that decrease the IOP.

1.6 Models of glaucoma

To investigate the biology of POAG, both in vivo models and in vitro models have been applied. In vivo models have more relevance to clinical glaucoma, but come with a higher cost for animal breeding and maintenance. In vitro models, including cells and organ culture, are more controllable for precise conditions, but have less relevance to glaucoma compared to in vivo models [68]. Overcoming these limitations and gaining a deeper understanding of existing models will increase research power for developing POAG therapies.

1.6.1 In vivo models

To study the response of the ocular tissues to glaucoma, animals such as macaque monkeys and transgenic mice have been applied. Yucel et al (1999) observed that decreased myelinated nerve fiber was associated with elevated IOP in monkey models [69]. Ju et al (2008) found that increased IOP damaged mitochondria in the optic nerve in transgenic mice [70]. More recently, Zhu et al. (2016) restored the normal function of TM via transplanting the TM-like cells into a high IOP transgenic mouse model [71], which proposed a novel treatment of glaucoma.

1.6.2 In vitro models

Cell models are also widely applied to studies of glaucoma pathogenesis, drug screening and potential therapeutic treatments. These cells can be derived from human or animal ocular tissue such as TM, Schlemm's canal endothelium, and retinal neurons [72,73]. TMCs can be harvested by treating TM tissue with collagenase-A and culturing in artificial medium [74]. These cells can be induced to mimic the progression of glaucoma by various methods, e.g. being exposed to chemical compounds including dexamethasone, transforming growth factor-β2, and oxidative stress factors such as H_2O_2 [56,75,76]. Also, primary human TMCs can be transfected with reconstructed plasmids containing mutant myocilin gene to induce mitochondrial function deficits and ROS generation[56]. However, primary TMCs start to develop senescence features such as increased size, vacuoles, and reduced doubling time by passage 9 or 10 in vitro, and the gene expression patterns also differ from early passage TMCs. Hence, it is preferable to use TMCs from human eyes before passage 7 [77]. This has led to demand to generate TMCs from stem cells, as it is sometimes not feasible to harvest enough TMCs from living eyes in glaucoma patients.

1.7 Cultured trabecular meshwork cell models generation

1.7.1 The development of trabecular meshwork

To generate a feasible differentiation procedure, we reviewed the development pathway of TM tissue. In the development of the anterior ocular segment, the TM and Sclemm's canal become differentiated from 15th to 20th week of gestation, shortly after the start of iris elongation. Briefly, a dense collection of mesenchymal cells aggregate in the chamber angle and begin to elongate and flatten, becoming separated from each other by spaces which are then filled with extracellular fibers. The fibers then become organized into lamellae or beams and covered by flat, endothelial-like cells. The formation of TM tissue should be completed around birth in humans[78]. Cell grafting and cell labelling experiments in mice have demonstrated that the ocular mesenchymal cells are derived from both cranial neural crest and cranial paraxial mesoderm[79]. A series of growth factors and transcription factors act on the mesenchymal stem cells (MSCs) to differentiate them to TMCs.

1.7.2 Transcription factors involved in the differentiation of trabecular meshwork

Retinoic acid (RA) is indispensable for the development of the eyes. The RA signal is transduced by two families of nuclear receptors, retinoic acid receptor (RAR) family (RARα, RARβ, and RARγ) and retinoid X receptor (RXR) family (RXRα, RXRβ, and RXRγ). These receptors work in the form of RXR/RAR heterodimers [80]. In periocular mesenchyme (POM), RA signaling is generated via the activation of RXRα/RARβ, and RXRα/RARγ. This signaling pathway plays an important role in embryonic development, cell proliferation, differentiation and apoptosis, thus blocking RA signaling could cause early embryonic death [81,82]. Also, impairment of RA synthesis could affect the expression of *FOXC1* and paired-like homeodomain 2(*PITX2*), which are both required for eye development [81]. The *FOXC1* transcription factor is expressed when mesenchymal cells have migrated into the eye. In *FOXC1*$^{-/-}$ mice models, severe anterior segment developmental defects are observed, including thickened cornea epithelium, disorganized stroma, and the absence of anterior chamber due to the lens not being separated from the cornea. In *FOXC1*$^{+/-}$ mice models, though the abnormalities are milder, all mice show hypoplastic TM and Schlemm's canal histologically [31,83]. *PITX2* is also a transcription factor expressed in the POM and its expression pattern is very similar to *FOXC1*. Both deficiency and over-expression of *PITX2* causes human ocular anterior segment dysgenesis, which indicates that normal anterior segment development needs precise regulation of transcription factors via various signaling pathways [31]. The transforming growth factor β (TGFβ) superfamily signaling pathway also plays an important role in ocular development. This super-family contains a group of signaling molecules which affect a series of biological processes, such as cell proliferation, differentiation, migration, and apoptosis [84]. BMP4 (bone morphogenetic protein 4) belongs to this superfamily and is expressed during ocular development. BMP4 $^{+/-}$ mice showed various degrees of anterior segment dysgenesis, including the TM, which exhibits a decrease in the trabecular beams and ECM [85]. BMP4 also influences the cell migration and differentiation via regulating the expression of ECM[31]. Another transcription factor, TGF-β2 also plays an essential role in ocular development. TGF-β2 is mainly expressed by the lens, and it is required for the expression of *FOXC1* and *PITX2* in the formation of TM and neural crest-derived cornea [86].

Overall, when RA signaling and TGFβ signaling occurs, MSCs may potentially exhibit some

characteristic properties of TMCs or POM. We hypothesized that when treated with RA, BMP4 and TGF-β2, mesenchymal stem cells could express the gene markers and exhibit the functional properties of TMCs.

1.7.3 Identification of trabecular meshwork cells

In order to verify that MSCs have successfully undergone differentiation into TMCs they ideally need to display the morphologic features, specific protein markers, and the cell behaviors of TMCs. TMCs are morphologically similar to fibroblast, which have an elliptical, speckled nucleus surrounded by branched cytoplasm (Fig. 5). There is not a single specific protein marker for TMCs yet. However, studies have identified TM-like cells differentiated from iPSCs through the expression of a group of proteins including Col IV, laminin, matrix Gla (*MGP*), and α-SMA, among others. [87–89]. Stamer et al. (2017) reviewed the characteristics of TMCs, which provides more information on specific TMC features (Table 2).[90]

Figure 5: *The appearance of fibroblast and trabecular meshwork cells, 80% confluent. A) Fibroblast; B) human primary HTMCs. Scale bar: 20 µm*

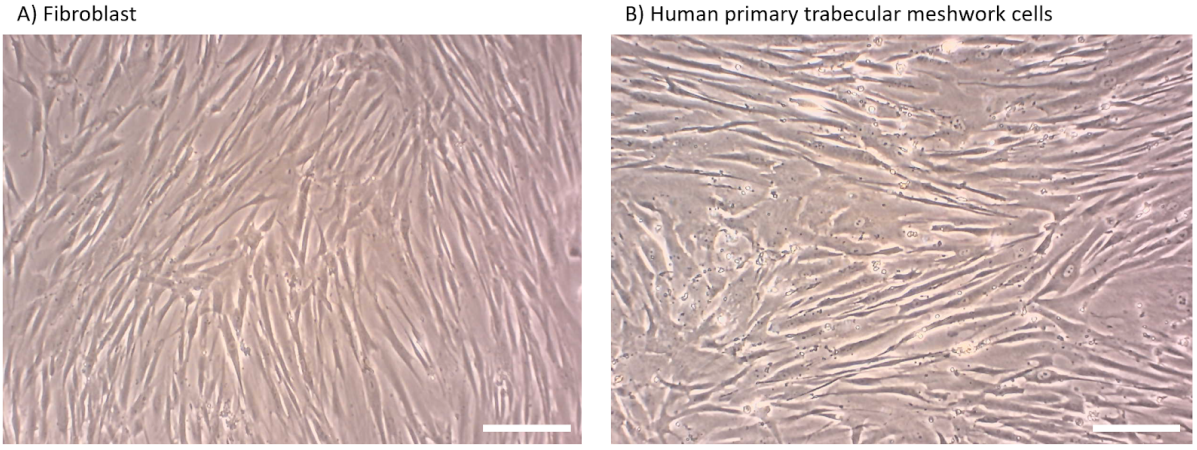

Table 2: *Identification of TM cells in culture* [90]

Positive Markers	Negative Markers	Cellular responses
Myocilin	VE-cadherin	Acetylated LDL uptake
Matrix GLA protein	Fibulin-2	αvb5/β3-mediated phagocytosis
Chitinase-3 like-1	Integrin α6	CS induction of myocilin, FN, CLANs
Aquaporin-1	Keratin	CS down regulation of tPA, phagocytosis
Smooth muscle actin	Desmin	PMA, TNFα and IL-1α stimulation of MMP-3/-9
Smooth muscle myosin	VEGFR3	TGFβ induction of alpha-B crystallin, PAI-I, MMP2, CLANs
Alpha-B crystallin	Prox-1	Stretch induction of MMP-2/-3

One of the behavioural properties of TMCs is upregulated expression of MYOC protein upon corticosteroid treatment, and that this behaviour is not shared by neighboring cells [90,91] . A possible mechanism is that corticosteroids such as dexamethasone regulate the activity of calcineurin/NFATc1 which promotes the expression of myocilin [91,92]. The TMCs are also phagocytic, as demonstrated by Ding, et al's 2014 study using pHrodo fluorescent bioparticles [87]. Another essential feature is the ability to contract to the extracellular matrix (ECM). TMCs can contract their extracellular collagen due to the adhesiveness of the cell to its matrix and the activation of the actin cytoskeleton. As mentioned, this can be prevented by ROCK-inhibitors,[93,94] which is an alternate means to screen for TMC-like behaviour.

TMCs can be identified by the combination of protein markers and behavioural characteristics as well as their morphology. In order to analyse these features, high throughput, human-independent methods are preferred for accurate and detailed characterisation of cells.

1.8 High throughput analysis of gene function

New technology including clustered regularly interspaced short palindromic repeats (CRISPR) technology, automated microscopy and single cell RNA sequencing (scRNA-seq) have improved large-scale gene function analysis by morphological profiling and mRNA expression profiling. These methods allow researchers to quickly and accurately characterise large numbers of cells, as well investigate the effect of many different single genes knockouts in a single experiment.

1.8.1 CRISPR technology in high-throughput genetic screens

CRISPR is an RNA-mediated defense system found in bacteria and archaea, designed to defend against viruses and plasmids, that has been adapted for genome editing within living cells [95–100]. This system contains a cas endonuclease protein and a single-guide RNA (sgRNA), which form the Cas-sgRNA ribonucleoprotein complex. This complex localises to a target DNA sequence following guide RNA:genomic DNA base-pairing rules [97]. The most commonly used CRISPR system utilises *Streptococcus pyogenes* Cas9 (SpCas9). When the SpCas9-sgRNA complex recognises the target DNA sequence, a double-strand break is created. In eukaryotic cells, DSBs can be repaired through non-homologous end joining (NHEJ) and homology-directed repair (HDR). NHEJ generally occurs more efficiently than HDR and results in stochastic insertions and deletions (indels) [101,102]. If NHEJ occurs in a coding region, it can introduce a frameshift mutation which causes loss-of-function in the targeted gene [99]. With the ease of desired DNA sequence targeting, the CRISPR system enables us to develop cell and animal knockouts which can be used to explore the causal linkages between genetic variations and biological phenotypes. Researchers have applied this powerful tool to high-throughput analysis to determine gene function, identify drug targets and explore cellular signaling pathways[103]. Cas9-mediated knockout screening has been a very successful method in many previous studies. In these experiments, libraries were designed with at least two sgRNAs targeting each gene to increase the likelihood of a knockout, and the CRISPR system was delivered into mammalian cells via viruses. Chen et al. (2015) identified a set of genes driving tumor growth and metastasis in mice models [104]. Shi et al. (2015) identified 25 drug targets in murine acute myeloid leukemia, in which 6 were

known drug targets [105]. Parnas et al. (2015) reported dozens of novel regulators of Tlr4 signaling in the host response to pathogens [106]. Zhou et al. (2014) identified host genes essential for the bacterial toxins against anthrax and diphtheria toxins [107]. Also, the Cas9-mediated knockout screens show a much higher reagent consistency for the hits in the Cas9 screen compared to the previous gene knockdown technique of RNAi (RNA interference)-based screens [103]. Thus, CRISPR can be used to generate a robust model with desired gene perturbation in large-scale experiments. CRISPR has also been applied to other ocular experiments. Hung et al. (2016) delivered the CRISPR/Cas9 system to the retinal of transgenic mice via adenovirus, successfully disrupted the expression of yellow fluorescent protein to assess the gene editing efficacy [108]. Jain et al. (2017) knocked down mutant *MYOC* via adenovirus mediated CRISPR/Cas9 system in human TMCs and a murine model, and the ER stress was released [109]. However, there has been no large-scale CRISPR mediated experiment undertaken for any ophthalmic application ocular research yet.

1.8.2 Image-based profiling

Automated microscopy enables us to perform large-scale imaging experiments and create an image based-profile of each cell population. These profiles contain complex phenotypic outcomes that are related to the disease states or responses in a drug screening. Bray et al. (2016) summarized the method named "Cell Painting" to evaluate the biological information about cellular state [110]. In Cell Painting, cultured cells are dyed by six fluorescent stains to reveal eight cellular substructures. After imaging in five channels, we are able to extract more than 1000 morphological features from each of the cells by designing pipelines with cellprofiler software. This method has been applied to compound library enrichment and genetic perturbation experiments. Gustafsdottir et al. (2013) reported that the Cell painting assay could identify cellular phenotypes and cluster compounds with similar chemical structure or annotated targets based on the cellular profiles [111]. Cell painting does have some limitations. Singh et al. (2015) studied the morphological profiles of RNAi-induced knockdown in U2OS cell line, and was unable to group cell profiles by RNAi targets in the same gene compared to different genes. The cause of this could be off-target effects [112], hence the more precise suppression technique, CRISPR, may potentially fix this problem, and is a novel approach.

1.8.3 Single-cell RNA sequencing

The technology of scRNA-seq enables us to establish the transcriptional profiles of individual cells by capturing and reading the cell's individual mRNA transcriptome [113]. With the development of technologies such as microfluidics, robotics, and reverse emulsion and hydrogel droplets, scRNA-seq can process hundreds of thousands of cells per experiment [114]. The methods of scRNA-seq differ in whether the mRNAs are reverse transcripted to full-length cDNA, such as SMART-seq2 (Switch Mechanism at the 5' End of RNA Templates sequencing)[115], or cDNA with a unique molecular identifier (UMI), such as Drop-seq [116]. These methods have been integrated into platforms such as SMART-seq2 (illumina) and 10X Genomics Chromium, among others. Briefly, in the droplet based system used by the 10X Genomics Chromium platform, a single cell suspension would be prepared, and then the cells are individually encapsulated into a water-in-oil droplet together with a gel bead which is labeled with oligonucleotides. The oligonucleotide consists of a unique barcode for each cell (16 bp), an UMI (8 bp), sequencing adapters, and an anchored oligo-dT. Next, reverse transcription, cDNA amplification and library construction occurs, followed by next generation sequencing (NGS). The downstream processing with the data generated by NGS involves data de-multiplexing, alignment, and then biological data interpretation, which should be designed specifically [117,118]. scRNA-seq gives us the opportunity to study heterogeneity in a whole organism and investigate the differential expression of genes at the cell level. For example, Kim et al. (2015) reported a subgroup which is related to anti-cancer drug resistance from tumor cells of lung adenocarcinoma [119]. Smillie et al. (2019) also identified 51 cell subgroups in human colon mucosa from patients with ulcerative colitis versus healthy individuals and found many ulcerative colitis risk genes were convergent onto limited sets of cell types and pathways [120]. Lukowski et al. (2019) identified 18 cell types by performing scRNA-seq on 20, 009 cells from the human retina [121]. Patel et al. (2020) identified 12 cell populations using scRNA-seq on 8,758 cells from human TMCs and neighboring tissues [122]. Single cell RNA-seq is a powerful tool to investigate subtle changes in cell transcription, combined with cell painting, we can gain a novel understanding of the morphological and transcriptional changes that occur as a result of Cas9-mediated gene knockout and potentially determine a causal relationship between certain genes and disease related phenotypes.

In summary, TMCs are vital models in studying the disease of glaucoma. Due to the difficulty in harvesting human TMCs and the limitation in the usage, we investigated whether MSCs could acquire TMCs properties in response to the combination of RA, TGF-β2, and BMP4. Also, we firstly utilised novel techniques of CRISPR, CellPainting and scRNA-seq together to study the effects of IOP-associated genes in human primary TMCs, where the morphological and transcriptome profiles illuminate their roles in the pathogenesis of glaucoma.

2. AIMS AND HYPOTHESIS

2.1 Characterize DP-MSCs under the treatment of combination of transcription factors, RA, TGF-β2, and BMP4.

Aim: To determine whether DP-MSCs could be induced to exhibit the phenotypic properties of human TMCs through the exposure of the transcription factors known be involved in the embryogenesis of the anterior segment;

Hypothesis: After the treatment of combination of transcription factors, RA, TGF-β2, and BMP4, DP-MSCs will express the gene markers of human TMCs. Also, the treated DM-MSCs will upregulate the expression of myocilin under the presence of dexamethasone and exhibit contractile properties.

2.2 Morphological and genetic profiles of CRISPR-induced gene knockout in human TMCs

Aim: To use Cell Painting and scRNAseq to generate morphological and transcriptome profiles of TMCs, in which genes implicated in IOP variation have been knocked out by CRISPR.

Hypothesis: That the morphological and transcriptional profiles of TMC knockout lines will indicate how that gene may contribute to TM dysfunction in POAG, and genes involved in the same regulatory pathway will cluster together.

3. METHODS:

3.1 Cell culture:

3.1.1 Cell type and culture medium:

Primary human TMCs were isolated from patients by Dr. Helena Liang in the Royal Victorian Eye and Ear Hospital (Ethics approved, Ref. 13-1151H). The primary human TMCs were cryopreserved at Passage 0 and delivered frozen. These TMCs were thawed and cultured in Dulbecco's Modified Eagle Medium (DMEM, Gibco, 11965118) with 10% fetal bovine serum (FBS, Gibco, 16000044), and supplemented with 0.5% antibiotic-antimycotic (Gibco, 15240-062). Commercial human TMCs were bought from ScienCell (Cat. 6590) and cultured in trabecular meshwork cell medium (TMCM, ScienCell, 6591). Human neonatal dermal fibroblast (HNDF, Thermofisher, C0045C), HEK-293A and HEK-293FT were all cultured in DMEM with 10% FBS supplement and 1% antibiotic-antimycotic. Dental pulp mesenchymal stem cells (DP-MSCs, Lonza, PT-5025) were cultured in the DP-MSC culture medium (Lonza, PT-3005). All cell lines were cultured at 37°C with 5% CO_2 in the incubator. Each fortnight cell lines were tested for mycoplasma using the PCR Mycoplasma Test Kit (PromoKine, PK-CA91-1096).

3.1.2. Cell Maintenance and Subculture

To maintain TMCs and DP-MSCs, the culture medium was changed every 3 days when cells were less 80% confluent. Once the confluence reaches 80%, the medium was changed every other day before subculturing. For HNDF, HEK-293A, and HEK-293FT, the medium should be changed every 3 days before subculturing. All cell lines were allowed to reach ~90% confluence in vessels, with different types of vessels used for different purposes (Table 3). For subculturing, cells were washed twice with DPBS (Gibco, 14190144) and then incubated with Trypsin/EDTA (Gbico, 25200056) at 37°C with 5% CO_2. For TMCs, the concentration of Trypsin/EDTA is 0.05%, diluted in DBPS. For DP-MSCs, HNDF, HEK-293A, and HEK-293FT, the concentration of Trypsin/EDTA is 0.25%. After 2-3 minutes of trypsinization the cells should round up and detach from the culture surface. The vessel may be gently tapped to assist with cell detachment. The trypsin is then neutralised with the culture medium (5X volume of 0.25% Trypsin/EDTA) or Trypsin Neutralizer Solution

(Gbico, R002100) (2X volume of 0.25% Trypsin/EDTA). Cells are then centrifuged at room temperature. For DP-MSCs, 220 x g for 5 minutes; for TMCs, HNDF, HEK-293A, and HEK-293FT, 300 x g for 5 minutes. After aspirating the supernatant, cells would be resuspended in the culture medium and cell number and viability would be determined by hemocytometer. To obtain a clear view of individual cells after subculturing, and given that the cell painting and phagocytosis assays require a low confluence, cells were seeded at a density of approximately 40%~50%. The optimal seeding number of different cell types and corresponding culture vessels are listed (Table 3).

3.1.3 Freezing and thawing

The procedure for freezing cells is similar to subculture, except that cells are resuspended in cold freezing medium (FBS with 10% DMSO (Merck, D2650)). Generally, one cryovial contains 1ml cell suspension with 1*10^6 cells. Cryovials are then stored in a Mr. Frosty container (Thermo Scientific, 5100-0001) and placed at -80°C for at least 6 hrs. These cryovials are transferred to liquid nitrogen the next day for long term storage. To quickly thaw cells, the cryovials are half immersed in a 37°C water bath on a floating plate for less than 2 minutes, then cells are gently resuspended in culture medium and plated into appropriate cultureware. The culture medium should be changed the following day and regular culture procedures followed.

3.2 Characterization of the trabecular meshwork cells

3.2.1 Treatment with dexamethasone in TMCs

TMCs were plated out in 6-well plates with/without coverslips ($1.5*10^5$ cells/well) and allowed to adhere overnight. The following day, TMCs were treated with different concentrations of dexamethasone in culture medium (Sigma-Aldrich, D4902) (100nM, 500nM, 1μM, 2 μM, 5μM) or 0.1% ethanol (EtOH; vehicle control), which was continued for three days. TMCs cultured without coverslips were harvested for RNA extraction to detect the level of *MYOC* mRNA, and TMCs cultured with coverslips were fixed in 4% paraformaldehyde (Sigma-Aldrich, 441244) for immunocytochemistry.

Table 3: *The use of different culture vessels and optimal seeding number of different cell lines*

Culture Vessel	Usage	Optimal seeding number for ~40% confluence (*10^6)	
		DP-MSCs TMCs HNDF	**HEK-293A HEK-293FT**
T-75 flask (Corning, 430641U)	Thaw, expand, and freeze cells	1	3
T-25 flask (Corning, 430639)	Thaw and freeze cells	0.3	1
6-well Tissue Culture treated plate (Corning, 3516)	qPCR, immunocytochemistry with glass coverslips	0.15	0.5
24-well Tissue Culture treated plate (Corning, 3524)	Lentivirus transfection	0.03	/
96-well Black/Clear Imaging plate (Flacon, FAL353219)	Cell Painting Assay	0.004	/
96-well Black/Clear Image plate (ThermoFisher, 165305)	Phagocytosis	0.03	0.1
10 mm tissue treated cell culture dish (Falcon, 353003)	Lentivirus preparation	/	8

3.2.2 RNA extraction, reverse transcription and quantitative real-time PCR

RNA was extracted using RNeasy plus micro kit (Qiagen, 74134) following the supplied manufacturer's protocol. Briefly, cells were washed once using DPBS and 350µL of Buffer RLT Plus was added to lyse cells. Cell lysates were transferred to the gDNA Eliminator spin column, and subsequently transferred to an RNeasy spin column for purification. The RNA was eluted in 30µL of RNase-free water and the concentration was measured by Nanodrop 1000 (Thermo Scientific).

Reverse transcription was performed to produce cDNA following Qiagen's protocol. Briefly, a volume of thawed RNA corresponding to the amount of cDNA required was added to 8 µL of master mix and RNase-free water was added up to a volume of 20 µL. For each reaction in the master mix, 2 µL 10* Buffer RT, 2 µL dNTP Mix (5 mM each dNTP), 2 µL Oligo dT Random Primer 9, 1 µL RNase inhibitor (10 units/µL) and 1 µL Omniscript Reverse Transcriptase (4 units/µL) was added and subsequently pipetted into individual reaction tubes. 200 mg of RNA was added per reaction, tubes were vortexed for less than 5 seconds, spun down and then incubated for 1 hour at 37°C. Finally, the cDNA samples were placed in ice for qPCR analysis or stored at -20°C.

For quantitative real time PCR reactions, cDNA samples were diluted to 2 ng/µL using nuclease-free water. qRT-PCR was performed using the LightCycler 480 system (Roche). TaqMan Probe/primers for *MYOC*, *EEF2* (Eukaryotic elongation factor 2) were selected. For each well, cDNA (5 µL) was added to 15 µL of TaqMan PCR mix (10 µL 2X TaqMan Master Mix, 1 µL 20X probe/primer mix, 4 µL nuclease-free water). 20 µL of total reaction was added to each well of a 96-well PCR plate, and each sample for each gene had a duplicate in the 96-well plate. qRT-PCR was performed using the following program: initial polymerase activation for 10 minutes at 95°C and 50 cycles of amplification (denaturation for 15 seconds at 95°C, annealing and extension for 1 minute at 60°C). The Ct value of each gene for each sample was calculated as the mean value of the Ct values of the duplicates. Relative gene expression analysis was performed using the $2^{-\Delta\Delta Ct}$ method as the relative expression of target mRNA was normalized against the housekeeping gene, *EEF2*.

3.2.3 Immunofluorescent staining of TMCs

For immunofluorescence experiments, TMCs were fixed in 4% paraformaldehyde for 20 minutes and then washed with phosphate-buffered saline (PBS, 0.01M) three times. Then the cells were permeabilized by 0.1% solution of Triton X-100 (Sigma, T8787) for 10 minutes with agitation and washed with PBS three times again. Cells were blocked in PBS containing 10% FBS for at least 30 minutes at room temperature. Then the cells were incubated with the primary antibodies (Table 4) at 4°C overnight. The following day, cells were washed with PBS four times with agitation and then incubated with corresponding secondary antibodies with agitation for 2 hours in darkness at room temperature, followed with 4,6-diamidino-2-phenylindole (DAPI, 1μg/ml) (Merck, 10236276001) for 10 minutes. Cells were then washed with PBS four times. The coverslips were mounted onto glass slides with mounting media (Dako, S202380-2), and allowed to dry overnight before sealing with nail polish. Images were taken by the fluorescent microscope olympus BX53.

Table 4: *List of antibodies used*

Antibody	**Company**	**Catalogue Number**	**Working Concentration & Dilution ratio**	**Host**	**Species Reactivity**
myocilin	Cloud-Clone Corp.	PAH586Hu01	5 μg/ml 1:40	*Rabbit*	*Homo sapiens*
Caveolin-1	Cell Signaling	3238S	1:400	*Rabbit*	*Homo sapiens*
TIMP3	Abcam	ab39184	5 μg/ml 1:200	*Rabbit*	*Homo sapiens*
Alexa Fluor 488 goat anti-rabbit	ThermoFisher	A11034	2 μg/ml 1:1000	*Goat*	*Rabbit*
Alexa Fluor 555 donkey anti-rabbit	Abcam	ab150074	2 μg/ml 1:1000	*Donkey*	*Rabbit*

3.2.4 Phagocytosis assay

In the phagocytosis experiment, TMCs, HNDF, and HEK293A were seeded into a 96-well black/clear bottom plate. Macrophages were also used as a positive control, which were a gift from Peng Chen at the Menzies Institute for Medical Research. The cells were incubated with 100 µL 1mg/ml S. *aureus* pHrodo red particles (ThermoFisher Scientific, A10010) for 2 hours at 37°C. Then each well was washed with DPBS (Gibco, 14040133) three times gently, no final aspiration. Plate was observed under the live cell fluorescent microscope Nikon Ti2.

3.3 Effects of transcription factors in DP-MSC

3.3.1 Treatment with the combination of transcription factors RA, TGF-β2, BMP4 and dexamethasone in DP-MSCs.

For this treatment, the concentrations of each growth factor were selected by previous study (McDonald,N.L., 2015). Prior to adding into the culture media, retinoic acid (RA, Sigma, R2625) was diluted to 1mM in DMSO, recombinant human transforming growth factor-β2 (TGF-β2, Invitrogen, PHG9114) and bone morphogenetic protein 4 (BMP4, Invitrogen, PHC9534) were diluted to 10µg/mL in 0.1% BSA/HBSS (Bovine Serum Albumin, Invitrogen, A8806; HBSS, Gibco, 14025134). Cells were treated with the culture medium containing 0.1µM RA, 5ng/mL TGF-β2, and 10ng/mL BMP4 or vehicle control (DMSO and 0.1% BSA/HBSS) for 48 hours. This was followed by a medium change with the same concentrations of growth factors or vehicle, with the addition of 1µM dexamethasone or 0.1% ethanol for another 24 hrs. After three days treatment, DP-MSCs were harvested for RNA extraction to detect the mRNA level of myocilin intracellularly and conditioned medium was collected for enzyme-linked immunosorbent assay to assess extracellular myocilin levels. The experiment was repeated three times from passage 4 to passage 6.

3.3.2 Quantitative PCR (qPCR) of candidate genes

The procedure for qPCR is previously described in chapter 3.2.2. TaqMan Probe/primers for *MYOC*, *MGP*, *FOXC1*, *PITX2*, *FOXC2*, *PAWR*, and *HPRT1* were selected. Relative gene expression analysis was performed using the $2^{-\Delta\Delta Ct}$ method as the relative expression of target mRNA was normalized against the housekeeping gene, *HPRT1*.

3.3.3 ELISA (Enzyme-linked immunosorbent assay)

To determine whether dexamethasone influences the expression level of *MYOC* secreted extracellularly, ELISAs were performed with the Cloud-Clone kit according to manufacturer instructions (Cloud-Clone Corp. USA, SEH586Hu). Briefly, the standard solution was diluted (concentration gradient: 50 ng/mL, 25 ng/mL, 12.5 ng/mL, 6.25 ng/mL, 3.12 ng/mL, 1.56 ng/mL, 0.78 ng/mL) and 100 µL was added to each well. Then 100 µL samples of culture supernatant from the cells or an equal volume of culture medium for blank samples was added. Then the plate was incubated at 37°C for one hour and the liquid was removed. 100 µL Detection Reagent A was added to each well and the plate was incubated for another hour at 37°C. Each well of the plate was washed with Wash Solution and dried on the absorbent paper. 100 µL Detection Reagent B was added to each well and the plate was incubated at 37°C for 30 minutes. The plate was then washed with Wash Solution five times. Then 90 µL of Substrate Solution was added to each well and incubated for 20 minutes at 37°C. 50 µL Stop Solution was added to each well to terminate the color reaction. The absorbance of each well was measured at 450 nm using a microplate reader (Tecan Spark).

3.3.4 Collagen contraction assay

In this experiment, DP-MSCs that had undergone five days treatment with the combination of the growth factors, RA, TGF-β2, BMP4 were investigated, together with HNDF and TMCs as positive controls. Collagen gel contraction assay was performed as described in the studies [93,94], with some modifications. The wells of 24-well culture clusters were each coated with 1% BSA at 37 °C for 1 hour. DP-MSCs, HNDF TMCs were trypsinized and resuspended in culture medium at a density of $2.2*10^6$ cells/ml without or with 10µM Y-27632 ROCK inhibitor (Sigma-Aldrich, Y0503). To prepare the 1.1 ml collagen gel mixture, 700µl Collagen type I (3mg/ml, ThermoFisher, A1048301), 110µl 10*DMEM (Sigma, D2429), 110µl 10X PBS, 17.5µl 1N NaOH, 62.5µl water and 100µl cells suspension were mixed in an ice bath (final concentration of collagen type I, 1.9mg/ml; final cell density, $2*10^5$ cells/ml). The mixture (0.5 mL) was added to each well of the BSA coated culture clusters, and collagen gel formation was induced by incubation at 37°C for 90 minutes. Growth medium (0.5mL), without or with 10µM Y-27632, was then added on top of the collagen gels. After 1 hour, the gels were freed from the wall of the culture wells with the use of a micro spatula. Photos were taken every 24 hours up to 72 hours and the area of each collagen gel was

measured using ImageJ. The extent of contraction of the collagen gels was calculated by comparing the decrease in gel diameter with the initial diameter. Each experiment was performed in quadruplicate and was repeated three times.

3.3.5 Statistical analysis for qPCR, ELISA and collagen contraction assay

Raw data from each experiment was collated in Microsoft Excel and statistical analysis was performed via GraphPad Prism V6.01. TMCs with dexamethasone treatment were analyzed using a one-way Analysis of Variance (ANOVA). DP-MSCs with growth factors and dexamethasone were analyzed using a two-way ANOVA. Significant results were differentiated using Tukey's post-hoc test. All data are represented as mean +/- standard deviation (SD). Significant results are defined as *p<0.05; **p<0.01; ***p<0.001, and ****p<0.0001.

3.4 CRISPR-induced gene knockout in primary human TMCs

The gene knockout procedure followed the method of modified CRISPR droplet sequencing (CROP-seq) [123]. Briefly, cells were transfected with lentivirus containing the CRISPR system in separate wells for each target gene (Arrayed CRISPR screen). After antibiotic selection and recovery in the culture medium, cells were harvested for cell painting and scRNA-seq (Fig. 6). In scRNA-seq, the CROP-seq sgRNA was detectable and unique in each well, that is we were able to use the sgRNA as the tag to identify which well the cell came from when we pooled all cells together.

Figure 6: *CROP-seq Workflow*

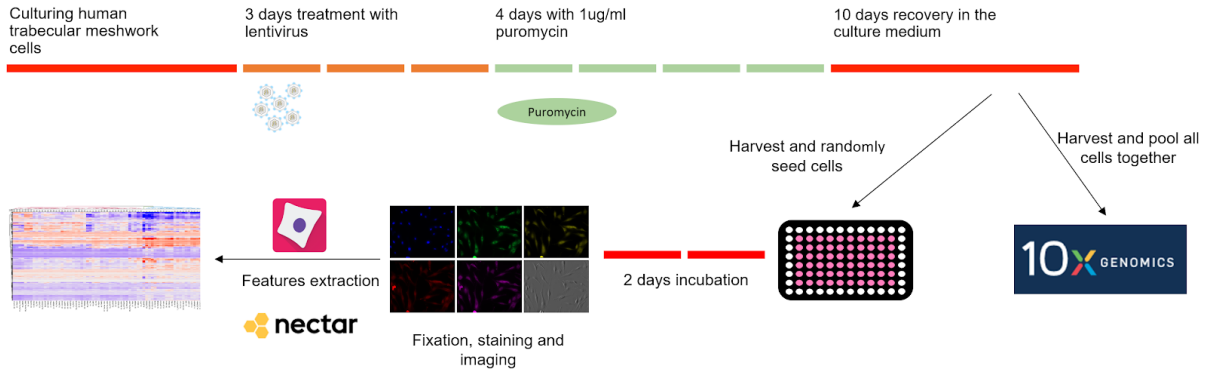

3.4.1 Cloning and validation of the single-vector CROPseq system

The cloning work to produce CROP-seq plasmids was done by Dr. Sandy Hung. To generate a single-vector system CROPseq plasmid to express both SpCas9 and sgRNA(CROPseq-EFS-SpCas9-P2A-EGFP; Addgene #99248), the EF1a promoter in the CROPseq-Guide-Puro [124] (supplied by Christoph Bock; Addgene plasmid # 86708) was replaced with the EFS promoter to drive the expression of SpCas9 using the Gibson Assembly method (NEBuilder HiFi DNA Assembly master mix; NEB). The EFS-SpCas9-P2A fragment was amplified from lentiCRISPRv2 [125] (a gift from Feng Zhang; Addgene plasmid # 52961) using Q5 high-fidelity DNA polymerase (NEB). Puromycin resistance gene was then subsequently replaced with EGFP using a amplified fragment from the pMLS-SV40-EGFP plasmid [126] (a gift from Stanley Qi & Jonathan Weissma; Addgene plasmid # 46919).

The expression and activity of the single-vector CROPseq plasmid was tested by cloning in a sgRNA targeting the DNMT3B (sgRNA sequence: CAGGATTGGGGGCGAGTCGG) [127] or LacZ control gene (sgRNA sequence: TGCGAATACGCCCACGCGAT) [128] using Gibson Assembly method and transformed into NEBStable bacteria (NEB) as outlined in Datlinger et al. [129] and tested in HEK293A cells (Life Technologies). EGFP expression was visualised using the Eclipse Ti-E inverted fluorescence microscope (Nikon). Cleavage activity of the SpCas9 was measured through the indel formation using SURVEYOR assay (Integrated DNA Technologies). Briefly, genomic DNA was extracted (QIAamp DNA mini kit; Qiagen) from HEK293A cells transfected with CROPseq-EFS-SpCas9-P2A-EGFP DNMT3B sgRNA plasmid using Fugene HD (Promega). PCR fragment for SURVEYOR assay was amplified using Q5 high-fidelity polymerase using the primers F: 5`-CAAGAGCATCACCCTAAGAATGC-3` and R: 5`-GTTGTCAGAGACTCTCCCCAAAG-3` from Datlinger el al. [130]. Q5 PCR conditions were as of manufacturer's protocol with the following thermocycling conditions: 98°C 30 secs; 35 cycles of 98°C 10 secs, 71°C 30 secs, 72°C 15 secs; 72°C 2 mins. PCR products were gel purified using the QIAquick gel extraction kit (Qiagen). 200ng of purified PCR product was used in the SURVEYOR assay as outlined in the manufacturer's protocol.

3.4.2 Confirmation of sgRNA sequence via Sanger sequencing

In total, 134 sgRNAs sequences were designed by Prof. Alex Hewitt to generate the 67 trabecular meshwork cell lines (124 sgRNAs for 62 genes and 10 sgRNAs for human non-targeting control, 2 sgRNAs for each cell line) (Table 5, Appendix. Table 2). Each of the sgRNAs was cloned into CROPseq-Guide-pEFS-SpCas9-p2a-puro backbone (Addgene: #99248) by Dr. Sandy Hung. The sequences of all sgRNAs templates were confirmed by in-house Sanger sequencing. Firstly, each template was amplified by the BigDye Terminator Cycle v3.1 Sequencing kit (Applied Biosystems, 4337454). The 10 µl reaction system contained 1 µl template, 1 µl 10µM primer, 0.25 µl Reaction Mix, 1.75 µl 5X Sequencing Buffer, and 6 µl nuclease-free water. Cycling was performed using the following program: initial polymerase activation for 1 minute at 96°C and 25 cycles of amplification (denaturation for 10 seconds at 96°C, annealing for 5 seconds at 50°C, and extension for 4 minutes at 60°C), then held at 15°C. Samples were purified with the CleanSEQ kit (Beckman Coulter, A29151) following the Agencourt CleanSEQ Dye-Terminator Removal protocol. Briefly, 10 µl of vortexed CleanSEQ reagent and 42 µl of 85% ethanol was added to each 10 µl sample and gently mixed. The sample was placed on the 96-well magnetic plate for 3-5 minutes until the magnetic beads formed a ring and the solution was clear. The supernatant was removed and samples were washed twice with 100 µl 85% ethanol with 30 seconds incubation, and then air dried for five minutes. Lastly, 30 µl nuclease-free water was added to each sample and incubated for 3-5 minutes on the magnetic tray to elute the purified DNA. Next, 15 µl of purified cycle sequencing product was added to the sequencing plate, then denatured by incubating at 95°C for 5 minutes (no heat on lid). The plate was loaded into the sequencer (Genetic Analyzer 3500, Applied Biosystems) and the default program for 850 bp length of DNA was used. Finally, the online alignment tool MAFFT (version 7) was used to confirm whether the sequences of all the 134 sgRNAs were matched with reference sequences.

Table 5: *CRISPR/Cas9 sgRNAs designed to target genes at loci previously associated with variation in intraocular pressure.*

sgRNA_name	Sequence	Gene	Exon	Protein domain targeted	Predicted On-target efficiency
GUIDES_sg001	GTTGACTGGGAGAGAACACG	*ABCA1*	46	ABC_tran	0.707186352
GUIDES_sg002	GTGTTCTAAAAGAGAAACAC	*ABCA1*	50	-	0.684107302
GUIDES_sg003	GTGCAGTGTCTCTCCTACAC	*ADAMTS6*	28	-	0.720054847
GUIDES_sg004	ACCAGTCATGTCCACCACAG	*ADAMTS6*	26	-	0.71972146
GUIDES_sg005	CAAGGGTAAAAAGCCCCCCG	*AFAP1*	16	-	0.759587174
GUIDES_sg006	GGAAAGAAAAGACCTTCGAG	*AFAP1*	17	-	0.753862205
GUIDES_sg007	CAACTATAACGTCAGCCCAG	*ALDH9A1*	10	Aldedh	0.764185557
GUIDES_sg008	TATGAACAATGCTGTAAAGG	*ALDH9A1*	6	Aldedh	0.704113168
GUIDES_sg009	GTGCTGTGAGCTGGGAAGTG	*ANAPC1*	39	-	0.69840945
GUIDES_sg010	ATGGCTCTTCCTGTAGGACG	*ANAPC1*	27	-	0.641611628
GUIDES_sg011	CCCCAGCCAATATTCACCGG	*ANGPT1*	9	Fibrinogen_C	0.666179972
GUIDES_sg012	AATATGGATGTCAATGGGGG	*ANGPT1*	8	Fibrinogen_C	0.630390739
GUIDES_sg013	TAACGTGTAGATGCCATTCG	*ANGPT2*	5	Fibrinogen_C	0.692502215
GUIDES_sg014	TGTGACATGGAAGCTGGAGG	*ANGPT2*	6	Fibrinogen_C	0.647042655
GUIDES_sg015	ACTCGCTCTCAGGTTCCAGG	*ANGPTL2*	5	Fibrinogen_C	0.761119961
GUIDES_sg016	CACCAGCATGTCACGCACAG	*ANGPTL2*	2	RasGEF	0.753686491
GUIDES_sg017	CTTTGTGGGAGAATCCACCA	*ANKH*	14	ANKH	0.705623542
GUIDES_sg018	TGAGGGCGCATCTCACCGGG	*ANKH*	13	ANKH	0.671178514
GUIDES_sg019	CTTCCGACATGCCCGCAACG	*ANTXR1*	10	Anth_Ig	0.66965417
GUIDES_sg020	CAGAACTGGAGATAAAAGAG	*ANTXR1*	12	Anth_Ig	0.661995855
GUIDES_sg021	CTGCTGGACCAGAAATTCGG	*ARHGEF12*	39	-	0.715629912
GUIDES_sg022	TCTCTGGGGTCATAATCATG	*ARHGEF12*	38	-	0.682338139
GUIDES_sg023	TACCAAATATGCCCCAACAG	*ATXN2*	21	-	0.746394842
GUIDES_sg024	ATTACAGGACTATAGACATG	*ATXN2*	22	-	0.705381212
GUIDES_sg025	ATGGGCCCAGGACTTCCAGG	*BCAS3*	35	-	0.763805308
GUIDES_sg026	TGAACTGGATGAGATAACTG	*BCAS3*	36	-	0.749363581
GUIDES_sg027	AGTTTTTAGGCTGAAACTGG	*CAPZA1*	6	F-actin_cap_A	0.671121892
GUIDES_sg028	GGAATAATGGTCTTTCACAT	*CAPZA1*	5	F-actin_cap_A	0.61837895
GUIDES_sg029	TAAACACCTCAACGATGACG	*CAV1*	3	Caveolin	0.697766064

sgRNA_name	Sequence	Gene	Exon	Protein domain targeted	Predicted On-target efficiency
GUIDES_sg030	TGGGGGCAAATACGTAGACT	*CAV1*	1	Caveolin	0.638532867
GUIDES_sg031	GATGTGCAGACAGCTGAGGG	*CAV2*	23	Caveolin	0.699222046
GUIDES_sg032	CGGCGTACTCGAGGCCGCTG	*CAV2*	22	Caveolin	0.674769146
GUIDES_sg033	TCAGGAAGCCAAAGTCCCAG	*CDH11*	19	Cadherin	0.765145054
GUIDES_sg034	GGATTGTGAATGATTTCAGG	*CDH11*	20	Cadherin	0.686839641
GUIDES_sg035	GGGTTATCTCGTGTGCCAAG	*COL24A1*	60	COLFI	0.662833491
GUIDES_sg036	GAAATTGCAGAAAACCTCAA	*COL24A1*	61	COLFI	0.614109727
GUIDES_sg037	AAGCGGCCAGACTTCCTGCG	*CTTNBP2*	25	-	0.737788504
GUIDES_sg038	GCCAGGTTGTCTTTTCACAG	*CTTNBP2*	24	-	0.682279464
GUIDES_sg039	AACATTCCCAGCATGTACGG	*DGKG*	22	DAGK_acc	0.746132205
GUIDES_sg040	GTACTTTGAATTTGGCACCT	*DGKG*	21	DAGK_acc	0.610555363
GUIDES_sg041	GACCACAAATGAATGCCGGG	*EFEMP1*	9	EGF_CA	0.7383367
GUIDES_sg042	TCACCACTTGGTATCCCTGG	*EFEMP1*	8	EGF_CA	0.711733541
GUIDES_sg043	ACGCTCTCTTTATCAGACTG	*EMCN*	19	Endomucin	0.716120299
GUIDES_sg044	GTTTTAGAAGGTGATGCATC	*EMCN*	15	Endomucin	0.500046723
GUIDES_sg045	AGGACTCCCAGGGACACCTG	*EMID1*	11	Collagen	0.633805274
GUIDES_sg046	GCTGCCCAGCAGAGCCTTGG	*EMID1*	13	Collagen	0.50154336
GUIDES_sg047	GCAGTGGACCAATCCAGCTA	*ETS1*	13	Ets	0.590477455
GUIDES_sg048	CACTAAAGAACAGCAACGAC	*ETS1*	8	SAM_PNT	0.507782957
GUIDES_sg049	ATGTTCAGTTGTAGGCACAA	*FBXO32*	7	-	0.680491123
GUIDES_sg050	AACTTGTCCGATGTTACCCA	*FBXO32*	8	-	0.665922839
GUIDES_sg051	ACAGTTCAGAGAGTGACGTG	*FER*	26	Pkinase	0.744231001
GUIDES_sg052	ATGTCTCGTCAAGAGGATGG	*FER*	25	Pkinase	0.666176654
GUIDES_sg053	GCCTGCAGATTAGCCTCCAA	*FERMT2*	17	PH	0.635135622
GUIDES_sg054	CTGAGGTTCATCTGATGAGC	*FERMT2*	15	PH	0.496718402
GUIDES_sg055	GGAGTTCATCCTCAACAATG	*FMNL2*	23	FH2	0.656016612
GUIDES_sg056	TTCACAAACCGGACAAAGAC	*FMNL2*	24	FH2	0.52306371
GUIDES_sg057	TGTGTACACACTACAGCTGG	*FNDC3B*	31	fn3	0.726749897
GUIDES_sg058	GCTCTTCCCAGTTCAGTACA	*FNDC3B*	30	fn3	0.69274705
GUIDES_sg059	GCTGAGCAACAAGACAGAGG	*GAS7*	19	-	0.715444147
GUIDES_sg060	GCTTGCGAAGGTCGGCAATG	*GAS7*	18	-	0.692490099
GUIDES_sg061	GCCCACACTCTCCAAGCACA	*GNB1L*	3	-	0.656080017

sgRNA_name	Sequence	Gene	Exon	Protein domain targeted	Predicted On-target efficiency
GUIDES_sg062	GCAGGCTCCAGATGTGTACC	*GNB1L*	2	WD40	0.572759585
GUIDES_sg063	TGAACAGAGAGACTTCTGAG	*KALRN*	59	PH	0.713929927
GUIDES_sg064	CTTCCTGAGATACAGTGAGA	*KALRN*	56	RhoGEF	0.590046749
GUIDES_sg065	TGATTACTGGAAGTACGGGG	*KREMEN1*	5	WSC	0.732200895
GUIDES_sg066	TTACTGGTGCCAGTTAGAGG	*KREMEN1*	4	WSC	0.660612633
GUIDES_sg067	CAGGGACTCGATGATCATGG	*LMO7*	34	LIM	0.767439497
GUIDES_sg068	GATCCTGACTTCAGCTCCTG	*LMO7*	35	LIM	0.666458078
GUIDES_sg069	CTTCGACGAGACCTCGAAGG	*LMX1B*	4	Homeobox	0.713403988
GUIDES_sg070	GTGCAAGGGTGACTACGAGA	*LMX1B*	3	LIM	0.675803927
GUIDES_sg071	ACGTCTCGGATGGTGCTGAG	*ME3*	18	Malic_M	0.711900963
GUIDES_sg072	AGAGAAAGAAGGTGTACCGA	*ME3*	14	Malic_M	0.683948993
GUIDES_sg073	TAGTACTTCCCATGTGCCAG	*MECOM*	24	-	0.69054325
GUIDES_sg074	ACTGTGGCAAGATTTTTCCA	*MECOM*	20	zf-C2H2	0.638498746
GUIDES_sg075	GGACTTCTGCTCAAAGAGGG	*MYOF*	56	-	0.689398449
GUIDES_sg076	TGCATGGGTTGGTGAACCAG	*MYOF*	58	-	0.68114604
GUIDES_sg077	AAAGGTACTCTGAAACATGG	*PARD3B*	24	-	0.748915706
GUIDES_sg078	TGGTCTCTTTCTGGAGACAG	*PARD3B*	25	-	0.687131379
GUIDES_sg079	TCTGGGAGATGAGCAAGCAG	*PDE7B*	11	PDEase_I	0.63710316
GUIDES_sg080	TCTTTCTGTTGATTACAAAG	*PDE7B*	12	PDEase_I	0.626787508
GUIDES_sg081	CGTGAGACTCCAGTCACAGG	*PKHD1*	20	-	0.721146822
GUIDES_sg082	ATGGGATAGCCCCAAGCAGG	*PKHD1*	16	-	0.648027027
GUIDES_sg083	TACTCAGGGGATCACCAGCG	*PLEKHA7*	28	-	0.733493753
GUIDES_sg084	CCCCGAACTCTACAGCCCAG	*PLEKHA7*	25	-	0.727012157
GUIDES_sg085	GCTGCCCACTGCATACACGA	*PRSS23*	3	Trypsin	0.707785666
GUIDES_sg086	AACATCAGTGAAGTTATCCA	*PRSS23*	3	Trypsin	0.589826381
GUIDES_sg087	CAGTGGTGTCGGGAACACCG	*PTPRJ*	26	Y_phosphatase	0.752294442
GUIDES_sg088	GTTCGGTAAAGGTCCTTGTG	*PTPRJ*	24	Y_phosphatase	0.742428198
GUIDES_sg089	TGGCAAAAAGGTTTCCATCG	*RALGPS1*	25	PH	0.63983389
GUIDES_sg090	CGAAAGAAGATAATTACAAG	*RALGPS1*	11	RasGEF	0.632295378
GUIDES_sg091	AGAGGTACCAGATGGGACTG	*RUNX2*	5	Runt	0.707376125
GUIDES_sg092	CATGGCGGAAGCATTCTGGA	*RUNX2*	11	RunxI	0.681198759
GUIDES_sg093	TGGAATTCCCTACCACAGCG	*SPTBN1*	36	PH	0.712246448

sgRNA_name	Sequence	Gene	Exon	Protein domain targeted	Predicted On-target efficiency
GUIDES_sg094	TCAGTCTTAACCATTCCCAT	*SPTBN1*	31	Spectrin	0.683179693
GUIDES_sg095	GGGCTGGCTATGATAAACTG	*TES*	6	LIM	0.774116567
GUIDES_sg096	CCATGAGTTGTCTCCCAGAG	*TES*	5	PET	0.735126362
GUIDES_sg097	GAAGCTTCCGAGAGTCTCTG	*TIMP3*	3	TIMP	0.703685264
GUIDES_sg098	CTATGATGGCAAGATGTACA	*TIMP3*	4	TIMP	0.591387438
GUIDES_sg099	AGTCCTTGGATGTAAGAAAG	*TMCO1*	9	DUF841	0.652850785
GUIDES_sg100	GAAACAATAACAGAGTCAGC	*TMCO1*	5	DUF841	0.622258097
GUIDES_sg101	AGAGACTTTGAAGTGAACGA	*TNS1*	42	PTB	0.715095311
GUIDES_sg102	CAGAAGGTGACAGTGTTGAG	*TNS1*	43	PTB	0.675343539
GUIDES_sg103	GCCGACTGGTGACCTCATGG	*TRIOBP*	3	-	0.713915639
GUIDES_sg104	GGGAGCAGGAGGCAGGAACG	*TRIOBP*	4	-	0.656603289
GUIDES_sg105	TAAACCACTGGAGTTCACGG	*TXNRD2*	20	Pyr_redox_dim	0.785275668
GUIDES_sg106	TCATCATTGCTACTGGAGGG	*TXNRD2*	8	Pyr_redox_2	0.706088692
GUIDES_sg107	GGTGAAGCTCCTGATTGCAG	*ZNF280D*	27	-	0.700021186
GUIDES_sg108	GAAGAAAGTAAAAGAAGTTG	*ZNF280D*	15	-	0.599965492
GUIDES_sg109	ATGGAGTTCCGCGACCACGT	*ABO*	7	CDS	0.6563
GUIDES_sg110	CCGGTCCCCAGCGTCACGCG	*ABO*	7	CDS	0.6687
GUIDES_sg111	CCACCTGGTACATCGCCTCA	*TEX41*	2	TRANSCRIPT	0.6631
GUIDES_sg112	AACTCAAGACATTGGAACCA	*TEX41*	5	TRANSCRIPT	0.6251
GUIDES_sg113	AATGTGGTAGCCCAAGACAG	*CYP1B1*	5	p450	0.775320729
GUIDES_sg114	GTGGCCACTGATCGGAAACG	*CYP1B1*	3	p450	0.726256031
GUIDES_sg115	GCAAGCCATGAGCCTGTACG	*FOXC1*	1	-	0.747984594
GUIDES_sg116	TCGTCGTCCCTGAGTCACGG	*FOXC1*	1	-	0.730741126
GUIDES_sg117	GATTGTGGTGAACTTCCGTG	*GMDS*	8	Epimerase	0.727535334
GUIDES_sg118	GTTGCAGAATGATGAGCCGG	*GMDS*	10	Epimerase	0.65599947
GUIDES_sg119	CCTCCCGCACGCGCACACAG	*LTBP2*	35	EGF	0.755863507
GUIDES_sg120	CAGGCAGACATAACCAGGCA	*LTBP2*	31	EGF_CA	0.708717
GUIDES_sg121	GGTCATACTCAAAAACCTGG	*MYOC*	3	OLF	0.763937898
GUIDES_sg122	ATGCCAGTATACCTTCAGTG	*MYOC*	1	-	0.722928246
GUIDES_sg123	TCTTGCGAAGGAAGTCCAGA	*TEK*	17	Pkinase	0.627785812
GUIDES_sg124	ATCTAATGAGACAATGCTGG	*TEK*	22	Pkinase	0.626682424

sgRNA_name	Sequence	Gene	Exon	Protein domain targeted	Predicted On-target efficiency
NonTargeting_Human_0001	ACGGAGGCTAAGCGTCGCAA	-	-	-	-
NonTargeting_Human_0002	CGCTTCCGCGGCCCGTTCAA	-	-	-	-
NonTargeting_Human_0003	ATCGTTTCCGCTTAACGGCG	-	-	-	-
NonTargeting_Human_0004	GTAGGCGCGCCGCTCTCTAC	-	-	-	-
NonTargeting_Human_0005	CCATATCGGGGCGAGACATG	-	-	-	-
NonTargeting_Human_0006	TACTAACGCCGCTCCTACAG	-	-	-	-
NonTargeting_Human_0007	TGAGGATCATGTCGAGCGCC	-	-	-	-
NonTargeting_Human_0008	GGGCCCGCATAGGATATCGC	-	-	-	-
NonTargeting_Human_0009	TAGACAACCGCGGAGAATGC	-	-	-	-
NonTargeting_Human_0010	ACGGGCGGCTATCGCTGACT	-	-	-	-

3.4.3 Lentivirus preparation

The plasmids containing the 134 sgRNAs were transformed into E. coli bacteria and stored in glycerol stocks by Dr. Sandy Hung. To harvest enough plasmids, the E. coli bacteria were streaked out on LB agar plates with 1% ampicillin and incubated at 37°C for 24 hours. A single colony was picked into 2-YT broth (Invitrogen, 22712-220) and incubated at 30°C for 16 hours. The plasmids were harvested using Wizard Plus SV Minipreps DNA Purification Systems (Promega, A1460) following manufacturer instructions, the plasmid DNA was eluted in 30 µl of nuclease-free water and the DNA concentration was measured by Nanodrop 1000 (Thermo Scientific). To prepare the lentiviruses, the plasmids were then transfected into HEK 293FT cells. For each gene knockout cell line, the plasmids of the two sgRNA were combined (5 µg each), together with 10 µg pCMV Δ8.91, and 1 µg pMD2.G in 2.5 ml

Opti-mem (Gibco, 31985088), then combined with another 2.5 ml Opti-mem containing 30 µl Lipofectamine 2000 (Invitrogen, 10000230649). The 5ml transfection mixture was incubated at room temperature for 10-20 minutes before being added to 8*10^6 HEK 293FT cells in a 10cm tissue culture treated petri dish. The cells were incubated at 37°C for 5 hours, then the medium was replaced with 8ml of culture medium and incubated at 37°C for 48 hours. The supernatant was collected and filtered through a 45 µm filter (Merck, SLHV033RS), 5X PEG-IT (System Biosciences, LV825A-1) was added to concentrate the virus and the solution was stored at 4°C for 48 hours. Subsequently, the virus suspension was centrifuged at 1500 x g for 30 minutes and the supernatant was removed. Each virus pellet was resuspended in 1 ml Opti-mem and stored in -80°C.

3.4.4 Lentivirus transduction and puromycin selection in TMCs

TMCs were first expanded in T-75 flasks and then seeded in to tissue culture treated 24 well plates (Table 3), 3.0*10^4 cells per well. The following day, 50 µl of lentivirus was added to the 0.5ml culture medium containing Lentiblast (OZ Bioscience, LB01500, Concentration: LentiblastA: 1:100, LentiblastB: 1:100) and the cells were incubated at 37°C for 72 hours. Cells were then cultured in medium containing 1 µg/ml puromycin (Gibco, A11138-03) for four days, changing the medium after two days, after which the no lentivirus control cells had all died. The cells were then allowed to recover in regular culture medium for one week, with medium changes every two days. The virus transduction was performed as triplicates on different days.

3.5 Cell Painting Assay

3.5.1 Cell seeding with FACS

For each group, 4.0*10^3 puromycin-selected TMCs were seeded to 96-well plates (Falcon, FAL353219) by fluorescence activated cell sorting (FACS) supported by Dr. Terry Pinfold at the Menzies Institute for Medical Research. Each group was split into triplicates in the 96-well plate randomly. The culture medium was changed the next day. The whole experiment was performed in three batches of TMCs, thus, 9 wells of cells were captured for each gene knockout group. The plate layout (the metadata) can be assessed on github: https://github.com/PeterLu0403/CROP_seq_Cellpainting/tree/master/metadata

3.5.2 Staining and fixation

TMCs were stained and fixed 48 hours after FACS. Previously described Cell Painting Protocol [110,111] was followed, and the concentration of each stain was manually confirmed on a pilot plate (Table 6, Fig. 7). Firstly, TMCs were incubated in culture medium containing 500 nM Mitotracker (Invitrogen, M22436) and 30 µg/mL Wheat Germ Agglutinin (WGA) Alexa594 conjugate (Invitrogen, W11262) for 30 minutes at 37°C. Then TMCs were fixed with 4% paraformaldehyde at room temperature for 20 minutes and washed with 150 µl of HBSS (Gibco, 14025134). Next, TMCs were permeabilized with 0.1% solution of Triton X-100 (Sigma, T8787) for 20 minutes and washed with 150 µl HBSS twice. Lastly, TMCs were incubated with HBSS staining solution containing 1% BSA (Merck, A8806), 50 µg/ml ConcanavalinA (Invitrogen, C11252), 3 µM Syto14 (Invitrogen, S7576), 5 µg/ml Hoechst (Invitrogen, H3570), and 1 unit/ml Phalloidin (Invitrogen, A12381) for 30 minutes at room temperature. TMCs were washed three times with HBSS without final aspiration and then sealed with parafilm. All 96-well plates were kept at 4°C in the dark before imaging.

Table 6: *Cell painting components*

Dye	Organelle or cellular component	Channel name
Hoechst 33342	Nucleus	DNA
Concanavalin A	Endoplasmic reticulum	ER
Syto 14	Nucleoli, cytoplasmic RNA	RNA
Phalloidin, Wheat germ agglutinin	F-actin, Golgi, plasma membrane	AGP
MitoTracker	Mitochondria	Mito

Figure 7: *Single staining for each of the dyes and combined. Scale bar: 20 µm*

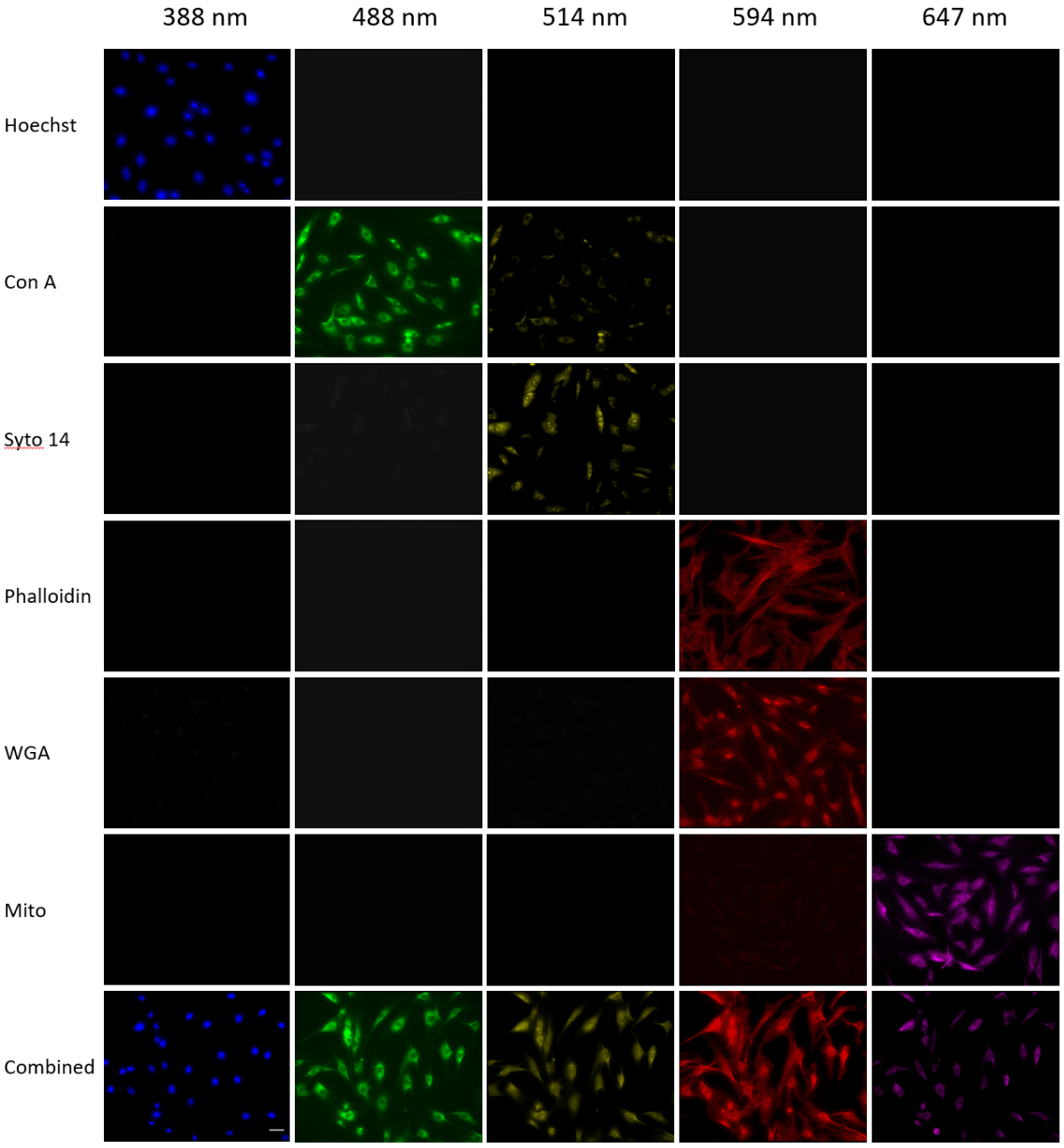

3.5.3 Automated Image acquisition

Images were captured at 20X magnification in Phase Gradient Contrast (PGC), and 5 fluorescent channels, DAPI (385/465 nm), AF488(470/517 nm), AF514 (511/543 nm), AF594 (590/618 nm), AF647 (625/668 nm) on ZEISS Celldiscoverer 7 system. In each well, 25 sites were imaged, with autofocus in the DAPI channel as the reference. Raw output files

were generated in "*czi*" format, and were processed using *Split Scenes* and *Image Export* with Zen Blue (Version 3.0). In *Image Export*, exporting file format as *TIFF*, ticking the modules of *Convert to 8 bit*, *Original Data and Shift Pixel*, *Use channel names* and *Use Full Set of Dimensions*.

3.5.4 Morphological image feature extraction

Version 3.1.9 of CellProfiler was used to locate and segment the cells for single-cell feature extraction. The pipelines in CellProfiler were set up to correct uneven illumination, flag aberrant images and identify the nuclei from DAPI channel and the entire cell from AF594 channel (Fig. 8), then measure the features of the size, shape, texture, intensity, and the local density of the nuclei, cell and cytoplasm.

Figure 8: *Identifying primary objects and secondary objects in Cellprofiler. Scale bar: 20 µm*

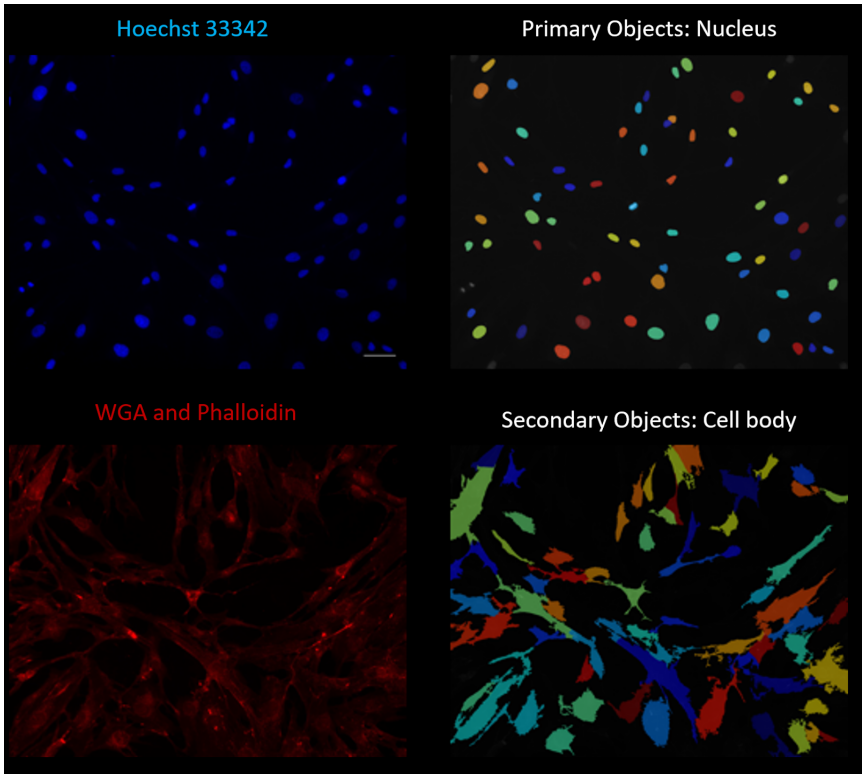

3.5.4.1 Establishing the CellProfiler pipeline

The pipelines consist of three parts: illumination correction, quality control and image analysis, and they are created for each batch of hTMCs (https://github.com/PeterLu0403/CROP_seq_Cellpainting/upload/master/Pipelines). These pipelines can be dragged to the panel of the CellProfiler directly, same as the images to be analyzed. The metadata should be extracted from the image name using regular expression. E.g. *hTMC_B1_Plate2-Scene-0001-P1-B03-Image Export-01_AF488_ORG.tif*: *(?P<Cell>.*)_(?P<Plate>.*)-Scene-(?P<Scene>[0-9]{4})-P(?P<Position>[0-9]*)-(?P<Well>.{3})-(?P<general>.*)_(?P<Channeln>.*)_ORG.tif*

Illumination correction pipeline is to improve fluorescence intensity measurement. For each fluorescent channel in each batch of images, the calculation was based on all images across cycles and then a *.npy file was generated which would be used in the other pipelines. Quality control pipeline is to identify and exclude aberrant images such as blurry images and debris, and a properties file would be generated. In CellProfiler Analyst (Version 2.2.1), the quality control features and corresponding thresholds were then selected for each batch of images. In the last pipeline of image analysis, blurry and saturated images were able to be removed by setting up the selected quality control features and thresholds in the modules of *MeasureImageQuality* and *FlagImages*. Uneven illumination was then corrected with the "npy" file. To identify the cell components, the nuclei was defined as the primary object, the cell body was defined as the secondary object, and the cytoplasm was defined as the tertiary object. Subsequently, the features of size, shape, granularity, colocalization, local density, and textures were measured, and the data was saved in the database of SQLite.

3.5.4.2 Configuration of CellProfiler pipelines on the Nectar Cloud

The first two pipelines of illumination correction and quality control were performed at a desktop workstation (CPU: Intel Xeon Gold 5122, RAM: 128 GB). The Nectar Cloud (The National eResearch Collaboration Tools and Resources project) was applied to process the analysis pipelines and in 8 instances, and the *c3xxlarge* flavor (32 virtual CPUs and 64 GB of RAM) was used. The image analysis outputs a set of SQLite files. The protocol describes how to set up virtual machines, install CellProfiler in Linux, and run a batch script and can be accessed on github (https://github.com/PeterLu0403/CROP_seq_Cellpainting/tree/master/NectarSetup).

3.5.4.3 Add metadata and merge all dataset

The software of R (Version 3.6.3) was used for data analysis. First, an R script was written to add metadata to each dataset, such as the knockout gene in each well. Then the datasets for each 96-well plates were all merged together into a csv file.

3.5.5 Data Preparation

The procedures of data preparation were done by R (Version 3.6.3) were described in Caicedo, et al. [131], which included feature transformation, normalization and batch-effect correction. Firstly, all the negative controls were selected to explore the distribution of the features and the batch effects. Two transformation methods were applied, generalized logarithmic function [132] and Box-Cox transformation [133]. To avoid nonpositive values, generalized logarithmic function used a shrinkage strategy while Box-Cox transformation used a shift strategy[131]. The Anderson-Darling test was performed to evaluate the normality of each feature[134]. Next, the value of each feature was normalized by subtracting the median value of each feature from the control group and dividing by the corresponding median absolute deviation (MAD) *1.4826 in each plate, respectively. The single-cell data was aggregated by the median value of each well to create profiles of each replicate. The Spearman's correlation was calculated for all replicates within a plate and across different plates. The replicates are selected with Spearman's correlation score > 0.2.

3.5.6 Data analysis

All gene knockout groups underwent hierarchical clustering and were plotted as a cluster tree. The optimal number of clusters was determined by the *silhouette* method. To annotate each of the clusters, the top features and tail features were extracted.

3.6 Single-cell RNA sequencing

3.6.1 Chromium Processing

The cells recovered in normal culture medium in 3.4.3 were taken to Garvan-Weizmann Centre for Cellular Genomics for single-cell RNA sequencing. Single-cell suspensions were prepared following the subculture procedure in 3.1.2. The cells from different wells were pooled, centrifuged and resuspended in DPBS containing 1% BSA (Sigma-Aldrich,

A8806-5G), and filtered by 37 μm strainer (STEMCELL, 27215). The estimated number of cells in each well in the Chromium chip was optimized to capture about 16,000 cells. The Chromium library was then generated following the protocol of the Chromium Single Cell 3' v2 Library (10X Genomics) by the technicians in Garvan Institute. Briefly, individual cells were allocated into nanoliter-scale Gel Bead-in-EMulsions, in which the bead carries the primers containing a read 1 primer sequence, a 16 nt 10x barcode, a 10 nt Unique Molecular Identifier, and a poly-dT primer sequence. A barcoded, full-length cDNA was produced from each poly-adenylated mRNA after incubation with the Gel Bead-in-EMulsions. Then all the cDNAs were pooled and amplified by PCR. In the library construction, P5, P7, a sample index, and read 2 primer sequences were added to each of the cDNA by End Repair, A-tailing, Adaptor Ligation, and PCR. The region of P5 and P7 allowed the library fragment to attach to the flow cell surface during the sequencing. Read 1 and read 2 sequences are standard Illumina sequencing primer sites used in paired-end sequencing. Then part of the library samples were sequenced on an Illumina NovaSeq 6000 system using the S4 flowcell with read depth of approximately 84000 reads per cell. The rest of the library samples after the NovaSeq procedure were used to amplify the sgRNA sequences for enriched MiSeq-based sequencing.

3.6.2 Computational analysis of single cell sequencing data

The first step of single cell RNA-seq mapping was performed by the service provider, Garvan-Weizmann Centre for Cellular Genomics. The library was mapped to the GRCH38 *Homo sapiens* genome, then the resulting mapped counts between all samples were depth-equalized via the *cellranger aggr* pipeline. Peter Tran performed the MiSeq-based sequencing, and Anne Senabouth from Garvan built up the repository for the processing and analysis of single-cell RNA-seq data (https://github.com/powellgenomicslab/CROP-seq). In the repository, our designed gRNAs are assigned to their respective cells.Then the scRNA-seq data was loaded into R via the Seurat package (Version 3.0), and SCTransform function was used to normalise the data. All cells targeted by sgRNAs were visualised in a uniform manifold approximation and projection (UMAP) plot and were clustered with the Louvain method. The differentially expressed genes (DEGs) of each gene knockout group were selected with log2 fold change > 2 compared to the human non targeting controls. Then a hierarchical clustering was performed on the subset of all DEGs of all gene knockout

groups. The optimal number of clusters was determined by the *silhouette* method. DEGs to the human non targeting controls were selected to present each cluster.

4. RESULTS: Characterization of human trabecular meshwork cells

4.1 Dexamethasone induced myocilin secretion assay in trabecular meshwork cells

The commercial TMCs were treated with different concentrations of dexamethasone (500 nM, 1 μM, 2 μM, and vehicle control) for 3 days (n = 3), after which RNA was extracted for RT-PCR, supernatant was collected for ELISA and cells underwent immunohistochemistry. In RT-PCR experiments, the expression of housekeeping genes was firstly assessed. Housekeeping genes were cellular maintenance genes which regulate basic cellular functions, and they would not change their expression levels across groups with different treatments. Therefore, housekeeping genes were involved in RT-PCR to act as internal controls for gene expression. The expression of four potential housekeeping genes was assessed and *EEF2* showed the most consistent expression in human primary TMCs, as demonstrated by the standard deviation in the fold change (*EEF2*, 0.41; *HPRT,* 0.42; *18sRNA*, 0.86 and *ACTB,* 0.91, Fig. 9A). Thus, *EEF2* was selected as the housekeeping gene. No *MYOC* RNA was detected in this commercial TMCs. In contrast, the expression of *MYOC* was upregulated (8 fold) under the treatment of dexamethasone (1 μM) in our human primary TMCs (Fig. 9B), and the extracellular concentration of myocilin measured by ELISA was also increased 1.015 ng/ml (Fig. 9C). Immunohistochemistry labelling demonstrated that the intensity of the myocilin in the dexamethasone treated primary TMCs (Fig. 9E) was stronger than the vehicle control TMCs (Fig. 9D). As a result, the primary TMCs were used in our next experiment rather than the commercial TMCs. The expression of *MYOC* following dexamethasone was assessed by immunocytochemistry in all CROP-seq knock-out lines. The mean intensity of myocilin for each cell was measured and normalized to mean intensity of the cell nuclei. For each gene knockout group, the normalized intensity of myocilin was slightly increased after the dexamethasone treatment (Fig. 10).

Figure 9: *Characterisation of TMCs: A) Assessment of housekeeping gene in human TMCs, expression level was normalized to each housekeeping gene without the dexamethasone treatment; B) Relative expression of MYOC with/without the treatment of dexamethasone normalized to EEF2; C) Secreted myocilin concentration by ELISA; D) Immunostaining of myocilin in primary TMCs without dexamethasone treatment; E) Immunostaining of myocilin in primary TMCs with dexamethasone treatment; F) Immunostaining of caveolin-1 in primary TMCs; G) Immunostaining of TIMP3 in primary TMCs. Scale bar: 20 µm.*

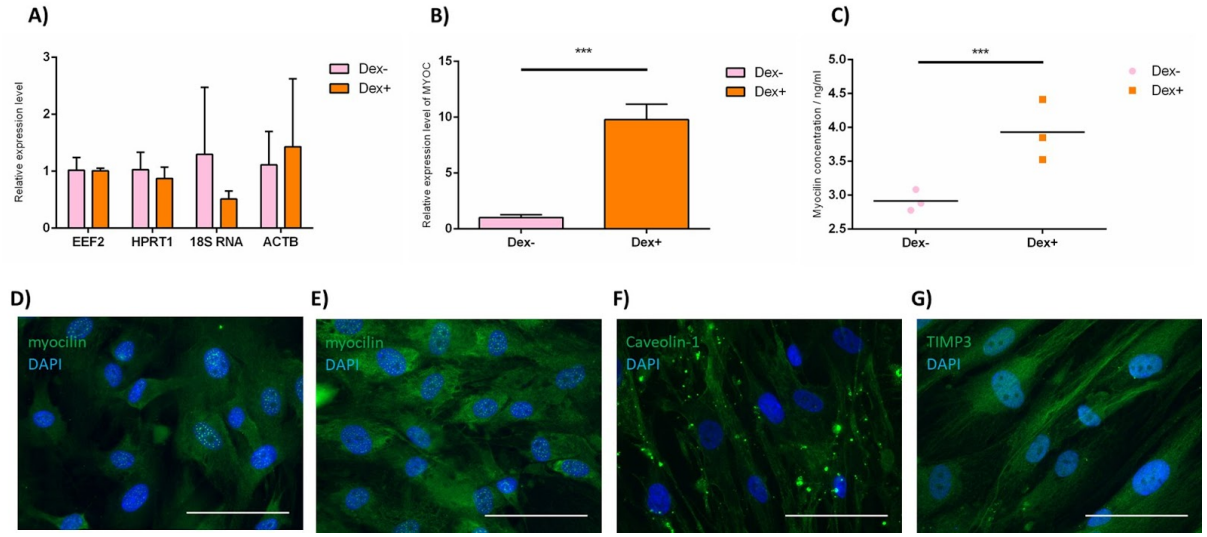

Figure 10: *Induction of MYOC expression across all cell lines following dexamethasone induction.*

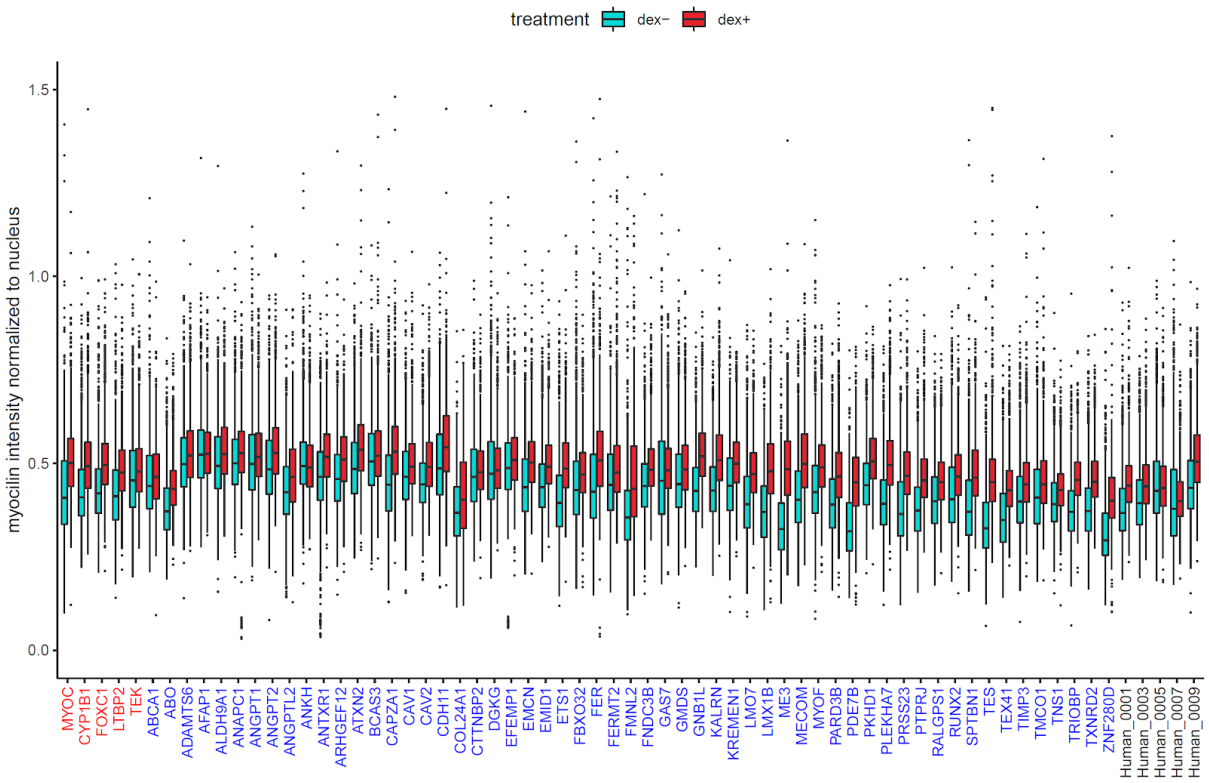

4.2 Evaluation of cell markers of trabecular meshwork cells

Primary human TMCs and human neonatal dermal fibroblast were assayed by qRT-PCR and immunocytochemistry for their expression of TMC markers. The expression of *AQP1, CHI3L1, LMX1B, MGP, MMP3, TIMP2, PITX2, FOXC1, FOXC2, PAWR* were all detected in TMCs, and their expression levels varied from TMCs to fibroblast. The expression levels of *AQP1, CHI3L1,* and *PAWR* did not show significant difference between TMCs and fibroblast (Fig. 11A, B, G). *LMX1B, MGP, PITX2, FOXC1* and *FOXC2* were expressed significantly higher in TMCs than those in fibroblast (Fig. 11C, D, G, H, I), while *MMP3* and *TIMP2* were expressed higher in fibroblast compared to TMCs (Fig. 11E, F).

Figure 11: *TMC markers in TMCs and human natal dermal fibroblast by qRT-PCR. A)-J): Relative expressions of AQP1, CHI3L1, LMX1B, MGP, MMP3, TIMP2, PITX2, FOXC1, FOXC2, and PAWR were normalized to EEF2.*

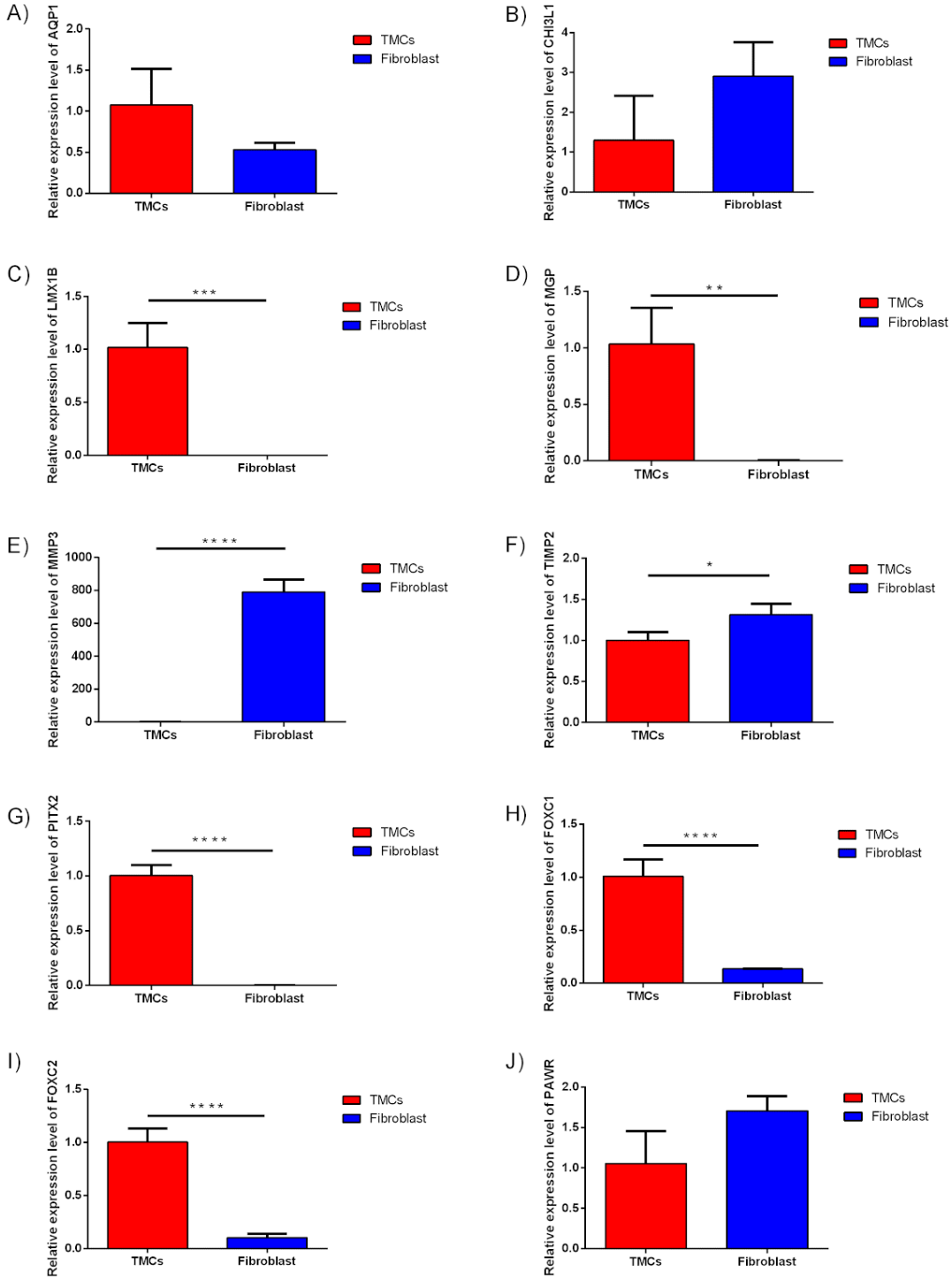

4.3 Phagocytic function in trabecular meshwork cells.

pHrodo bioparticles were used to measure phagocytosis activity in cell culture. The particles emit fluorescence when phagocytosed and transported to acidic subcellular structures. After 2 hours of incubation with the pHrodo red bioparticles at 37°C, our primary TMCs show phagocytic ability (Fig. 12A) that is stronger than the fibroblast (Fig. 12B), but weaker than the HEK and macrophages (Fig. 12C, D).

Figure 12: *Phagocytosis assay using pHrodo bioparticles (Red). A) TMCs, B) fibroblast , C) HEK 293A, D) Macrophage. Scale bar: 20 µm.*

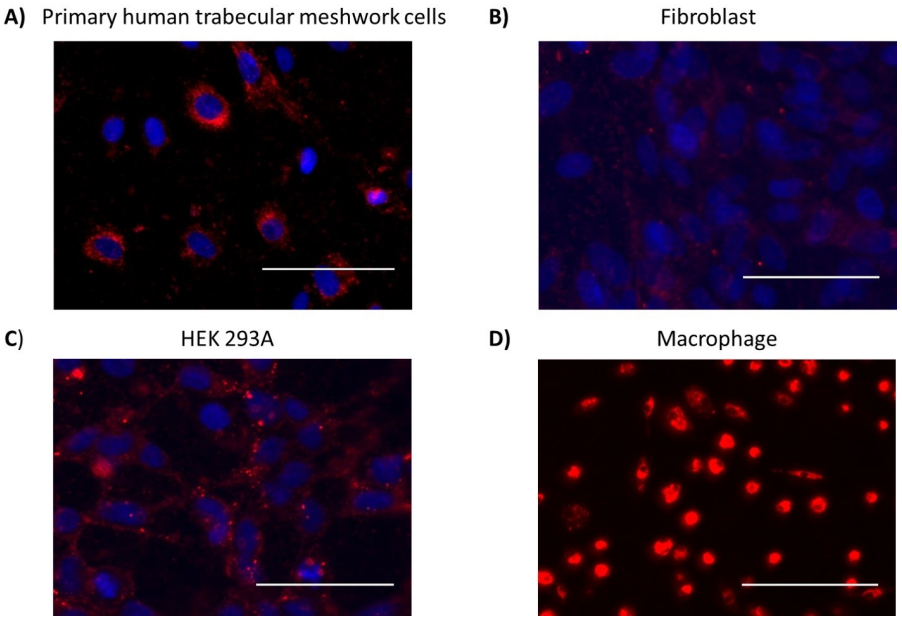

5. RESULTS: Differentiation of TMCs from mesenchymal cells

5.1 Effects of combination of retinoic acid (RA), transforming growth factor β-2 (TGF-β2), and bone morphogenetic protein 4 (BMP4) in dental pulp mesenchymal stem cells (DP-MSCs)

In previous work from the laboratory [135], DP-MSCs were treated with different combinations of RA, TGF-β2, and BMP4, and three treatment regimens were designed. T1: all growth factors were applied for five days; T2: TGF-β2 were applied for the first 2 days, then RA and BMP4 were applied for the last 3 days; T3: RA and BMP4 were applied for all 5 days, but TGF-β2 was only applied the first 2 days (Fig. 13). In the regimen of T1, the expression of *MYOC, MGP, FOXC1,* and *PAWR* were significantly increased with the treatment of 5 days, the expression of *PITX2* and *FOXC2* were also increased after 2 days treatment but not 5 days treatment. In the regimen of T2, only the expression of *PITX2* was increased after 2 days treatment but not 5 days treatment. In the regimen of T3, the expression of *PITX2* was also increased after 2 days treatment but not 5 days treatment, and the expression of *PAWR* was significantly increased for both 2 days treatment and 5 days treatment. Thus, the regimen of T1 is the most promising method of the differentiation from DP-MSCs to TM-like cells. With the treatment of all three growth factors for 5 days, TMC markers were assessed and functional assays were performed.

Figure 13: *Different combinations of RA, TGF-β2, and BMP4 alter the expression of TMC markers in DP-MSCs. A)-F): Relative expressions of MYOC, MGP, PITX2, FOXC1, FOXC2, and PAWR were normalized to EEF2, T1, T2, and T3 are different treatment regimens. T1: all growth factors were applied for five days; T2: TGF-β2 were applied for the first 2 days, then RA and BMP4 were applied for the last 3 days; T3: RA and BMP4 were applied for all 5 days, but TGF-β2 was only applied the first 2 days (adapted from McDonald, 2015 [135]).*

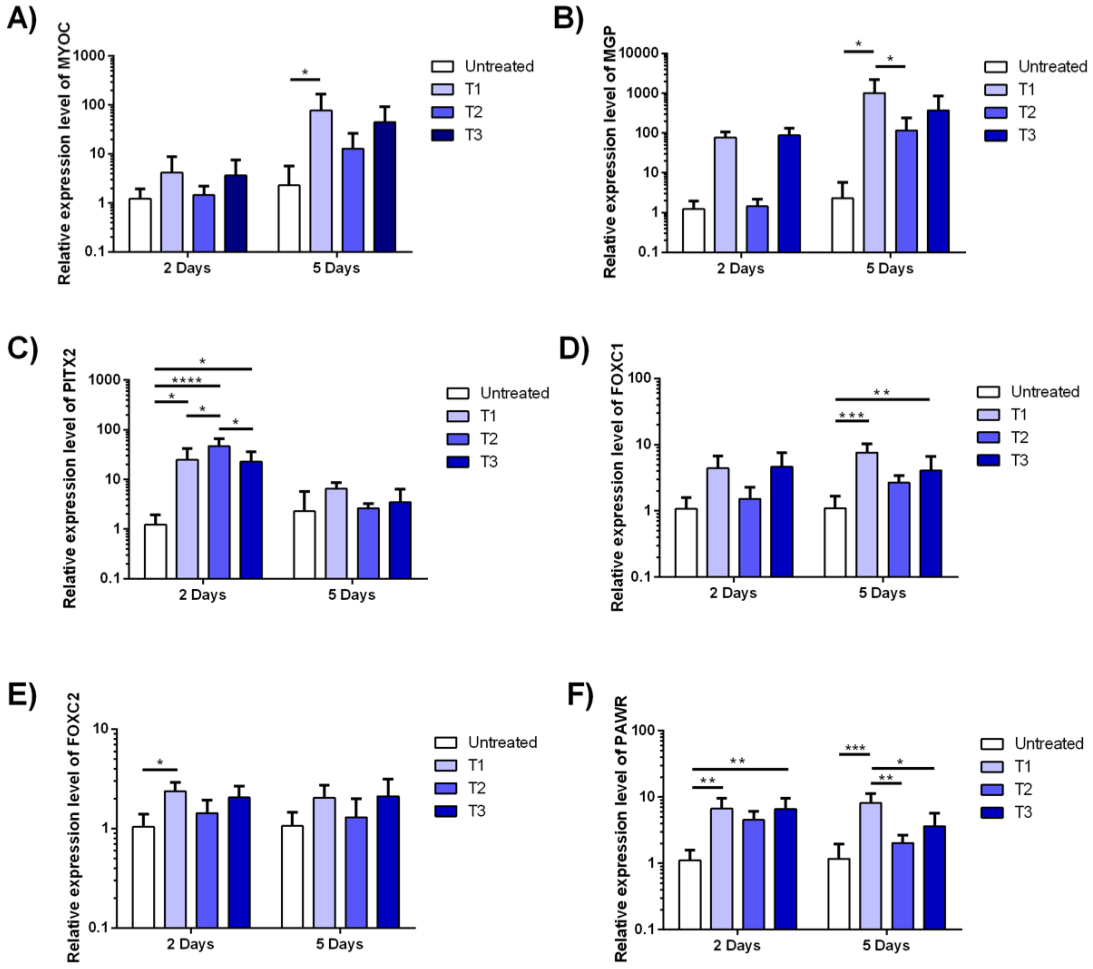

5.2 TM gene markers in DP-MSCs in response to RA, TGF-β2 and BMP4

This growth factors treatment experiment was performed three times for each group (N=3), and the expression of TMC gene markers was determined by qRT-PCR. The expression of *AQP1, CHI3L1,MGP* and *MMP3* showed no statistical difference between human TMCs and DP-MSCs with/without growth factors. The expression of *TIMP2* and *FOXC2* showed no difference between DP-MSCs with/without growth factors, but had lower expression in TMCs. The expression of *PAWR* was higher in DP-MSCs than TMCs, and increased further following treatment with growth factors. *LMX1B* was expressed in TMCs, but was not detectable in DP-MSCs with/without growth factors. The expression of *PITX2* was detected in TMCs, but was substantially lower in growth factor treated DP-MSCs, and was not detected in DP-MCSs without growth factors (Fig. 14).

Figure 14: *Trabecular meshwork cell markers in trabecular meshwork cells and dental pulp mesenchymal stem cells with or without the treatment of growth factors. A)-J): Relative expression of AQP1, CHI3L1, LMX1B, MGP, MMP3, TIMP2, PITX2, FOXC1, FOXC2, and PAWR were normalized to EEF2.*

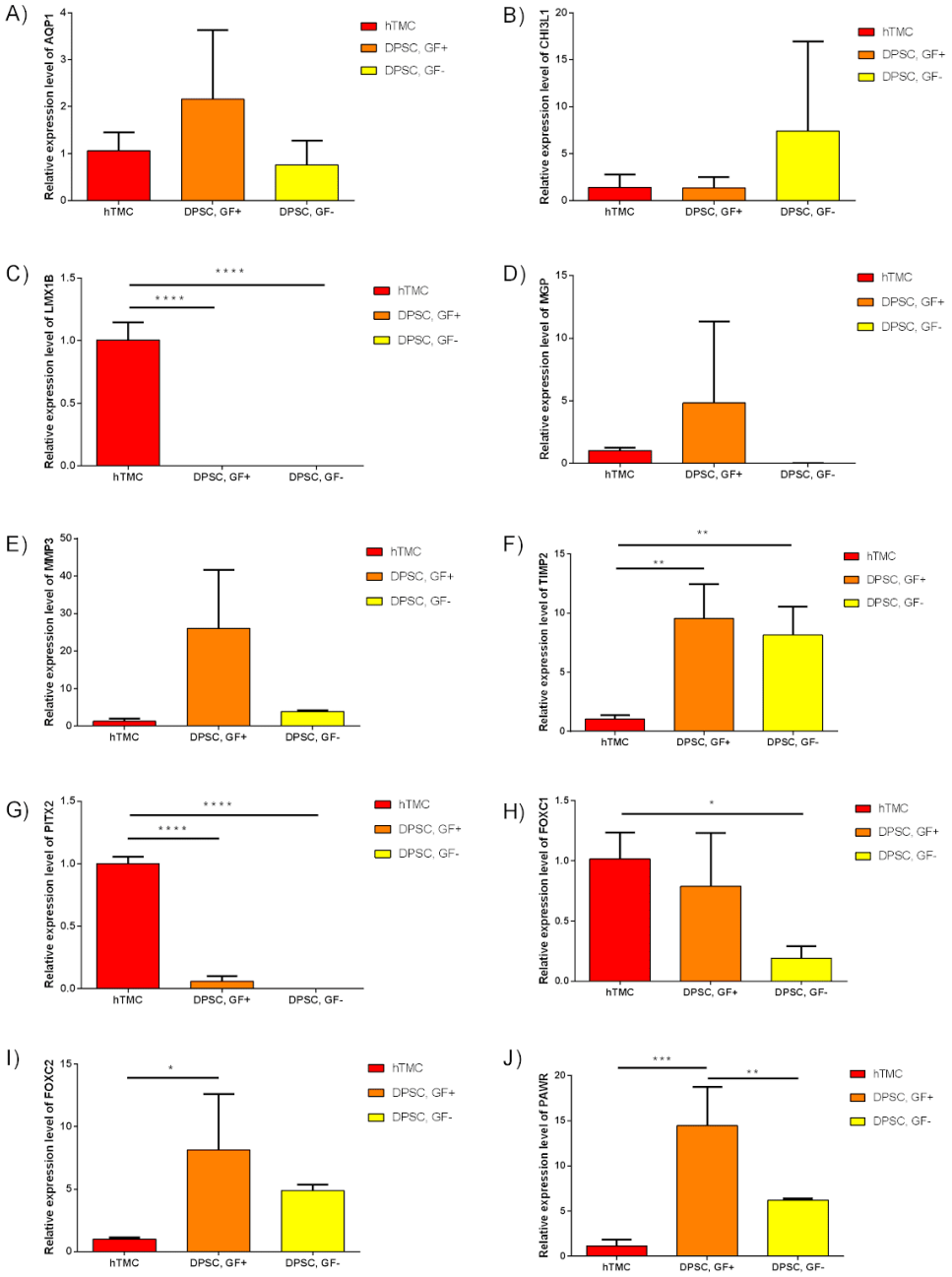

5.3 Expression of *MYOC* in response to dexamethasone in DP-MSC after the treatment with the combination of RA, TGF-β2, and BMP4.

As human primary TMCs showed a characteristic of upregulated expression of MYOC in response to dexamethasone, we applied this assay to DP-MSCs that had been treated with growth factors. In this experiment, after applying the established growth factor treatment, 1 μM dexamethasone or 0.1% ethanol is added for the last three days. The relative expression level of *MYOC* mRNA in the growth factors groups (GF+, DEX- and GF+, DEX+) was significantly higher (9 fold) compared to the concentration in groups not exposed to these growth factors (GF-, DEX- and GF-, DEX+) ($P < 0.001$). However, levels of *MYOC* mRNA did not show significant changes associated with dexamethasone treatment in the growth factor treated cells or the non-treated cells (Fig. 15A). The concentration of secreted myocilin was determined by ELISA and it showed a similar result. The concentration of *MYOC* protein in growth factors groups was significantly higher compared to the concentration in cells which were not exposed to the growth factors for both dexamethasone treated cells, which increased from 1.266±0.116 ng/ml to 2.657±0.235 ng/ml (p-value <0.001) and non-dexamethasone-treated groups, which increased from 1.332±0.071 ng/ml to 3.21±0.18 ng/ml (p-value <0.001). However, the secretion of myocilin in cells was not significantly affected by treatment with dexamethasone. (Fig. 15B).

Figure 15: *Dexamethasone induced myocilin secretion assay in DP-MSCs after the treatment of the combination of growth factors of RA, TGF-β2, and BMP4. A) Relative expression of MYOC with/without the treatment of dexamethasone normalized to EEF2; B) Secreted myocilin concentration by ELISA.*

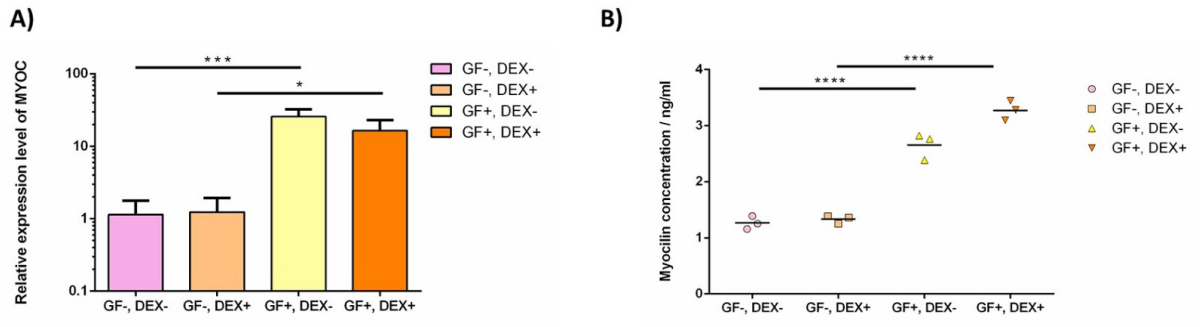

5.4 Contractile ability in TMCs and DP-MSCs

Primary human TMCs and growth factor treated DP-MSCs were tested for their ability to contract to the extracellular matrix. TMCs and fibroblast showed a great contractility to the collagen gel and this ability can be inhibited by Y-27632. The collagen gel area was decreased by 1.005±0.019 cm^2 and 1.007±0.074 cm^2 in the groups of TMCs and fibroblast, respectively, within 24 hours. While 10 μM Y-27632 was included, the change of the collagen gel area was shrunk to 0.231±0.219 cm^2 and 0.604±0.098 cm^2, respectively. However, there was no detectable contraction of the collagen gel area in the DP-MSCs with or without the treatment with the growth factors over the whole experimental time period of 72 hours (Fig. 16).

Figure 16: *Collagen gel contraction assay. A) Representative photographs of collagen gel cultures of DP-MSCs with/without growth factors, TMCs with/without 10μM Y-27632 and fibroblast with/without 10 μM Y-27632; B) The decrease in area of the collagen gel during culturing was calculated. Data are means ± SD of triplicate results.*

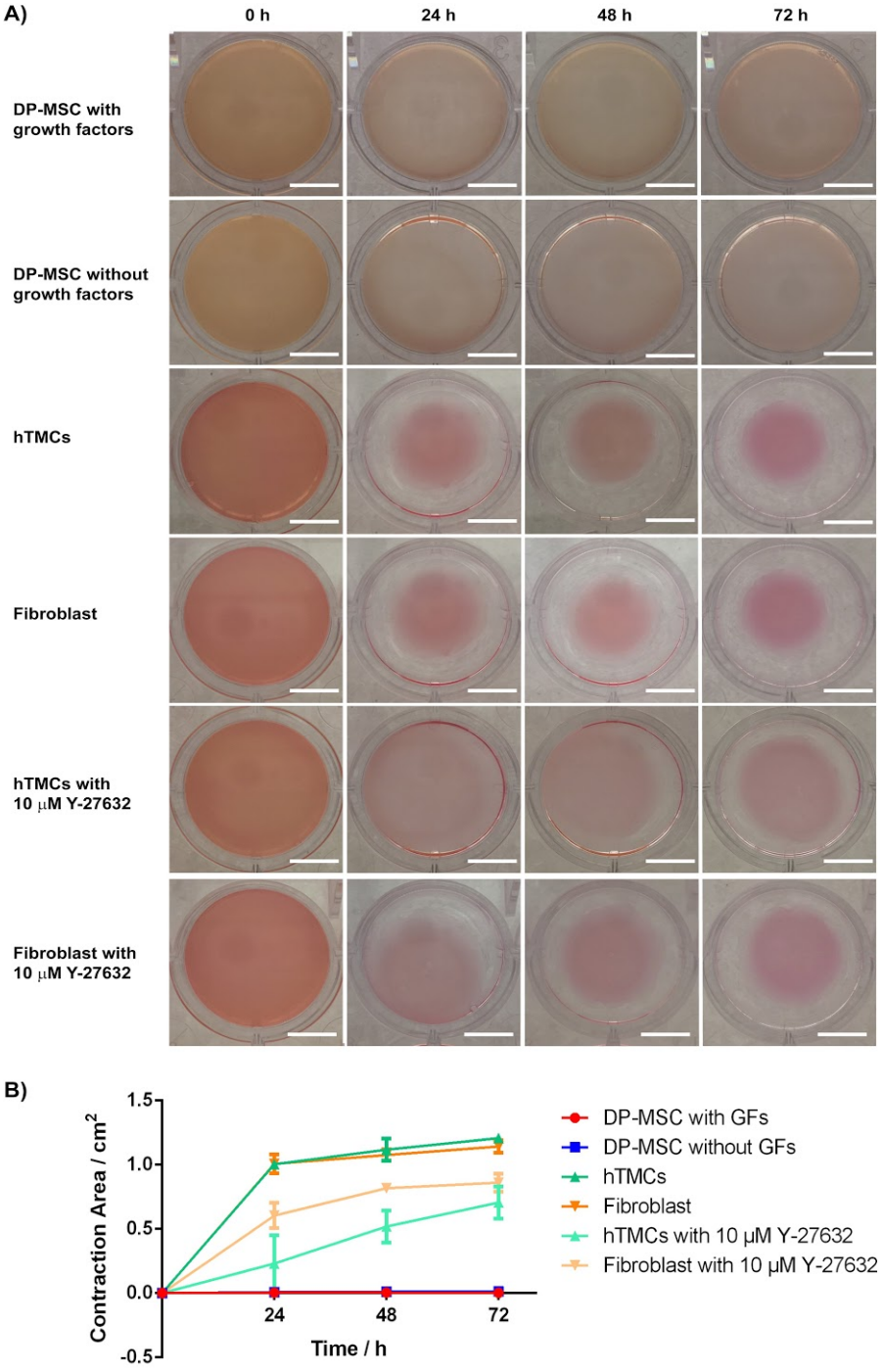

6. RESULTS: Structural and functional profiling in trabecular meshwork cells of genes putatively involved with variation in intraocular pressure.

6.1 Cell painting Assay for Crop-seq experiment in trabecular meshwork cells

In this assay, we aimed to create image profiles for each of the gene knockout and identify any distinct morphological groups. A total 210,243 individual cells were identified by the software of CellProfiler, together with 1053 morphological features (Appendix. List 1).

6.1.1 Feature transformation and normalization

The shape of the distribution varies across the features (Fig. 17). It is important to transform the feature values when approximately normally distributed data have centered mean value and comparable standard deviation value. Proper distribution of features enables us to extend the data from individual cells to the whole well. The algorithms of the generalized logarithm and Box-Cox transformation were applied to our non-targeting control groups. Anderson-Darling test was performed to compute ratios of deviation from normality. The lower the value of Anderson-Darling test, the more similar the distribution is to the normal distribution. The Box-Cox transformation shows a better effect compared to the generalized logarithm on the normality transformation (Fig. 18) and hence was used for next analysis. The procedure of normalization was introduced in the Method section 3.5.5.1.

Figure 17: *Diversity of feature distributions in morphological profiling. A)-F) Morphological features exhibit various types of distributions, including A) normal, B),C),E) skewed, D) uniform, F) discrete distribution. These histograms were obtained with feature value from our human non-targeting control cells (45,446 cells). The x axes show the feature values, and the y axes show frequencies (cell counts).*

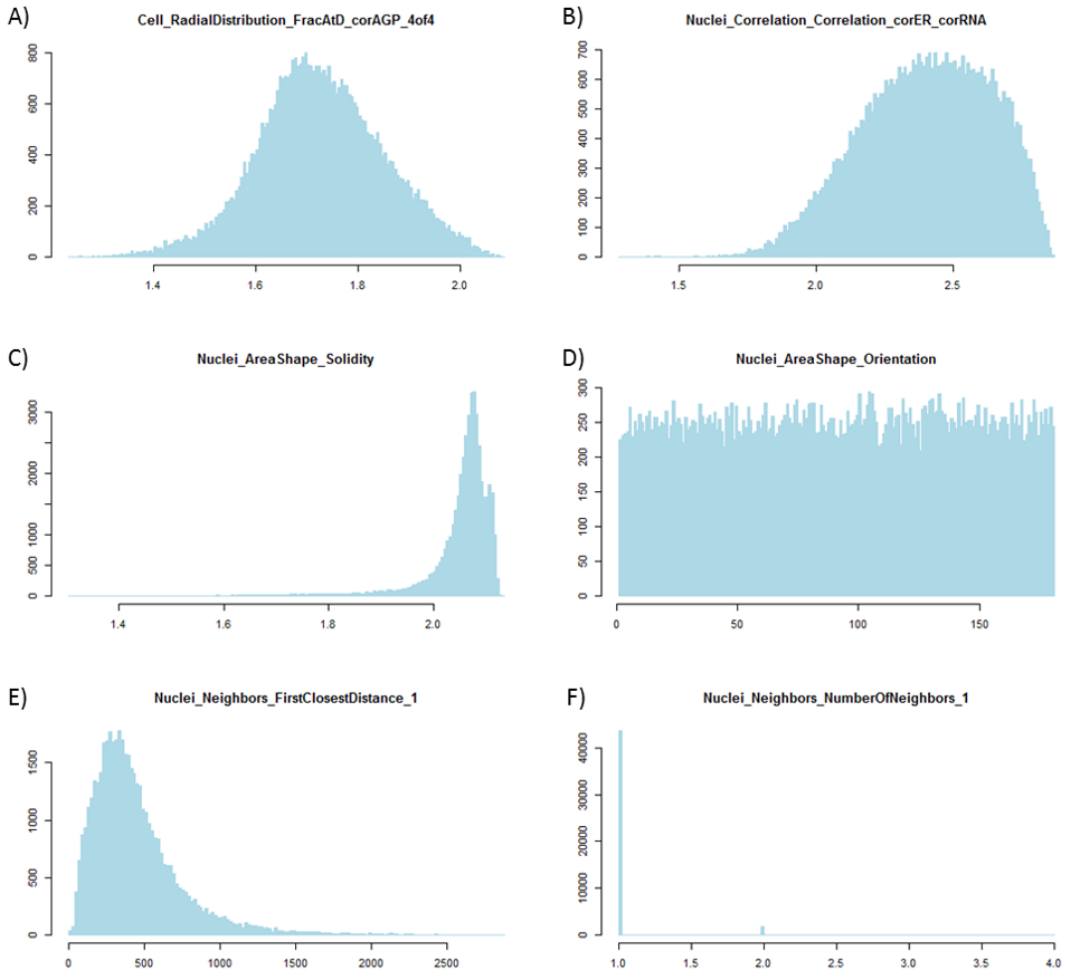

Figure 18: *Anderson−Darling normality test in the morphological profiles of control groups. The y axes show the statistic A value, the lower the value is, the closer to normality distribution of the feature, and the x axes are the features re ordered by the mean statistic A value of the three groups: raw data(Blue), generalized logarithm transformation(Green), and Box-Cox transformation(Red).*

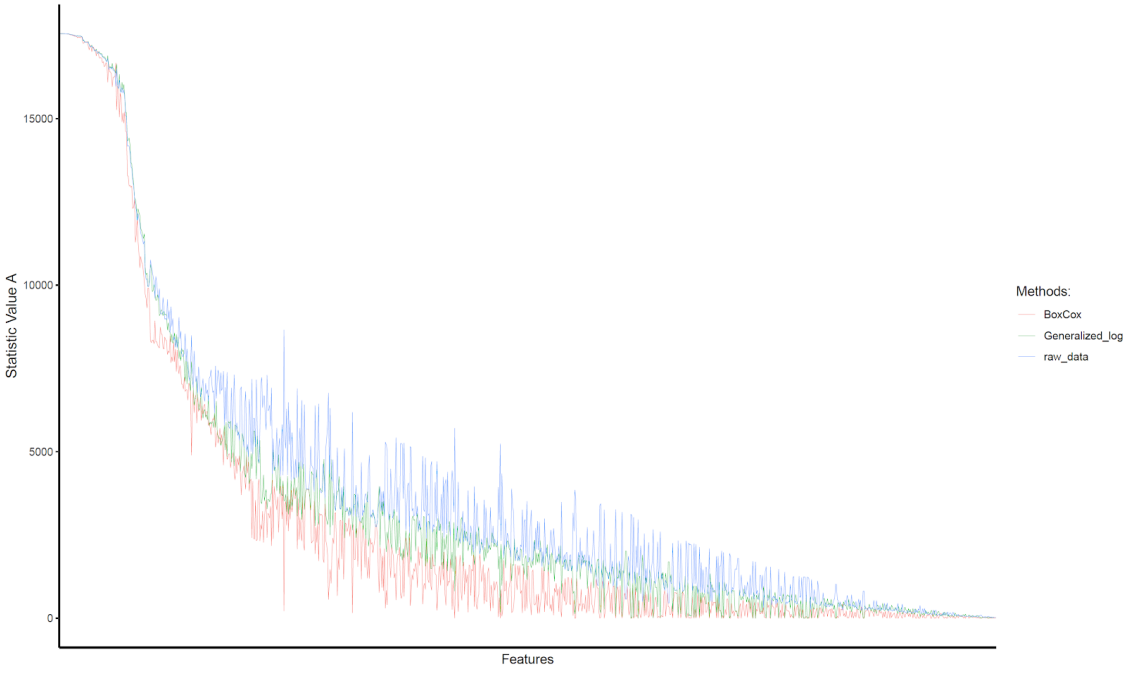

6.1.2 Investigation of well-well variation:

In the cell painting experiment, we set up three wells for each gene knockout group with triplicates in each plate, so each gene knockout group has nine wells total. To minimize the plate layout effect, we only used the inner wells of a 96-well plate, all groups including controls were randomly located across fifteen 96-well plates, and located in edge wells. In the gene knockout groups of *ANAPC1* and *LTBP2*, one batch of cells was lost during the puromycin selection, so only six wells of cells were seeded for these two groups. For the human non-targeting control group, we set up five different pairs of human non-targeting gene control groups which were seeded with triplicates in each plate, so our control group has 225 wells. In total, 777 wells were seeded and captured for 62 gene knockout groups and human non targeting groups.

Well profiles were created by aggregating the value of individual cells to the median value. For each of our gene knockout groups and human non targeting controls, the Spearman's rank

correlation coefficient was calculated between each pair of replicates. We initially checked how batch effects, which are subgroups of measurements that result from undesired technical variation such as instrument calibration, sample manipulation and changes in laboratory conditions, may be affecting our data. The batch effect varies across different groups (Fig. 19,). The groups such as *BCAS3, LMX1B, ME3* showed a strong batch effect and low correlation coefficient (Fig. 20_14, 39, 41) but other groups such as *CAPZA1, CAV2, ETS1* showed less batch effect (Fig. 20_15, 16, 26), also, our human non targeting controls also showed a low correlationship when involving all the control wells (Fig. 19, Fig. 20_63). To minimize the batch effects, we only selected the wells with a Spearman's rank correlation coefficient > 0.2, which was 397 wells out of 777 (Fig. 21). This procedure enables us to aggregate the data of each feature from individual cells to their corresponding groups.

Figure 19: *Spearman's rank correlation coefficient in each of the gene knockout group and human non targeting group. The x axes are the gene knockout groups and human non-targeting control groups. The y axes show the Spearman's rank correlation coefficient value between each pair of replicates in that group.*

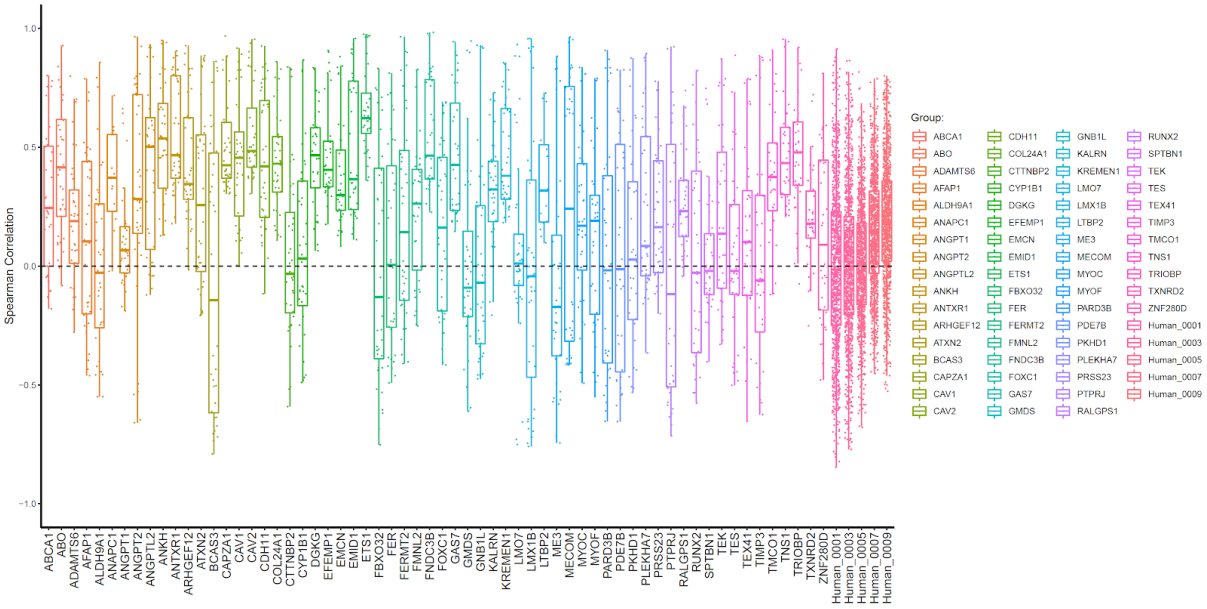

Figure 20: *Spearman's rank correlation coefficient matrix in each gene knockout group and human non targeting control group. The matrix shows the Spearman's value between each pair of replicates. The title of each matrix is the gene which is knockout in that group, the groups of ANAPC1 and LTBP2 have 6 wells and rest groups have 9 wells. The matrix of Spearman's value for non targeting controls has 225 wells.*

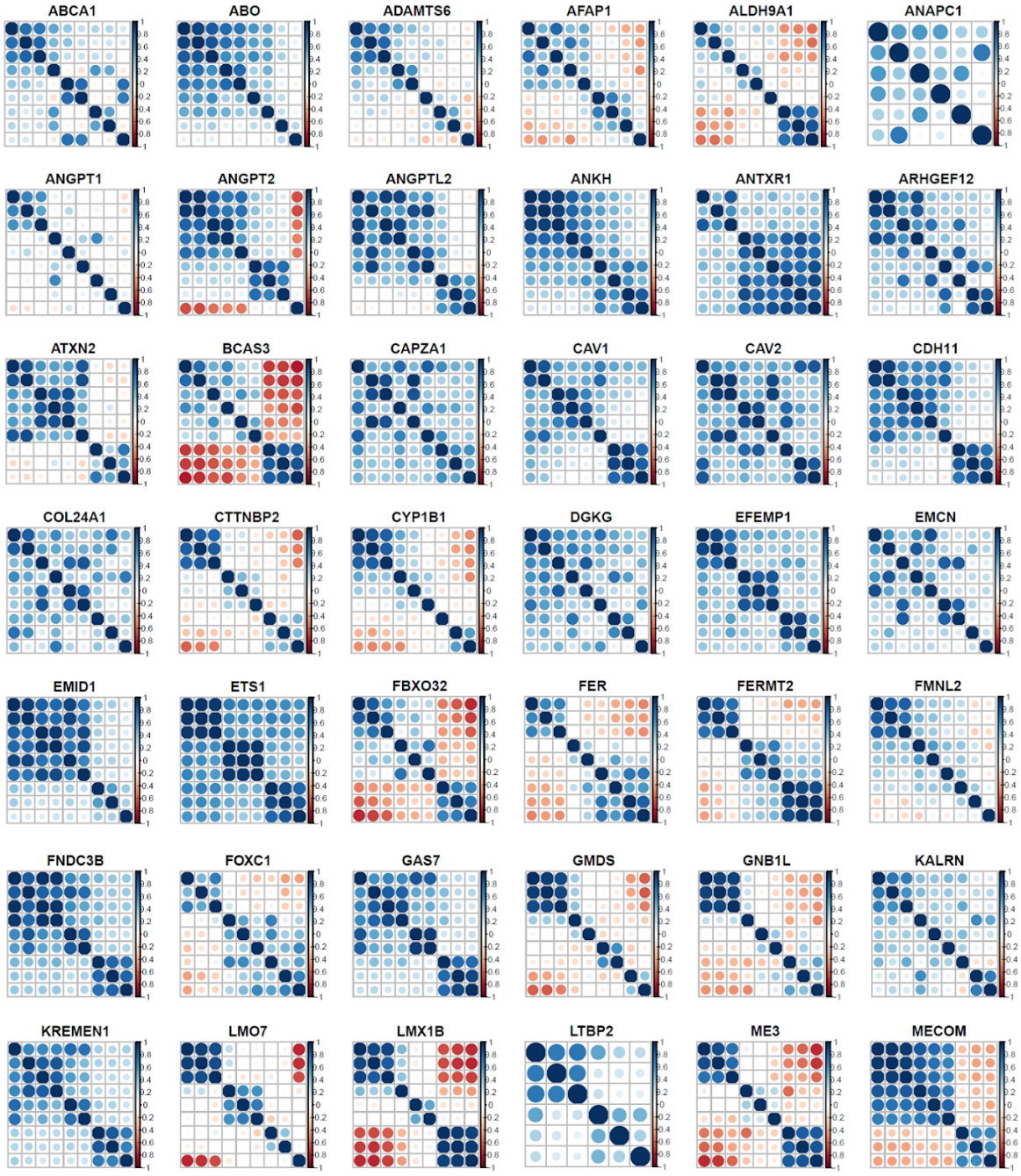

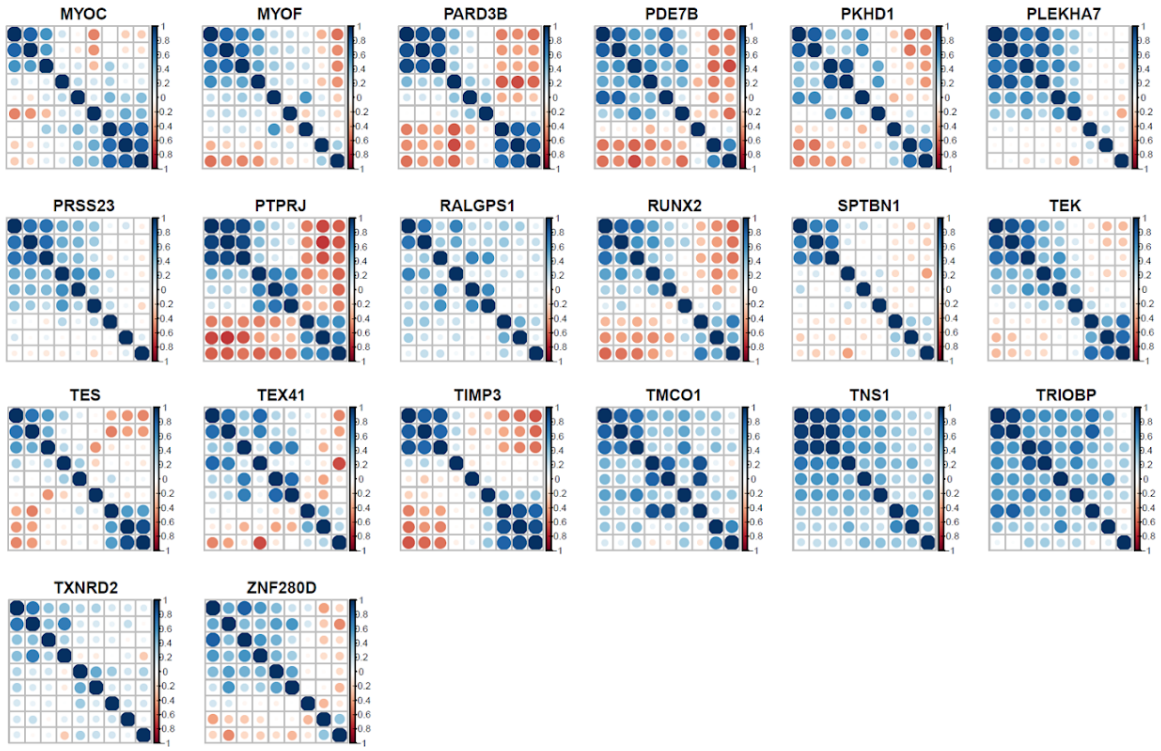

Human NonTargeting Controls

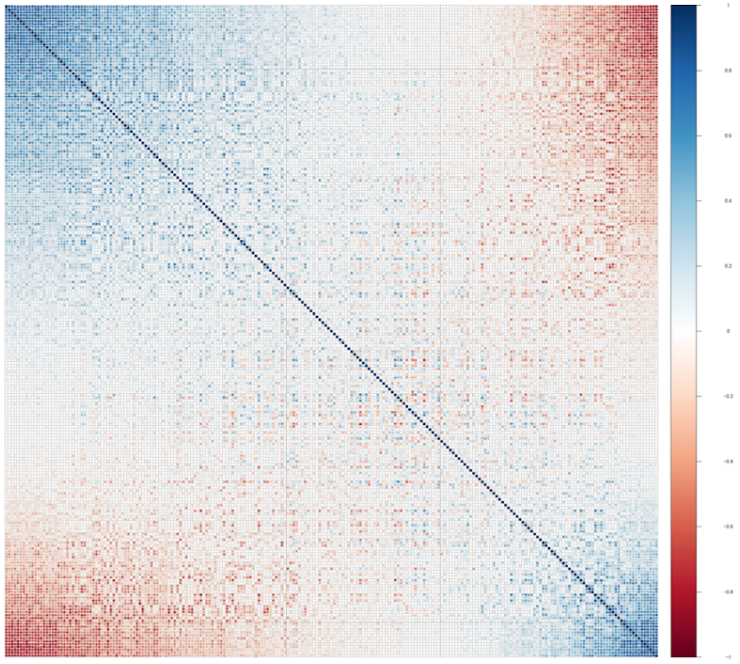

Figure 21: *Filter wells with Spearman's rank correlation coefficient > 0.2 for each gene knockout group and human non targeting control group.*

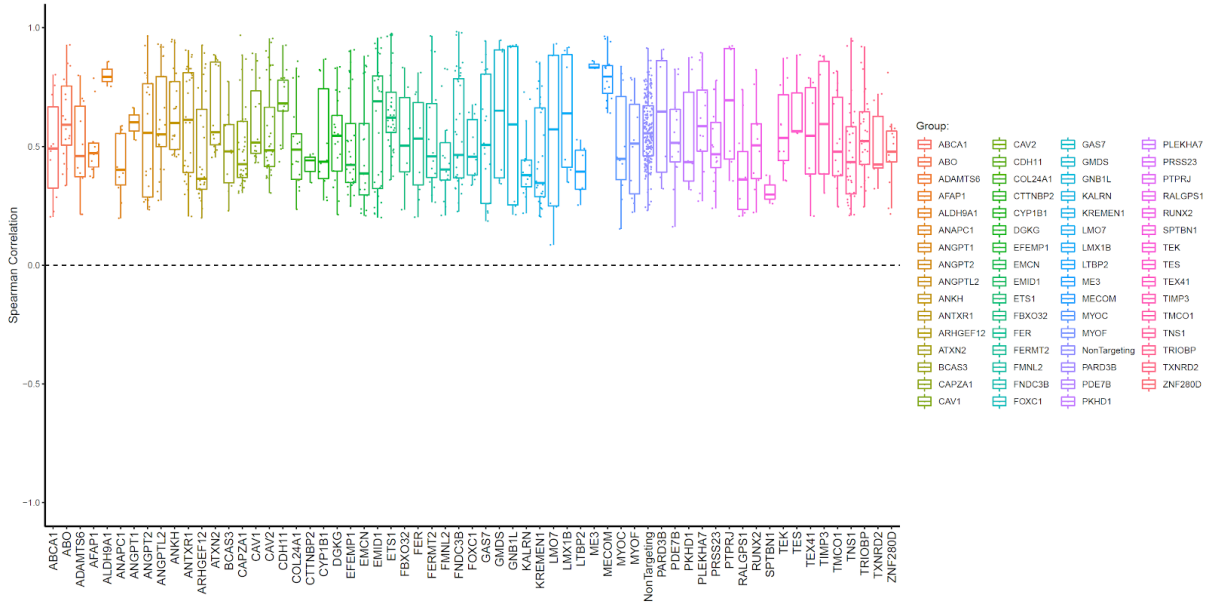

6.1.3 Feature selection

To reduce the redundancy of the features, the method of *correlation_threshold* was applied to the individual cell data. This method iteratively removed highly correlated features (*i.e.* those with a pearson value >0.9 compared the rest of the features). Finally, the profiles of each gene knockout group and human non-targeting control were created by aggregating the individual cell data to the median value and a data frame was generated with a dimension of 63 groups across 425 features (Fig. 22).

Figure 22: *Heatmap displaying the median value of each feature for each gene knockout group and human non targeting control group. The x axes are the groups, and the y axes are the 425 morphological features. The granularity features are zoomed in at the left panel.*

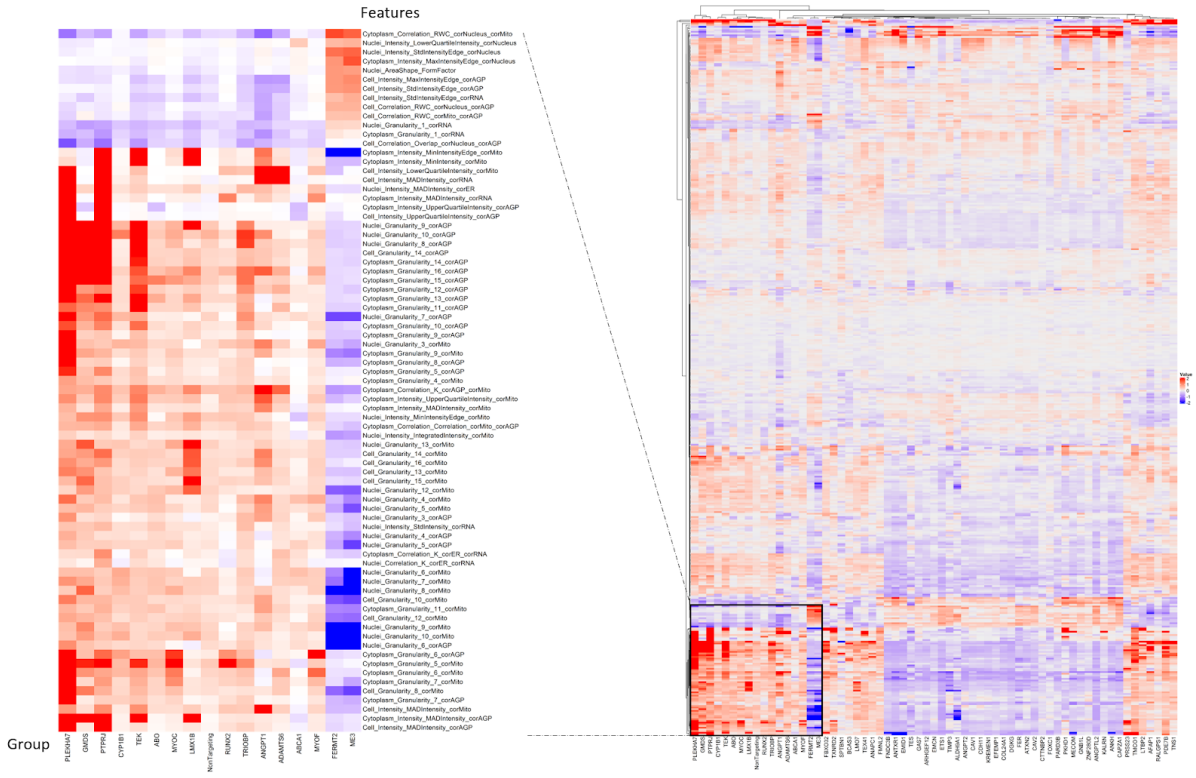

6.1.4 Morphological features-enriched hierarchical clustering

To determine how the morphological profiles of the knockout genes might be related to one another, we performed clustering analysis. The *euclidean* distance was computed between each pair of the groups (Fig. 23), and the hierarchical clustering method of *ward.D2* was applied to generate the cutree, where the distance between each group within one branch is closer than those located in different branches (Fig. 24). The gene knockout groups of *PLEKHA7, GMDS, PTPRJ* were clustered together with a morphological pattern of high granularity value features in the AGP channel, in which the phalloidin and WGA were used to stain the actin, golgi apparatus, and plasma membrane (Fig. 22, Fig. 25 A).

In the comparison between the genes at the overlapping loci, *CAV1, CAV2*, and *TES* at chromosome 7 showed a similar morphological pattern, as well as *EMID1* and *KREMEN1*,

GNB1L and *TXNRD2* at chromosome 22 (Fig. 22, Fig. 25 A). At chromosome 1, the *TMCO1* showed a more similar pattern to the non-targeting control groups than the gene knockout group of *ALDH9A1*, and the *ALDH9A1* group showed a low granularity in the AGP channel and mitochondrial channel (Fig. 22, Fig. 25 A). At chromosome 9, the gene knockout group showed a pattern with lower granularity than the groups of *RALGPS1* and *LMX1B* (Fig. 22, Fig. 25 A). At chromosome 11, *ME3* showed a low granularity pattern in the AGP and mitochondrial channel while the group of PRSS23 was more similar to the non targeting controls (Fig. 25 A, B).

In the groups of genes related to the congenital glaucoma, *GMDS, CYP1B1, TEK, FOXC1,* and *LTBP2*, the *GMDS* knockout groups showed a high granularity pattern while the *FOXC1* groups showed a low granularity pattern (Fig. 22, Fig. 25 A, B).

Figure 23: *Euclidean distance matrix between each of the gene knockout groups and human non targeting group of the morphological features. Groups are ordered by the hierarchical clustering methods of ward.D2. The bottom grid shows the genes within or nearby the same loci at the chromosome and the potential positive genes (blue) associated with congenital glaucoma, human non targeting control group is marked in red.*

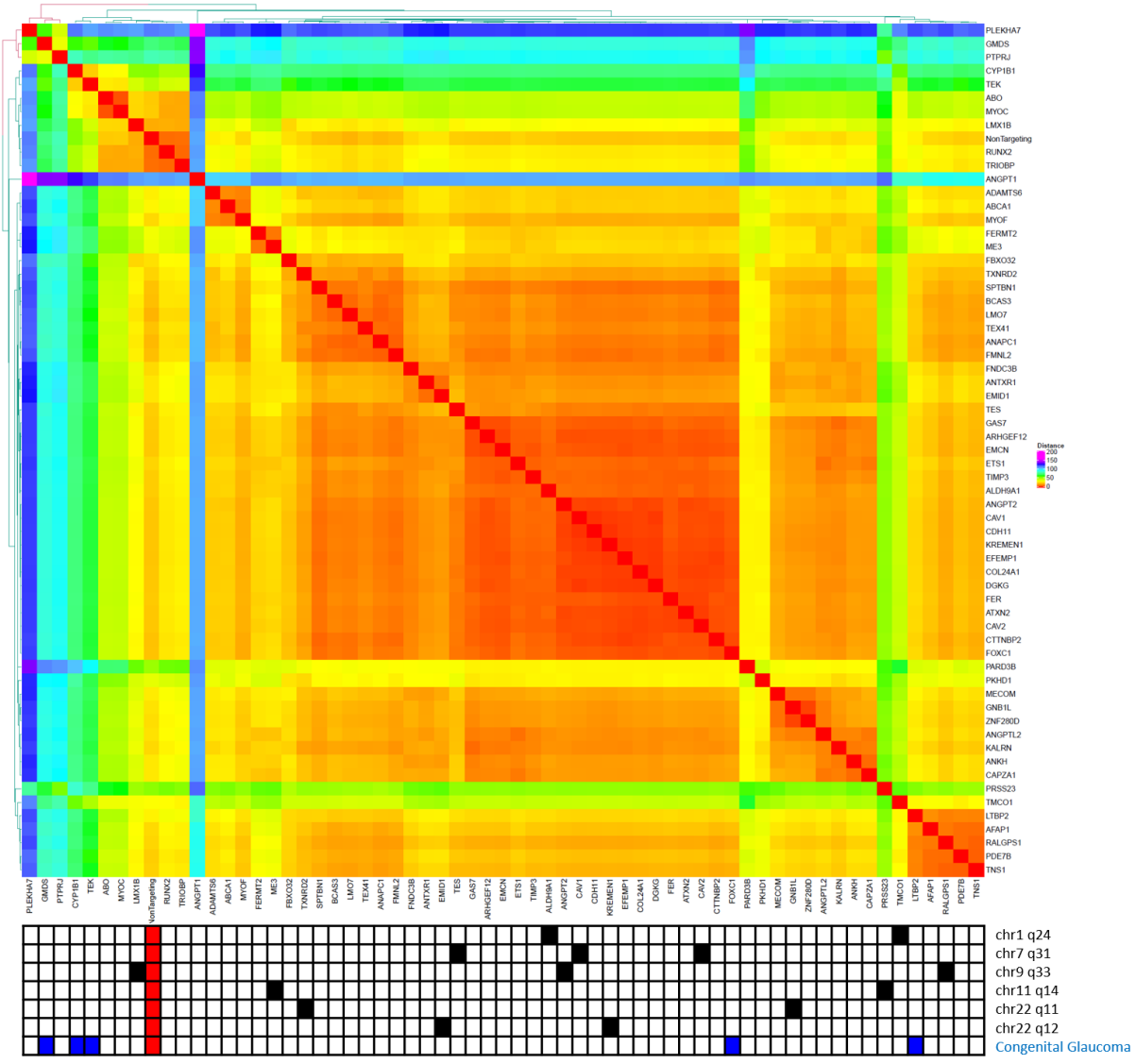

Figure 24: *Cluster tree displaying the hierarchical clustering of each cell line based on the morphological profiles. The method of ward.D2 was applied, the distance between each group within one branch was closer than those located in different branches. The bottom grid shows the genes within or nearby the same loci at the chromosome and the potential positive genes (blue) associated with congenital glaucoma, human non targeting control group is marked in red.*

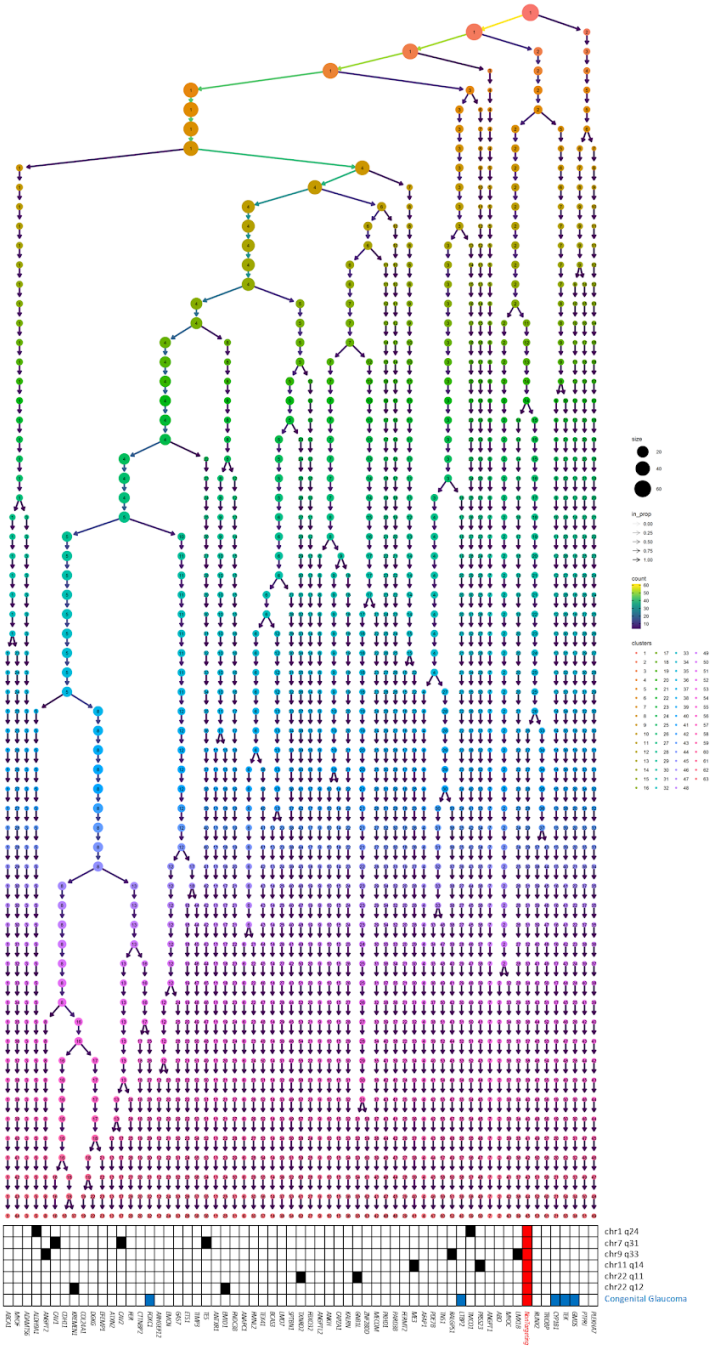

Figure 25: *The median value of selected features, Cytoplasm_Granularity_15_corAGP(A) and Nuclei_Granularity_9_corMito(B) in each gene knockout group and human-non targeting control group. The x axis shows each group, the bottom grid shows the genes within or nearby the same loci at the chromosome and the potential positive genes (blue) associated with congenital glaucoma, human non targeting control group is marked in red. The y axis is the value of the features. The names are provided by the CellProfiler software.*

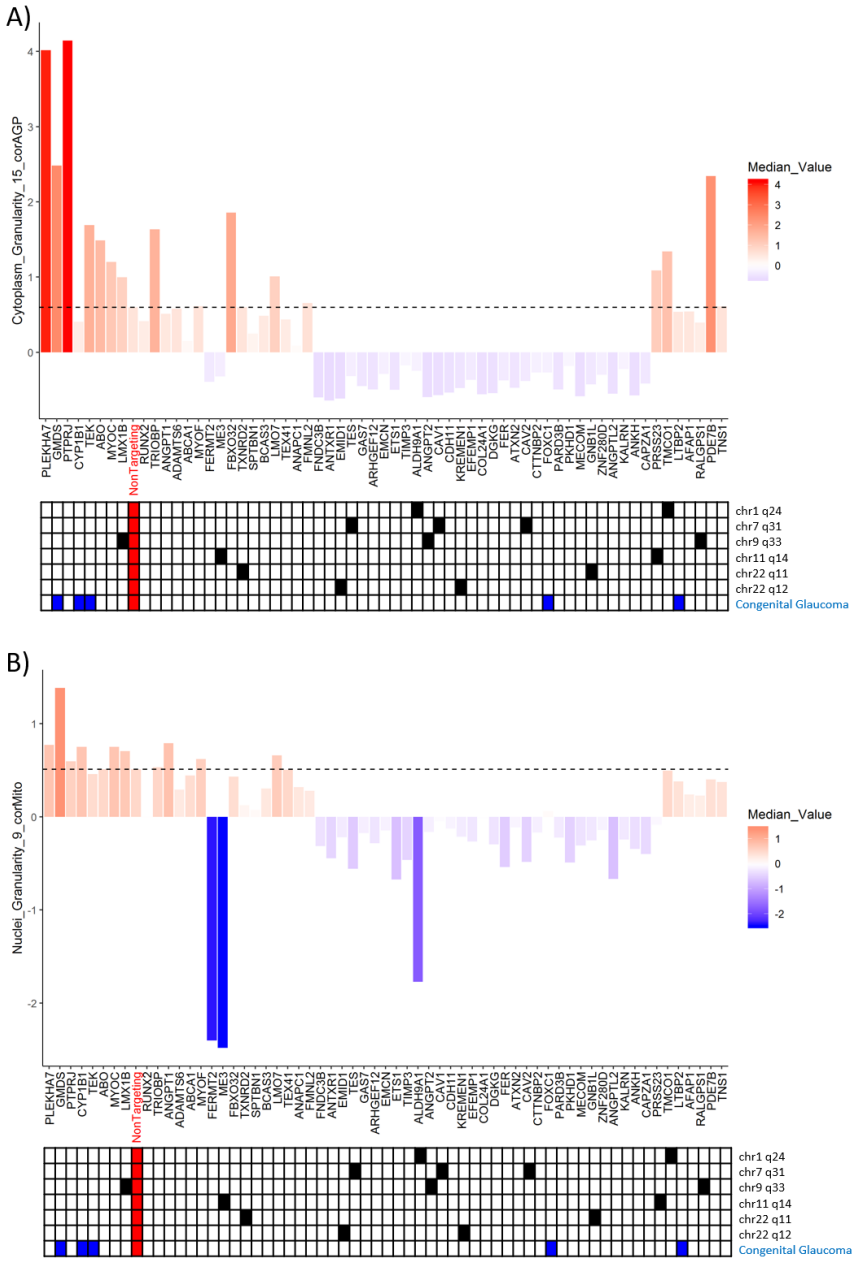

6.2 Single cell transcriptional profiling of trabecular meshwork cells

In this assay, the sgRNAs of each knockout gene were assigned to individual cells when the sgRNA was the only designed sgRNA found in the cell or the reads of the sgRNA were more than three times of the sum of other sgRNAs which targeting other genes. The data of single cell transcriptome was normalised using SCTransform and stored in a Seurat object via R. (https://github.com/powellgenomicslab/CROP-seq). Total 25,879 high quality single cell transcriptomes were obtained (Fig. 26).

Figure 26: *UMAP plots of the scRNA-seq. 25,879 cells are plotted and coloured by their corresponding gene knockout group or non-targeting control group.*

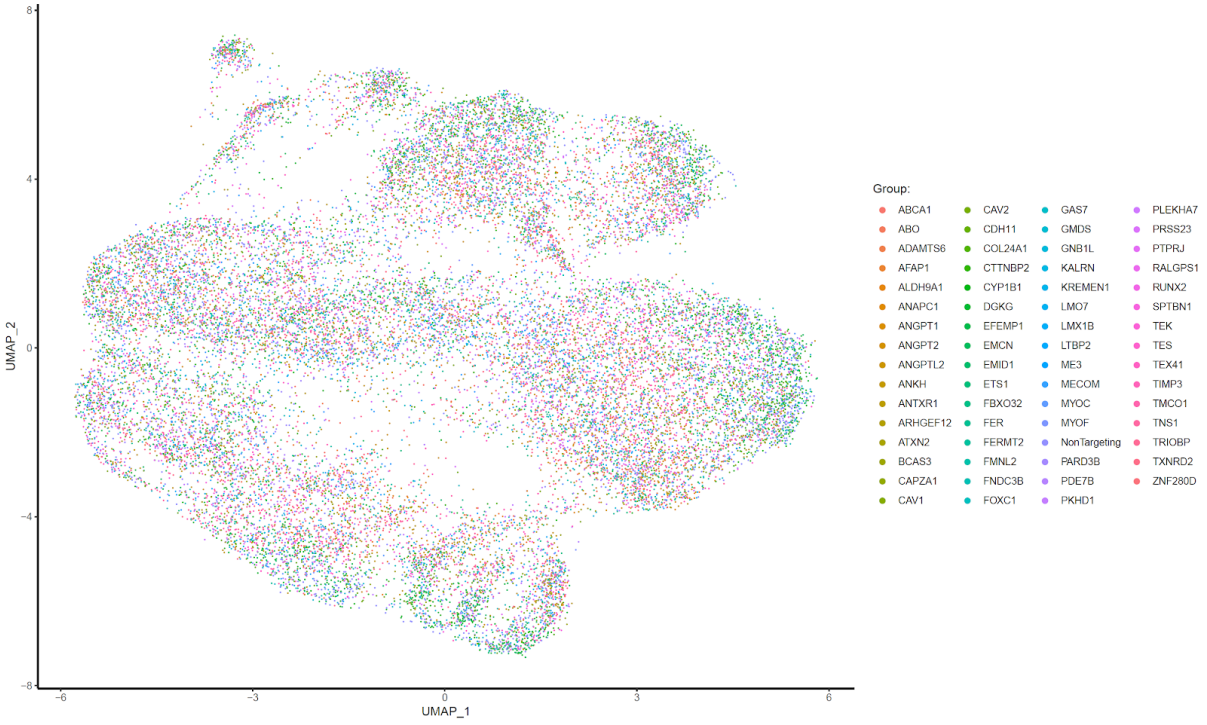

6.2.1 Differential expression analysis

To study the effects of each sgRNA on the transcriptome, we compared the gene expression level of each 62 gene knockout groups to the human non-targeting control group (Fig. 27, Appendix Figure 1). The differentially expressed genes (DEGs) were selected with the rules of *log2_fold_change* > 2 and *p value* < 10^{-6} (Appendix. Table 3). Among these 62 comparisons, total 240 DEGs were selected. Then we generated a data frame of the *log2_fold_change* value of DEGs for all 62 gene knockout groups together with the human non-targeting controls. The *log2_fold_change* value was set to 0 for the human non targeting controls (Fig. 28).

Figure 27: *Differential expressed genes between gene knockout groups compared to non-targeting control groups. 1) ABCA1, 2) ABO, 3) ADAMTS6, 4) AFAP1, 5) ALDH9A1, 6) ANAPC1, 7) ANGPT1, 8) ANGPT2, 9) ANGPTL2, 10) ANKH, 11) ANTXR1, 12) ARHGEF12, 13) ATXN2, 14) BCAS3, 15) CAPZA1, 16) CAV1, 17) CAV2, 18) CDH11, 19) COL24A1, 20) CTTNBP2, 21) CYP1B1, 22) DGKG, 23) EFEMP1, 24) EMCN, 25) EMID1, 26) ETS1, 27) FBXO32, 28) FER, 29) FERMT2, 30) FMNL2, 31) FNDC3B, 32) FOXC1, 33) GAS7, 34) GMDS, 35) GNB1L, 36) KALRN, 37) KREMEN1, 38) LMO7, 39) LMX1B, 40) LTBP2, 41) ME3, 42) MECOM, 43) MYOC, 44) MYOF, 45) PARD3B, 46) PDE7B, 47) PKHD1, 48) PLEKHA7, 49) PRSS23, 50) PTPRJ, 51) RALGPS1, 52) RUNX2, 53) SPTBN1, 54) TEK, 55) TES, 56) TEX41, 57) TIMP3, 58) TMCO1, 59) TNS1, 60) TRIOBP, 61) TXNRD2, 62) ZNF280D*

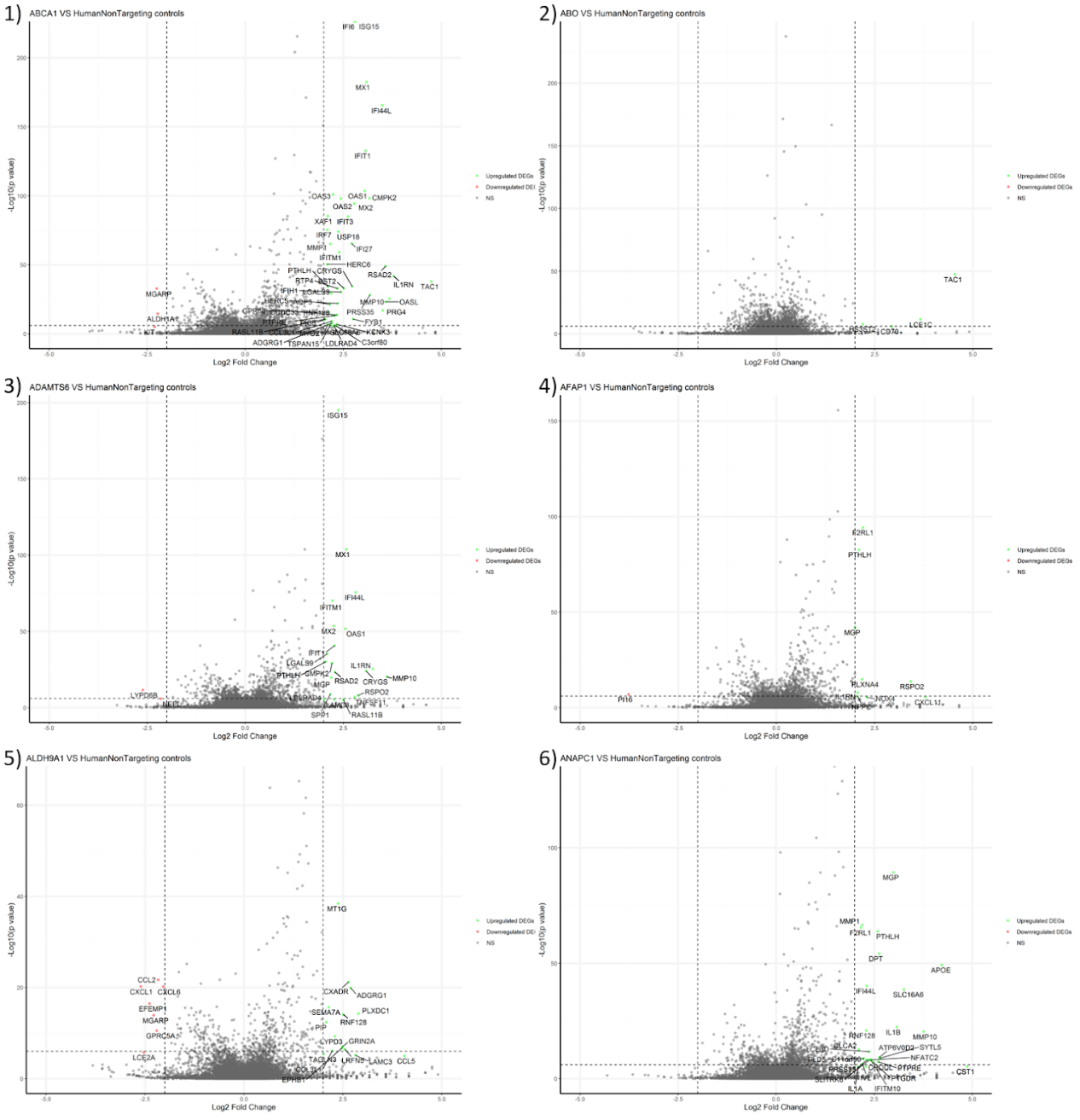
1) ABCA1 VS HumanNonTargeting controls
2) ABO VS HumanNonTargeting controls
3) ADAMTS6 VS HumanNonTargeting controls
4) AFAP1 VS HumanNonTargeting controls
5) ALDH9A1 VS HumanNonTargeting controls
6) ANAPC1 VS HumanNonTargeting controls
-Log10(p value)
Log2 Fold Change
Upregulated DEGs
Downregulated DEGs
NS

7) ANGPT1 VS HumanNonTargeting controls

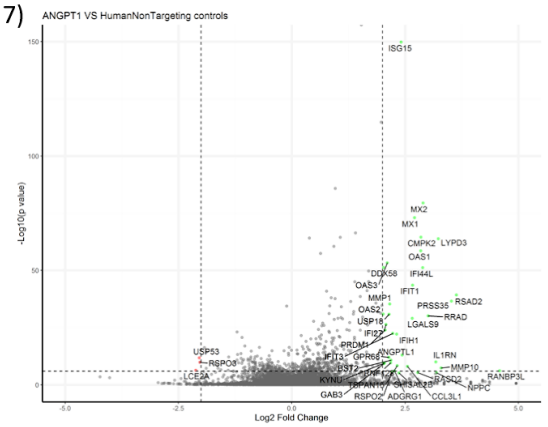

8) ANGPT2 VS HumanNonTargeting controls

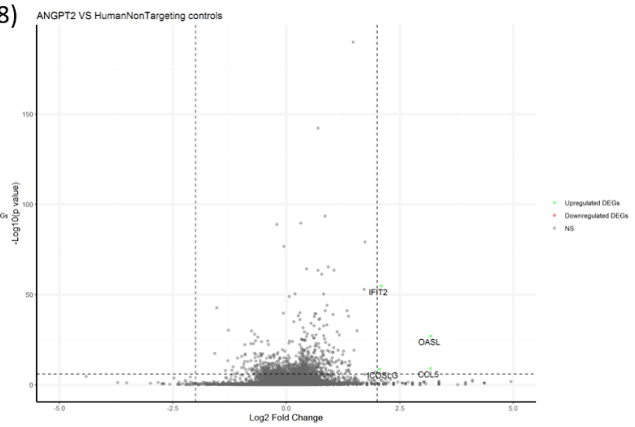

9) ANGPTL2 VS HumanNonTargeting controls

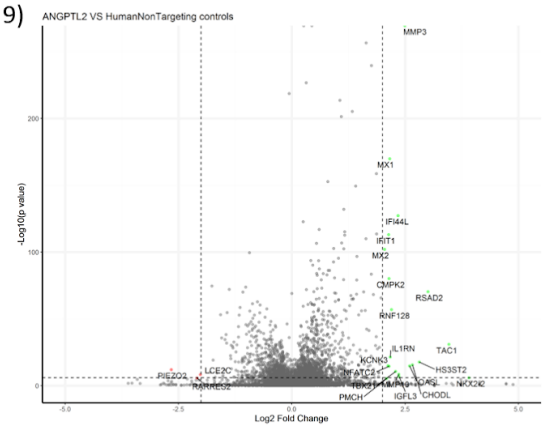

10) ANKH VS HumanNonTargeting controls

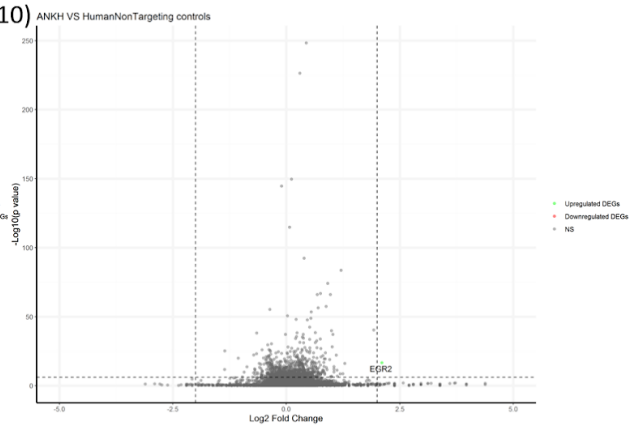

11) ANTXR1 VS HumanNonTargeting controls

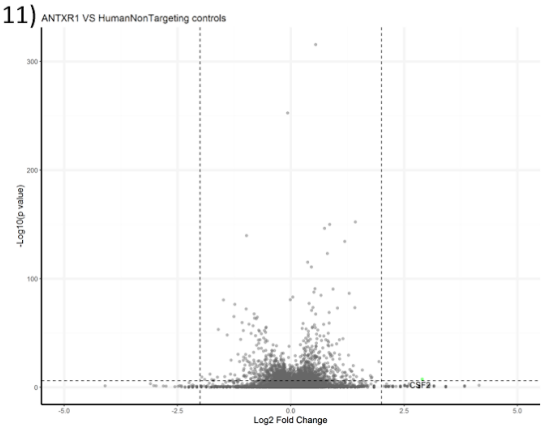

12) ARHGEF12 VS HumanNonTargeting controls

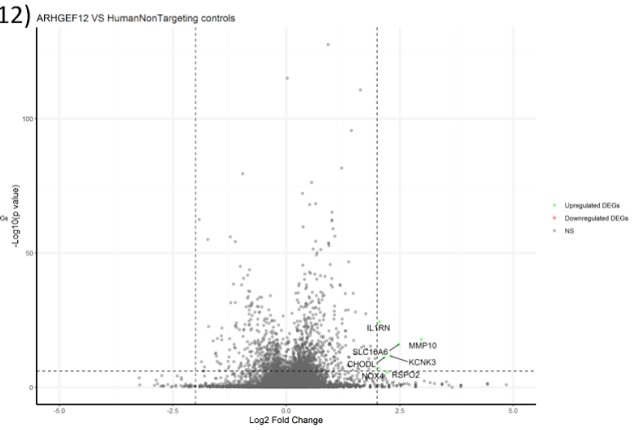

13) ATXN2 VS HumanNonTargeting controls

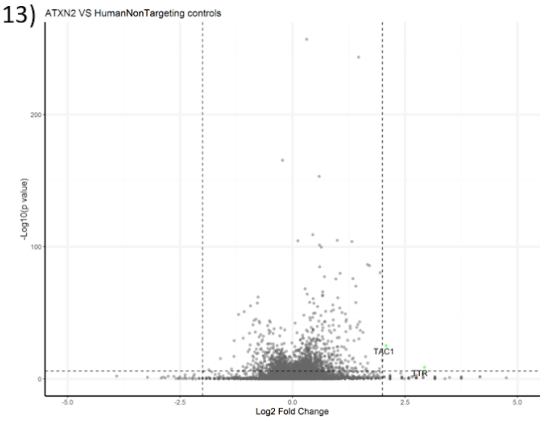

14) BCAS3 VS HumanNonTargeting controls

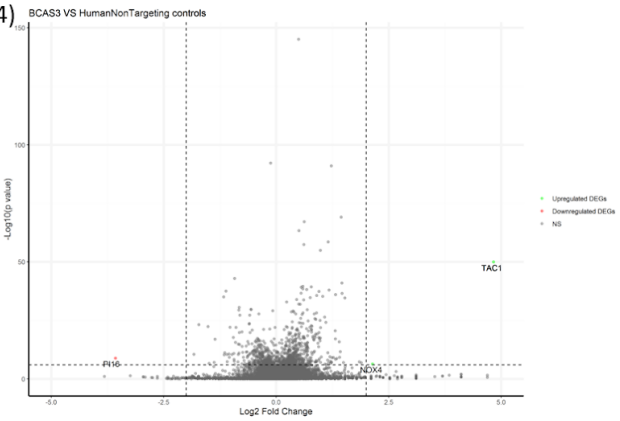

15) CAPZA1 VS HumanNonTargeting controls

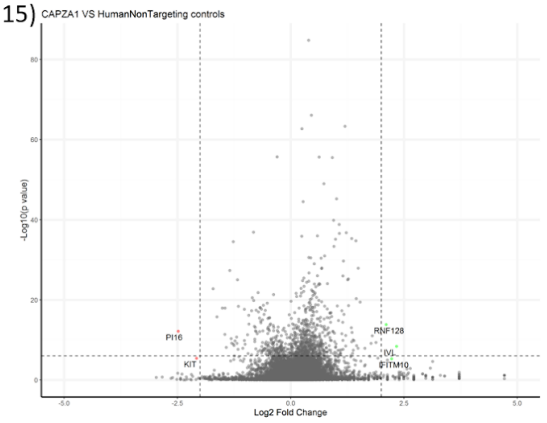

16) CAV1 VS HumanNonTargeting controls

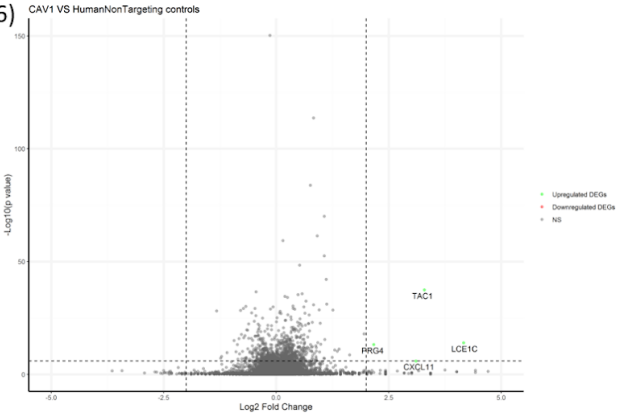

17) CAV2 VS HumanNonTargeting controls

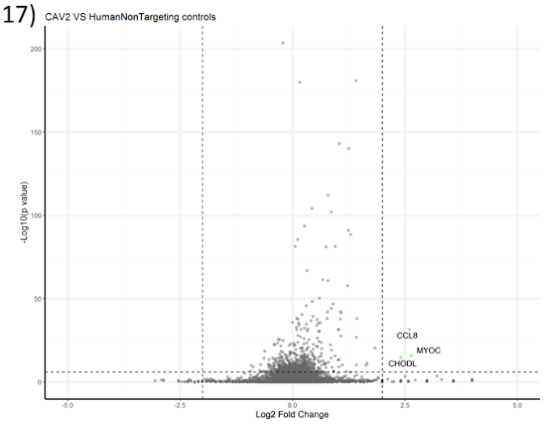

18) CDH11 VS HumanNonTargeting controls

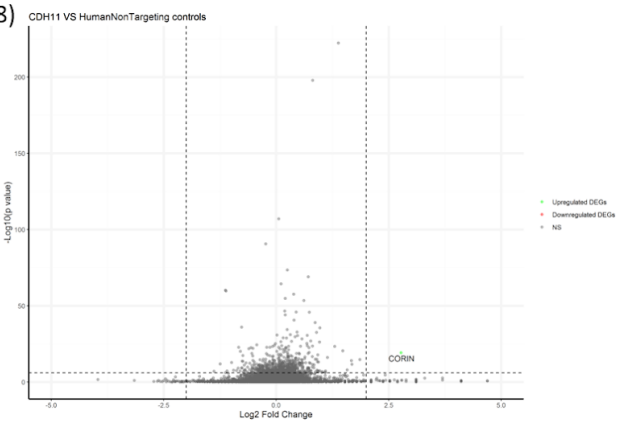

19) COL24A1 VS HumanNonTargeting controls

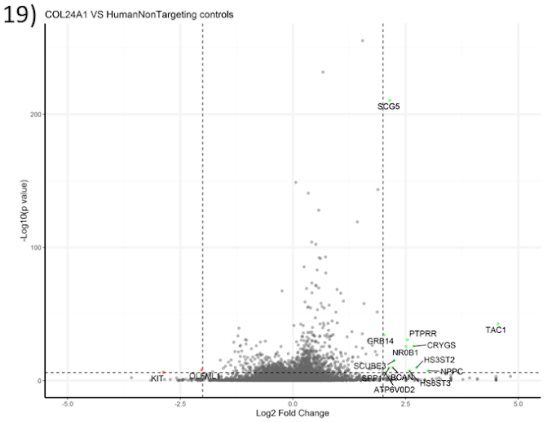

20) CTTNBP2 VS HumanNonTargeting controls

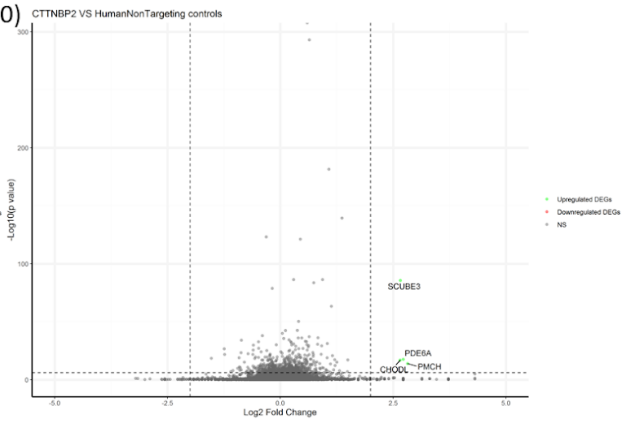

21) CYP1B1 VS HumanNonTargeting controls

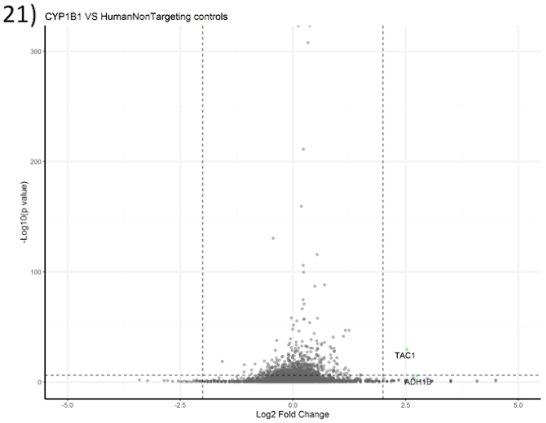

22) DGKG VS HumanNonTargeting controls

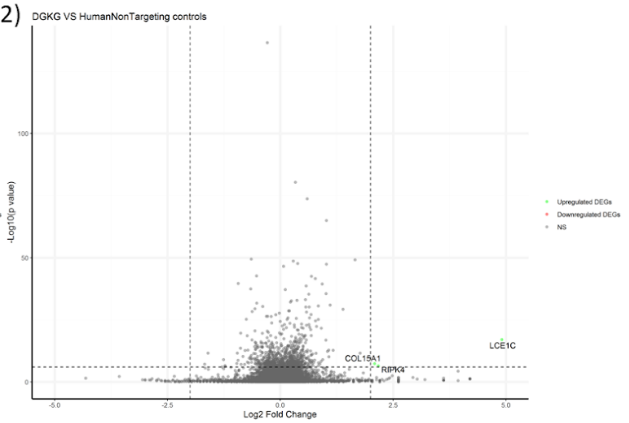

23) EFEMP1 VS HumanNonTargeting controls

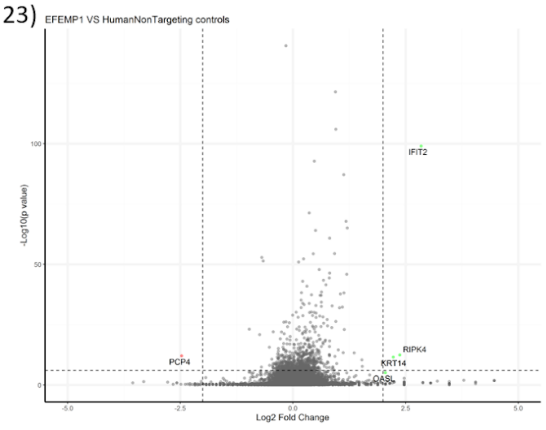

24) EMCN VS HumanNonTargeting controls

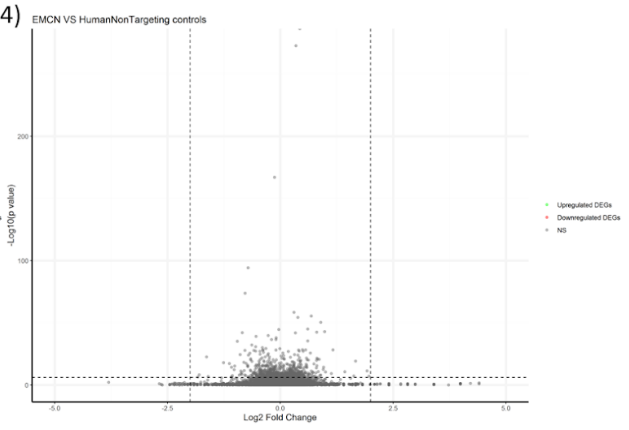

25) EMID1 VS HumanNonTargeting controls

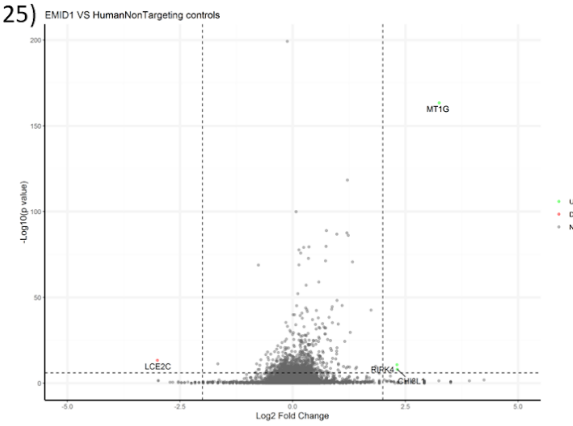

26) ETS1 VS HumanNonTargeting controls

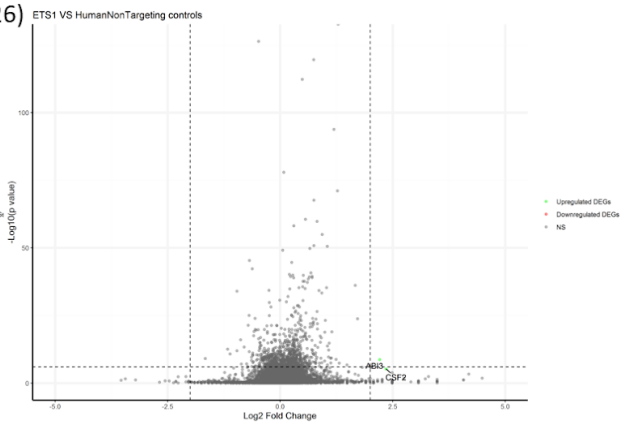

27) FBXO32 VS HumanNonTargeting controls

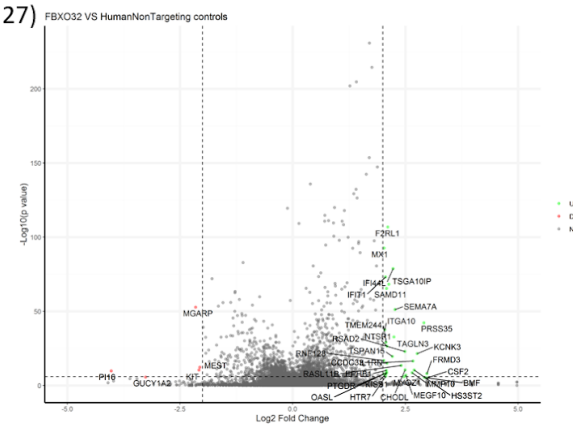

28) FER VS HumanNonTargeting controls

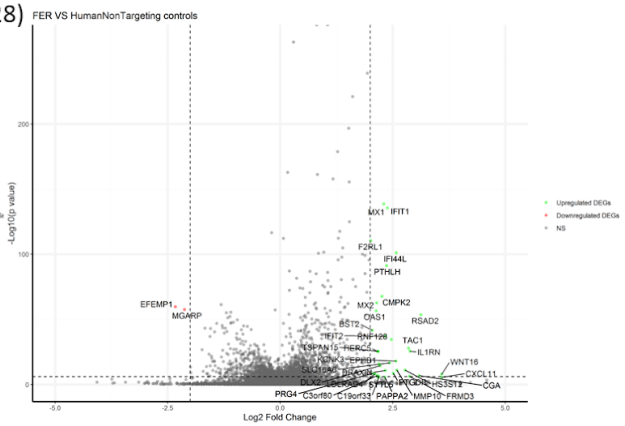

29) FERMT2 VS HumanNonTargeting controls

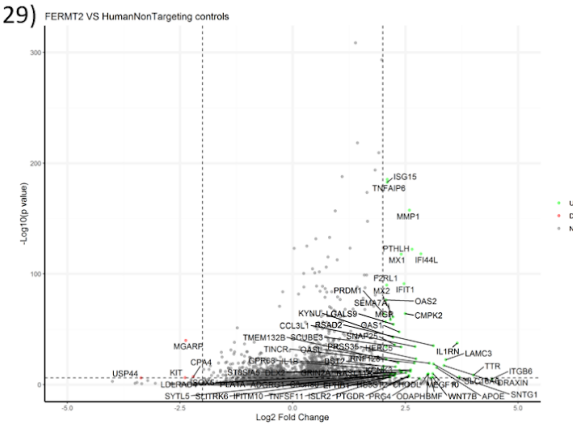

30) FMNL2 VS HumanNonTargeting controls

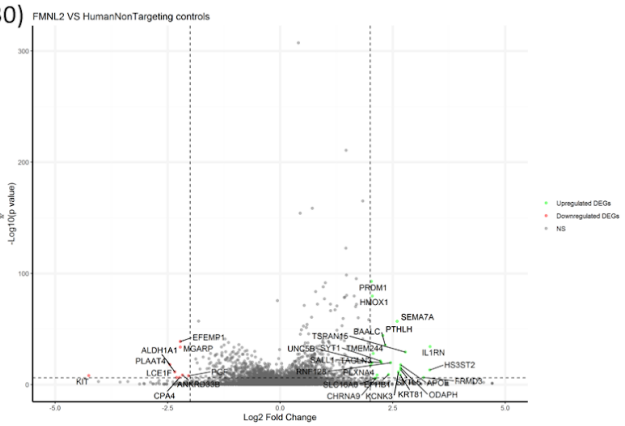

31) FNDC3B VS HumanNonTargeting controls

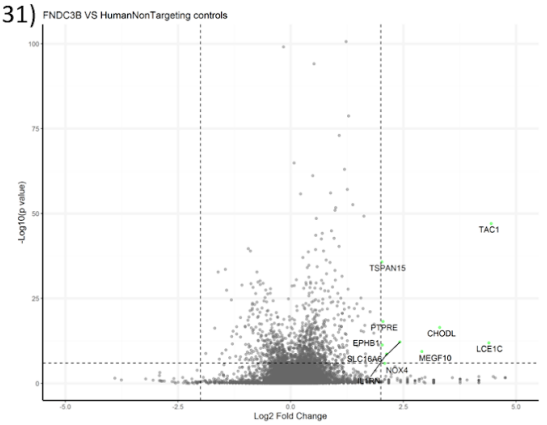

32) FOXC1 VS HumanNonTargeting controls

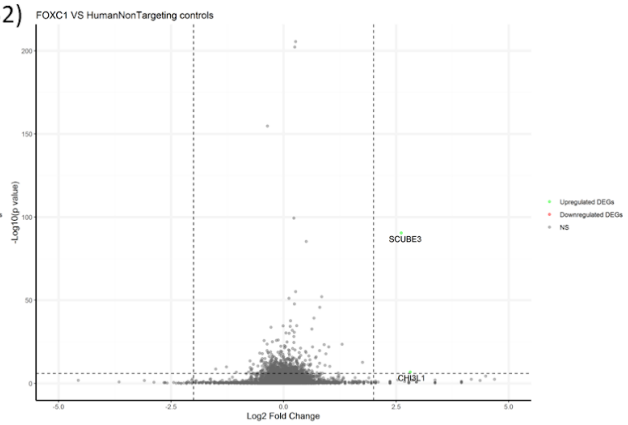

33) GAS7 VS HumanNonTargeting controls

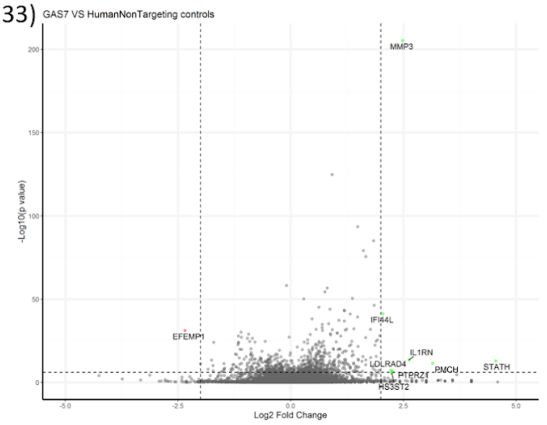

34) GMDS VS HumanNonTargeting controls

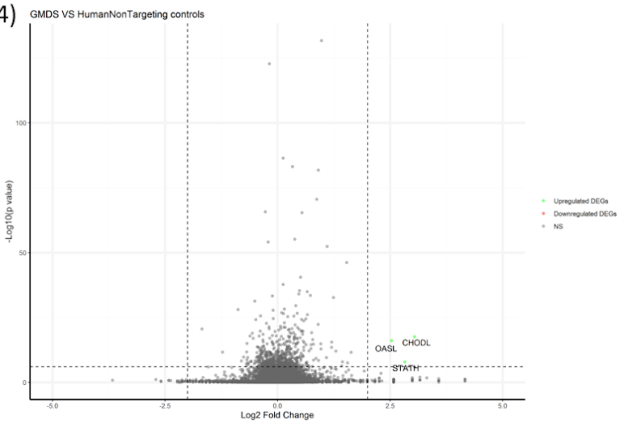

35) GNB1L VS HumanNonTargeting controls

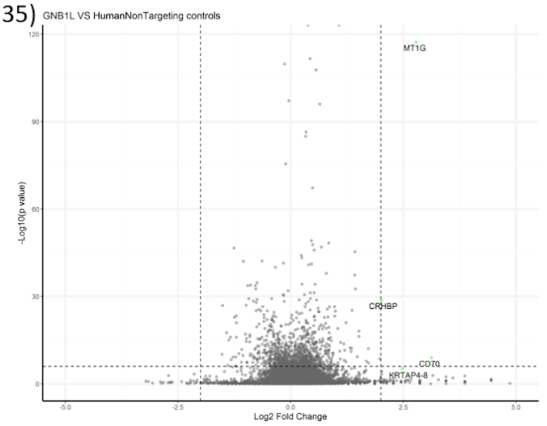

36) KALRN VS HumanNonTargeting controls

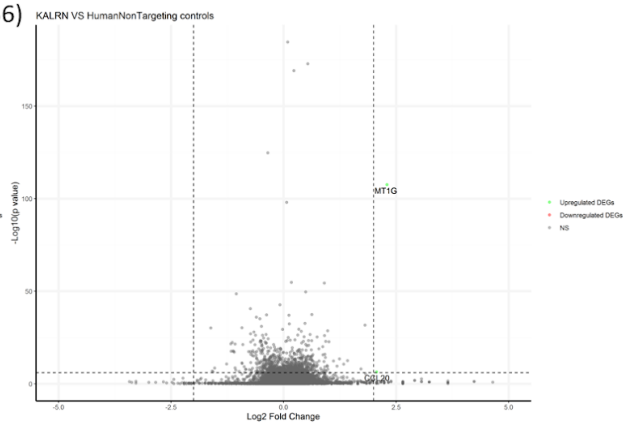

37) KREMEN1 VS HumanNonTargeting controls

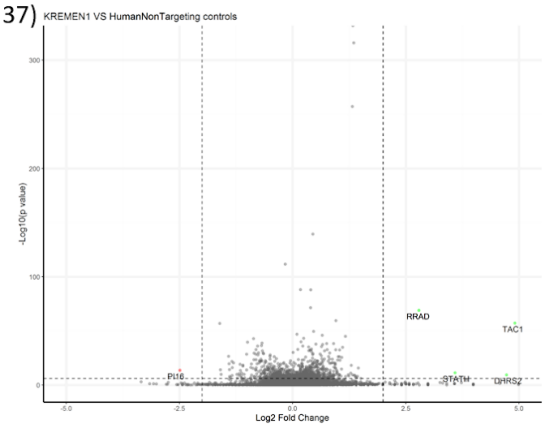

38) LMO7 VS HumanNonTargeting controls

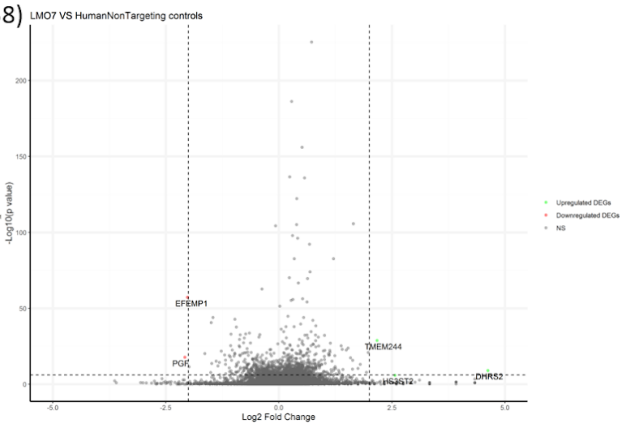

39) LMX1B VS HumanNonTargeting controls

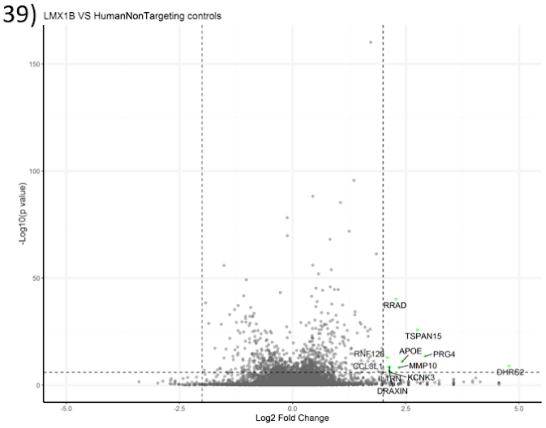

40) LTBP2 VS HumanNonTargeting controls

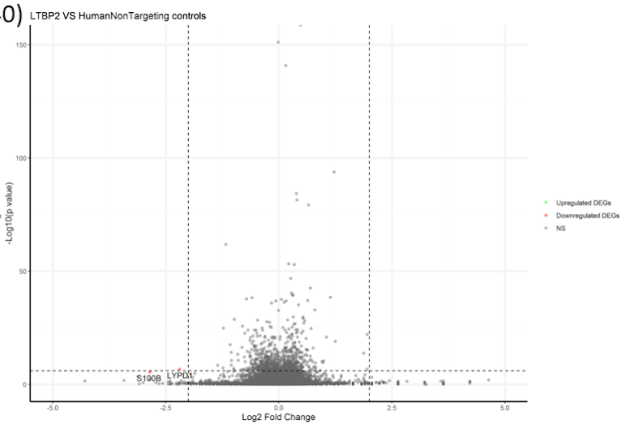

41) ME3 VS HumanNonTargeting controls

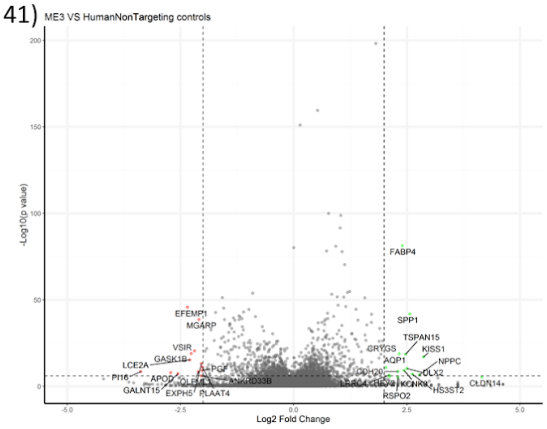

42) MECOM VS HumanNonTargeting controls

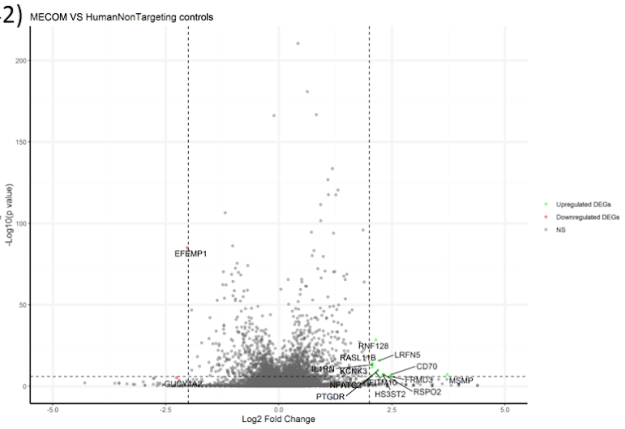

43) MYOC VS HumanNonTargeting controls

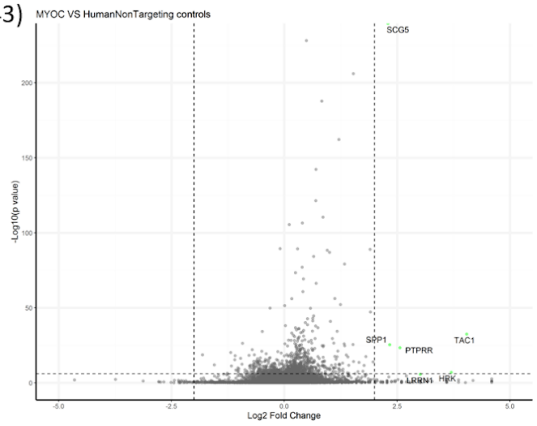

44) MYOF VS HumanNonTargeting controls

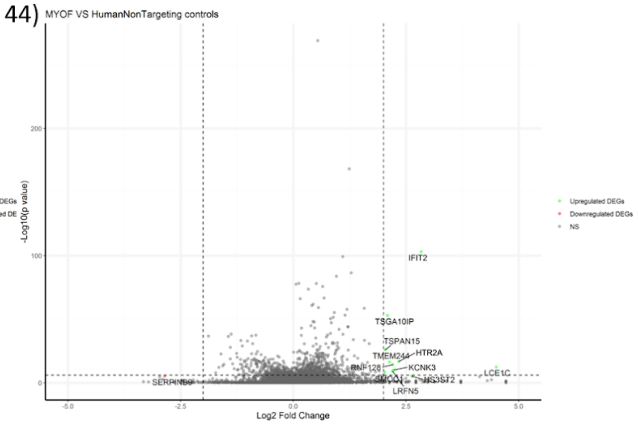

45) PARD3B VS HumanNonTargeting controls

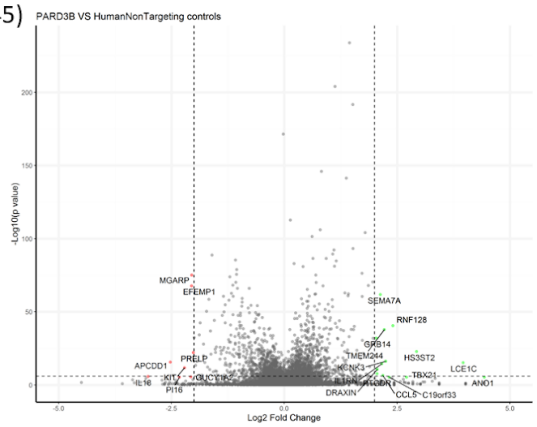

46) PDE7B VS HumanNonTargeting controls

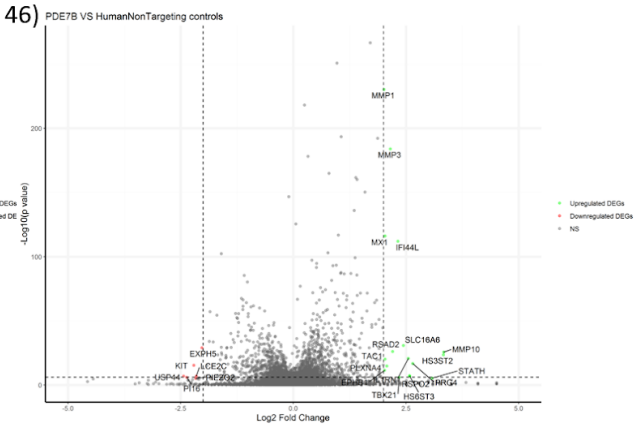

47) PKHD1 VS HumanNonTargeting controls

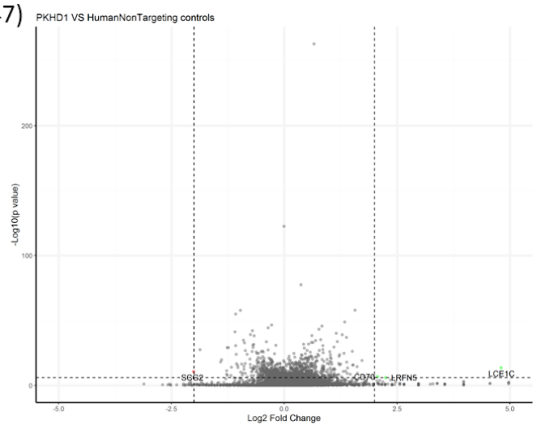

48) PLEKHA7 VS HumanNonTargeting controls

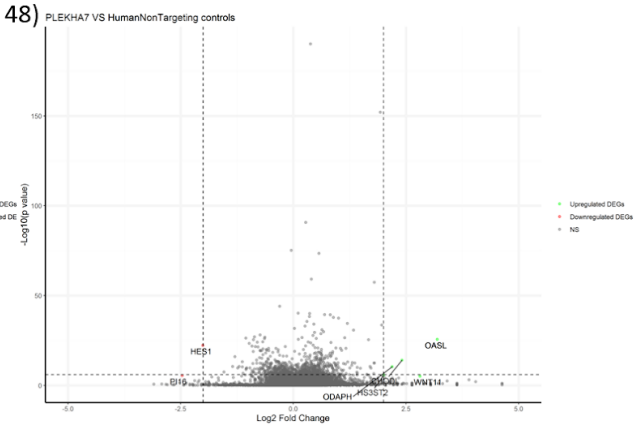

49) PRSS23 VS HumanNonTargeting controls

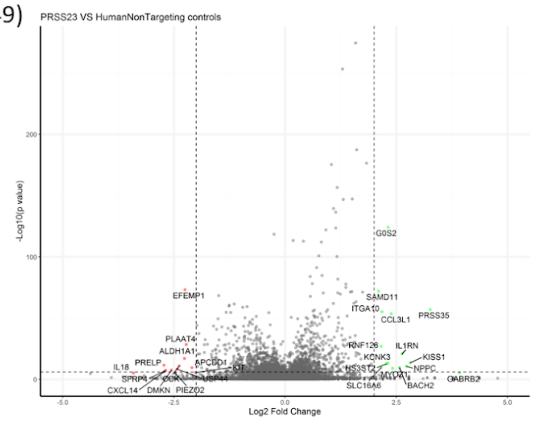

50) PTPRJ VS HumanNonTargeting controls

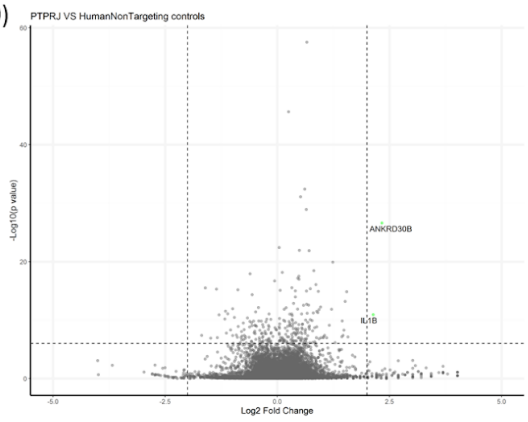

51) RALGPS1 VS HumanNonTargeting controls

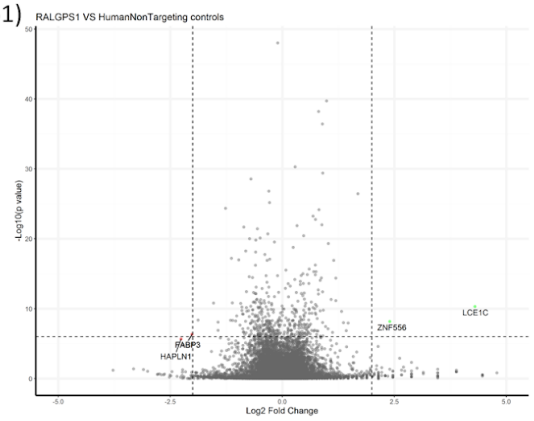

52) RUNX2 VS HumanNonTargeting controls

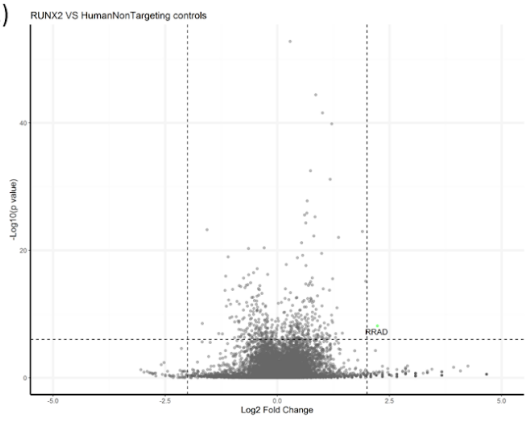

53) SPTBN1 VS HumanNonTargeting controls

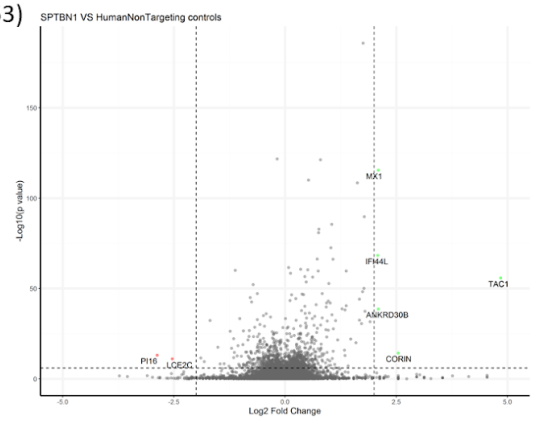

54) TEK VS HumanNonTargeting controls

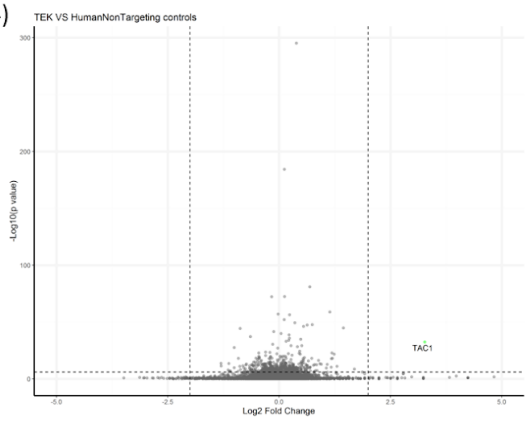

55) TES VS HumanNonTargeting controls

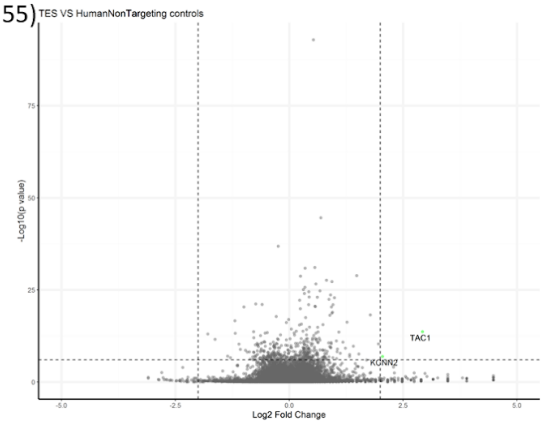

56) TEX41 VS HumanNonTargeting controls

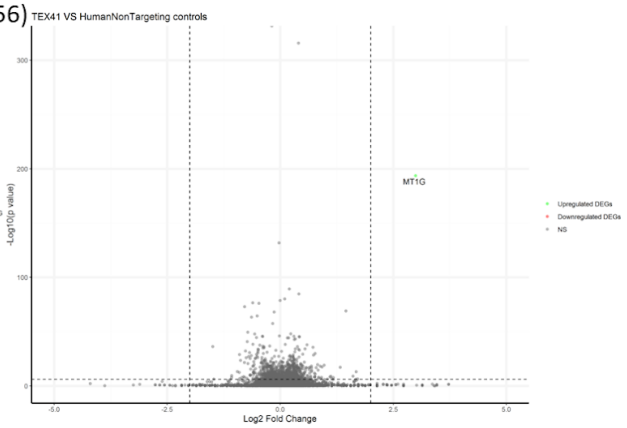

57) TIMP3 VS HumanNonTargeting controls

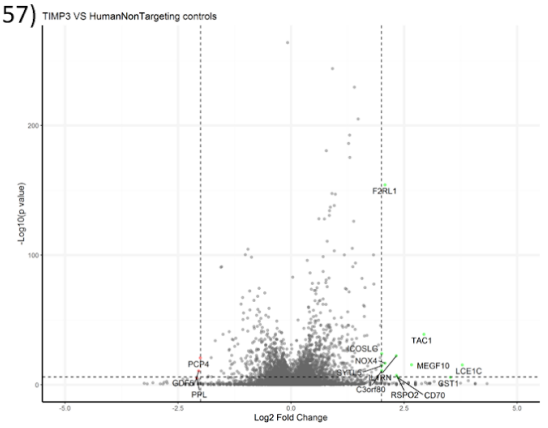

58) TMCO1 VS HumanNonTargeting controls

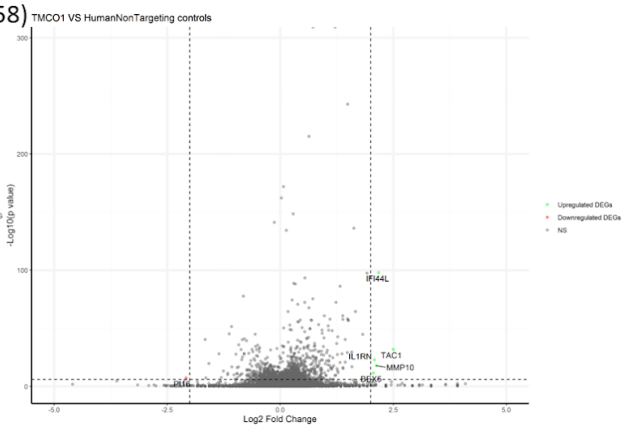

59) TNS1 VS HumanNonTargeting controls

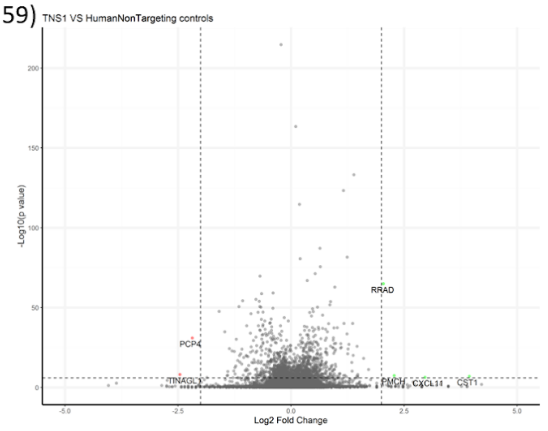

60) TRIOBP VS HumanNonTargeting controls

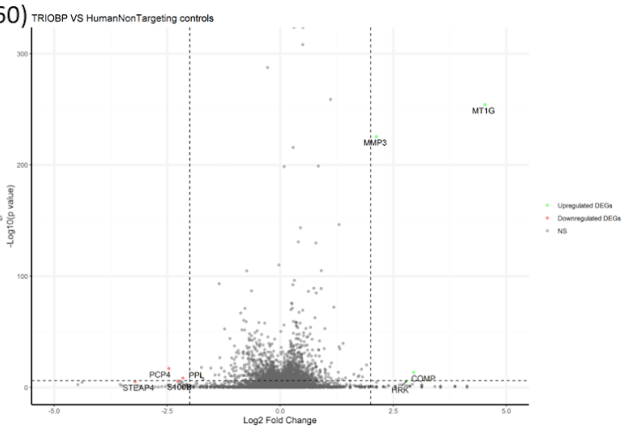

61) TXNRD2 VS HumanNonTargeting controls

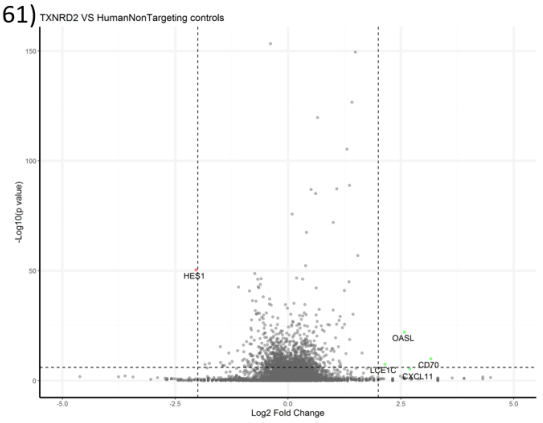

62) ZNF280D VS HumanNonTargeting controls

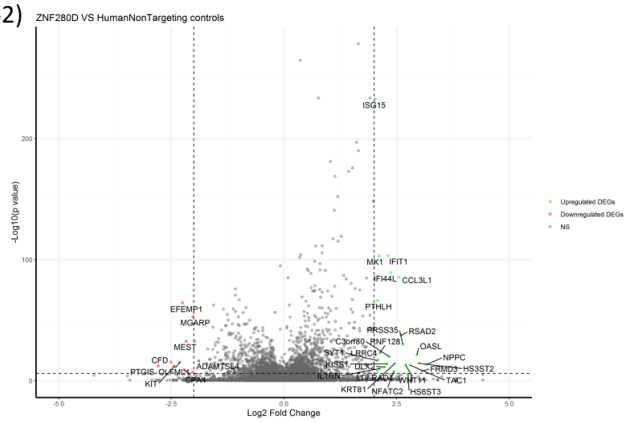

Figure 28: *Heatmap displaying the log2 fold change of each differentially expressed gene (DEG) for each gene knockout group and human non targeting control group*

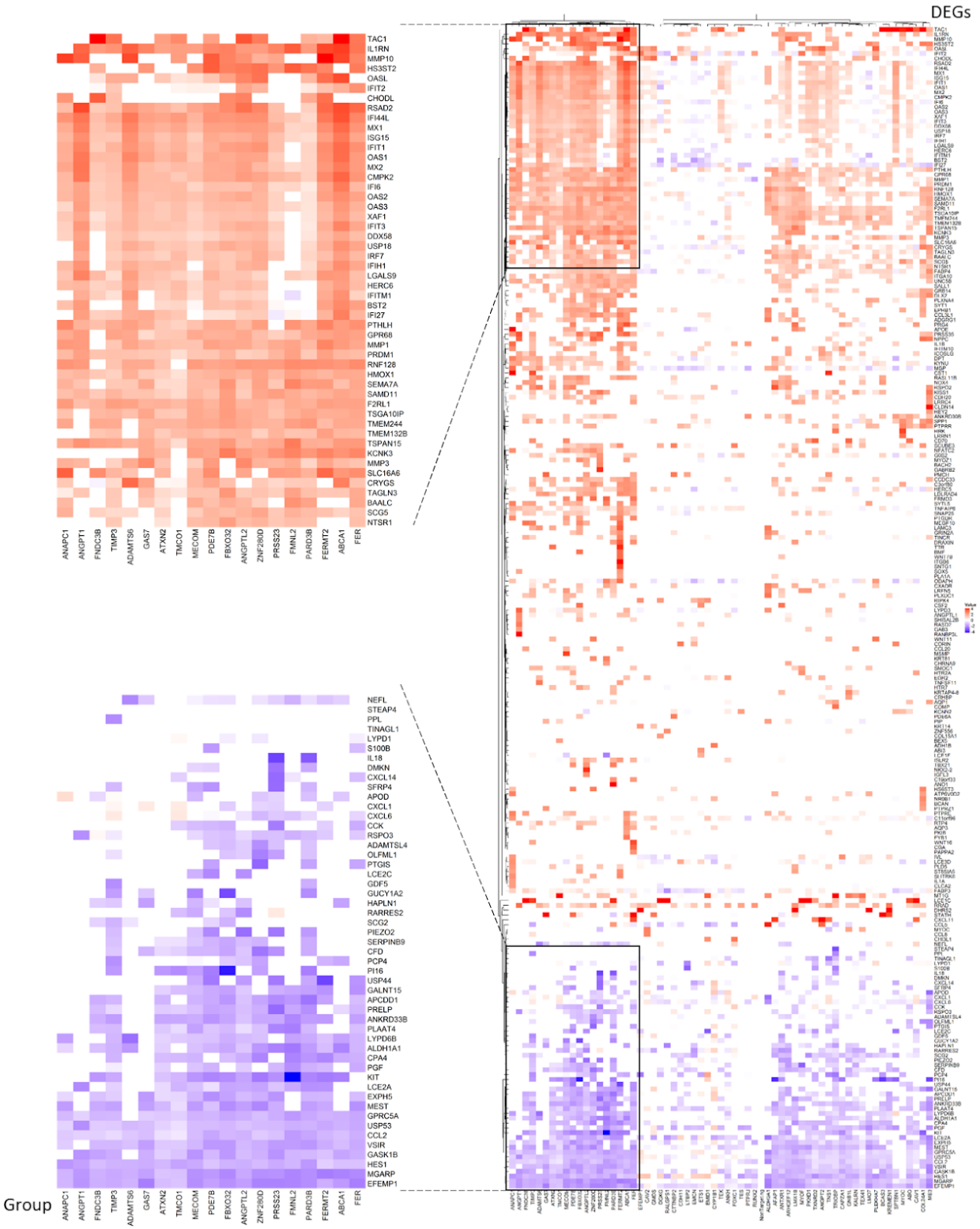

6.2.2 Hierarchical clustering of enriched differentially expressed genes

In clustering analysis, the *euclidean* distance was computed between each pair of the groups with the expression level of DEGs (Fig. 29), the hierarchical clustering method of *ward.D2* was applied to generate the cutree (Fig. 30). The gene knockout groups of *ABCA1, ADAMTS6, ANAPC1, ANGPT1, ANGPTL2, ATXN2, FBXO32, FER, FERMT2, FMNL2, FNDC3B, GAS7, MECOM, PARD3B, PDE7B, PRSS23, TIMP3, TMCO1, and ZNF280D* are clustered together and were more distant to other groups including the control (Fig. 28, Fig. 29, Fig. 30). In this cluster, the top 20 upregulated DEGs are *TAC1, IL1RN, MMP10, HS3ST2, OASL, IFIT2, CHODL, RSAD2, IFI44L, MX1, ISG15, IFIT1, OAS1, MX2, CMPK2, IFI6, OAS2, OAS3, XAF1,* and *IFIT3*, and the tail 20 downregulated DEGs are *APCDD1, PRELP, ANKRD33B, PLAAT4, LYPD6B, ALDH1A1, CPA4, PGF, KIT, LCE2A, EXPH5, MEST, GPRC5A, USP53, CCL2, VSIR, GASK1B, HES1, MGARP, EFEMP1* (Fig. 28). The gene ontology analysis on these DEGs were performed using the online tool *metascape* (https://metascape.org/)[136] and 13 upregulated DEGs are found related to the interferon alpha/beta signaling including *IL1RN, OASL, IFIT2, RSAD2, MX1, IFIT1, OAS1, MX2, IFI6, OAS2, OAS3, XAF1, IFIT3* (Fig. 31).

In the comparison between the genes at the overlapping loci, the gene knockout groups of *TMCO1* (at chromosome 1) and *PRSS23* (at chromosome 11) present distinct DEG patterns to the control groups (Fig. 27_58, 41). Other groups show a similar DEGs patterns to the control groups, including *ALDH9A1* (at chromosome 1) (Fig. 27_5), *CAV1, CAV2*, and *TES* (At chromosome 7) (Fig. 27_16, 17, 55), *ANGPT2, RALGPS1, and LMX1B* (at chromosome 9) (Fig. 27_8, 51, 39), *ME3* (at chromosome 11) (Fig. 27_43), *EMID1* and *KREMEN1* (at chromosome 22 q11) (Fig. 27_25, 37) , *GNB1L* and *TXNRD2* (chromosome 22 q12) (Fig. 27_35, 61).

All the gene knockout groups related to the congenital glaucoma showed similar patterns to controls, including *GMDS (Fig. 27_34), CYP1B1 (Fig. 27_21), TEK (Fig. 27_54), FOXC1 (Fig. 27_32),* and *LTBP2 (Fig. 27_40).*

Figure 29: *Euclidean distance matrix between each of the gene knockout groups and human non targeting group of the differential expressed genes. Groups are ordered by the hierarchical clustering methods of ward.D2. The bottom grid shows the genes within or nearby the same loci at the chromosome and the potential positive genes (blue) associated with congenital glaucoma, human non-targeting control group is marked in red*

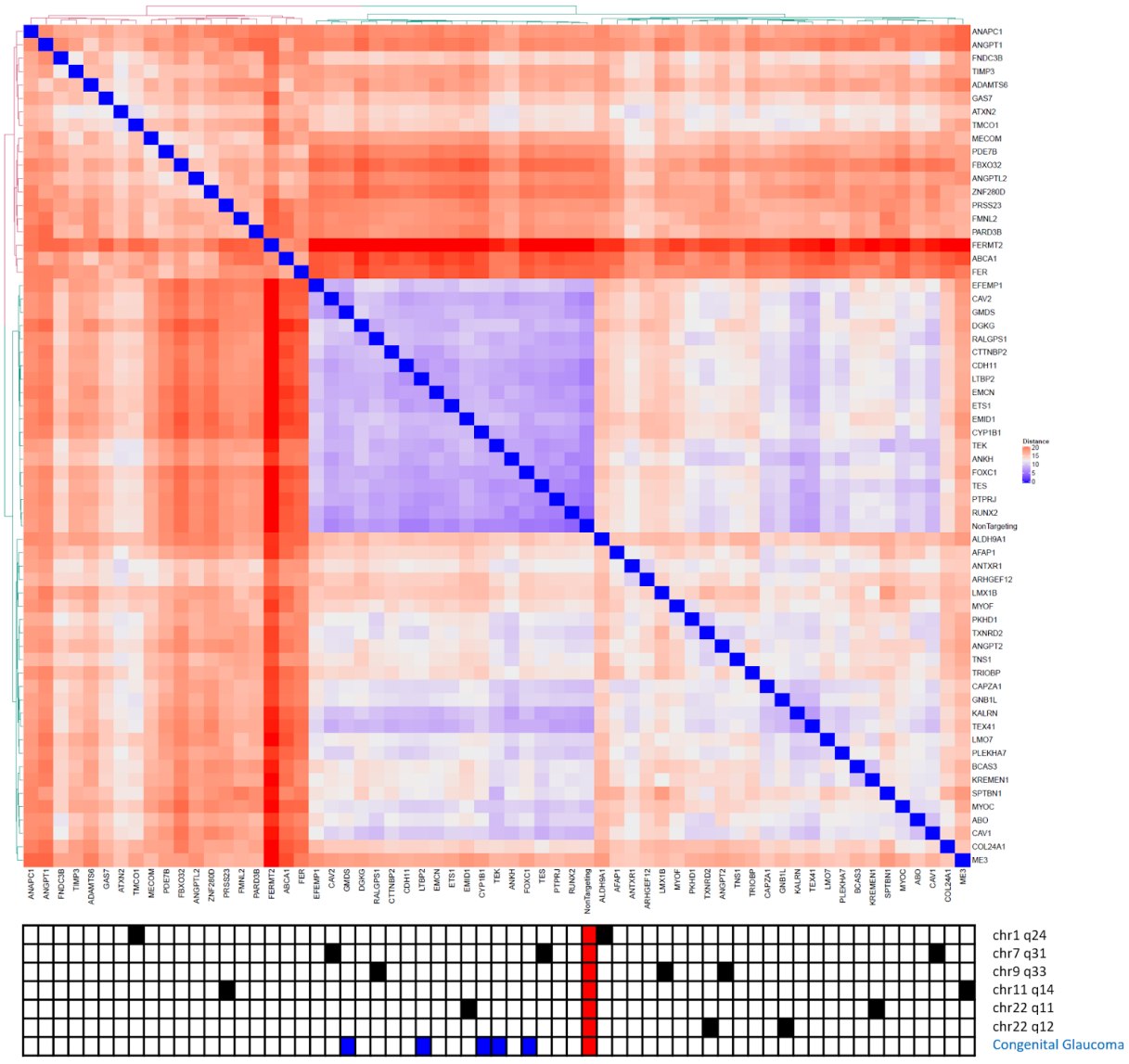

Figure 30: *Cluster tree displaying the hierarchical clustering of each cell line based on the RNA expression profiles. The method of ward.D2 was applied, the distance between each group within one branch was closer than those located in different branches. The bottom grid shows the genes within or nearby the same loci at the chromosome and the potential positive genes (blue) associated with congenital glaucoma, human non-targeting control group is marked in red.*

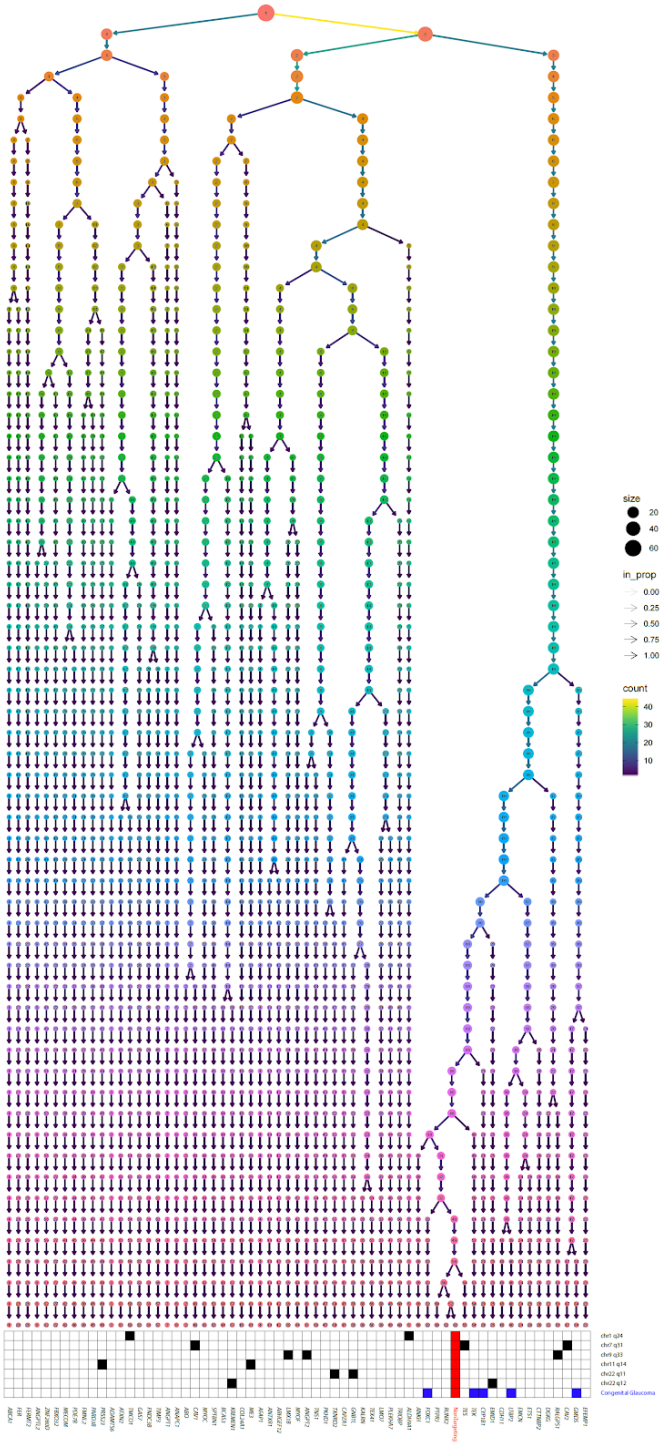

Figure 31: *Gene ontology enrichment analysis of the selected DEGs. Top 8 clusters with their representative enriched terms. For each given gene list, pathway and process enrichment analysis was performed with the ontology sources: KEGG Pathway, GO Biological Processes, Reactome Gene Sets, Canonical Pathways and CORUM. All genes in the genome have been used as the enrichment background. Terms with a p-value < 0.01, a minimum count of 3, and an enrichment factor > 1.5 (the enrichment factor is the ratio between the observed counts and the counts expected by chance) are collected and grouped into clusters based on their membership similarities. Each cluster has "Log10(P)" is the p-value in log base 10.*

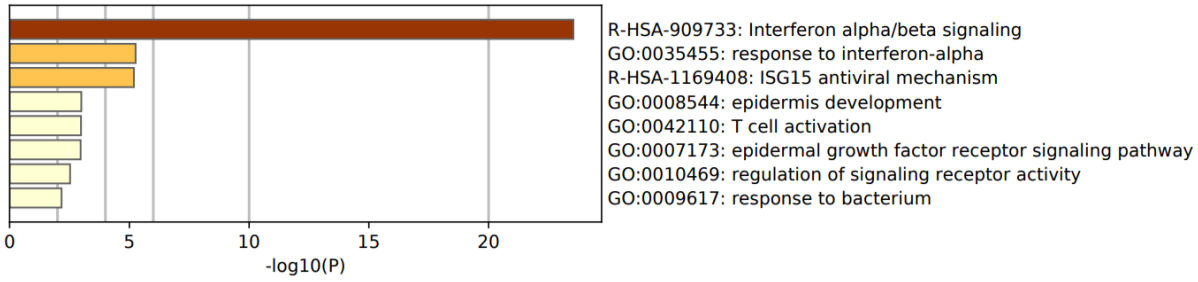

7. DISCUSSION

POAG is a heterogeneous disease influenced by complex interactions of risk factors including the age, ethnicity, family history, the use of corticosteroids, and intraocular pressure. Although the genetic basis of POAG is complex, many genetic risk factors have been identified and their roles in pathogenesis of POAG have become more clear [137]. For example, mutations in *MYOC* cause an elevated IOP and dysfunction of TMCs, while OPTN and TBK1 mutations are more closely related to the nervous system processes in glaucoma with a normal IOP [14,15,138]. To investigate cellular changes occurring in glaucoma, there is a demand to find more relevant models to study the gene mutations. TMCs are always the first choice since they are related to the IOP directly, however, the difficulty in harvesting the cells from TM tissue limits the usage of TMCs. Since TMCs are isolated from TM tissue and cultured in vitro, they should be treated as "secondary" cultures (passage 2), and they have a finite number of doublings. Their appearance begins to change after 6 passages, such as vacuoles, increased size and reduced doubling time. Thus, the human primary TMCs can only be used no later than 7 passages [77]. Although there exists a commercial cell line called TMCs, they are of doubtful quality since they did not show a TMC-like response to the treatment with corticosteroids [90].

Our first aim is to investigate whether the combination treatment of the growth factors, RA, TGF-β2, and BMP4 could induce DP-MSCs to become TM-like cells. The results show that the 5 days treatment of these growth factors can upregulate the expression of POM markers of *PITX2*, *FOXC1*, and *FOXC2*, as well as the *PITX2* regulator *PAWR*. These four genes interact with each other and are involved in a common regulatory network for the development of anterior segment of the eye. *FOXC1* and *FOXC2* have similar structure and expression patterns. *PITX2* can inhibit the activity of *FOXC1*, while *PAWR* can inhibit the activity of *PITX2* alone, but together with *FOXC1* or *FOXC2*, *PAWR* increases the activity of *PITX2* [139]. Thus, the upregulation of these genes may cause DP-MSCs to develop some features of TMCs. Our results show the TMC marker *MYOC* mRNA and secreted MYOC protein were upregulated in DP-MSCs with the growth factors treatment. However, for some genes, the data is highly variable, which may in part due to many genes being lowly expressed with Ct values close to threshold for DP-MSCs, either with or without the

treatment of growth factors. This variability may mean that the experiments were underpowered for quantifying expression of some genes such as *AQP1, CHI3L1, MGP,* and *MMP3*, and should be repeated with additional replicates. However, the mRNA expression levels of several other genes including *LMX1B, TIMP2, PITX2, FOXC2,* and *PAWR* did reveal statistically significant differences between human TMCs and DP-MSCs with the growth factors treatment, and the growth factors treated DP-MSCs did not present the functional properties associated with TMCs such as the response to dexamethasone and the contractile ability to collagen. Therefore, it is clear that exposure to RA, TGF-β2 and BMP4 is insufficient to differentiate DP-MSCs to TM-like cells.

The second study sought to investigate the effects of IOP-associated gene knockouts on the morphological and transcriptome profiles of primary human TMCs. It is the first time we combined the techniques of CellPainting, scRNA-seq and CRISPR together to study the gene knockout effects *in vitro*.

In the gene knockout groups with genes related to congenital glaucoma, *GMDS, FOXC1, LTBP2, TEK, and CYP1B1*, we expected to see distinct patterns on the gene expression and morphology. However, no distinct patterns were observed in the transcriptome of these gene knockout groups. In contrast, the *GMDS* knockout group exhibits a pattern with high value of granularity in AGP channel and the *FOXC1* knockout group exhibits a pattern with a low value of granularity features in both AGP channel and mitochondrial channel. The features in AGP channels are related to the status of actin, golgi apparatus and plasma membrane and the features in mitochondrial channel refer to the activity of mitochondria. Previous study of *FOXC1* knock down with small interfering RNA demonstrates that *FOXC1* can affect the expression 849 genes, 357 of which were enriched to the gene ontology term membrane [140]. Thus, the morphological profiles of *FOXC1* knockout group may reflect changed gene regulation in TMCs.

In the gene knockout groups with genes at overlapping loci, *TMCO1* and *ALDH9A1* at chromosome 1 q24, *CAV1, CAV2* and *TES* at chromosome 7 q21, *ANGPTL2, RALGPS1,* and *LMX1B* at chromosome 9 q33, *ME3* and *PRSS23* at chromosome 11 q14, *TXNRD2* and *GNB1L* at chromosome 22 q11, and *KREMEN1* and *EMID1* at chromosome 22q12, we aimed

to see distinct patterns of gene expression and morphology in each pair of genes when compared to the control group, so we could identify the true hit for that loci. In the transcriptome profiles, the gene knockout groups of *TMCO1* and *PRSS23* exhibit a pattern distinct to control groups, which contains a group of upregulated DEGs related to the interferon alpha/beta signaling. The rest of the gene knockout groups seem to be similar to the controls. Interestingly, *MYOC* was upregulated significantly in the gene knockout group of *CAV2*, which suggests *CAV2* is involved in the regulation of myocilin.
The morphological profiles present a different scenario to the cell transcriptomes in some cases. The gene knockout group of *ALDH9A1* and *ME3* show distinct patterns with a low e granularity of features in the mitochondrial channel compared to the controls. *ALDH9A1* encodes aldehyde dehydrogenases, which has a high level of oxidation activity [141]. *ME3* encodes an NADP-dependent malic enzyme involved in carbohydrate metabolism, and it was found to be associated with POAG in a study of mitochondrial genetic variation [142]. Thus, *ALDH9A1* and *ME3* should be positive hits associated with POAG.

The differences between the transcriptome and morphological profiles could be due to the different calculation method for each profile. In transcriptome profiles, DEGs were selected by comparing each gene knockout group versus the control group following the criteria of fold change > 4 and the p value < 10^{-6}, then the relative expression level compared to the controls was selected to represent each gene knockout group. However, the relative expression level reflects the mean expression level of all the cells in that group, which could be affected by the distribution of the dataset and the outliers. A recent scRNA-seq study identified 19 cell types in the human primary TMCs which suggests the dataset could follow a multimodal distribution across different cell types [143], hence our group mean expression levels may not be truly representative of the data. In contrast, we generated the morphological profiles using the median value of each feature, which is more robust when the dataset was not normally distributed or contained outliers [131]. Consequently, our morphological profiles should be more representative.

In summary, this work is the first time that high-throughput morphological profiling (CellPainting) has been combined with scRNA-seq analysis. Together, these platforms have uncovered unifying pathways involved in the homeostasis of TMCs, variation in IOP, and the

pathogenesis of glaucoma. Robust pipelines have been generated to create the profiles of transcriptome and cell morphology. These results demonstrate the gene perturbation can be reflected in the cell morphology with corresponding regulatory pathway, and as a consequence this resource further improves our understanding of gene function in disease.

8. CONCLUSIONS AND FUTURE DIRECTIONS

There are two main overarching conclusions from this body of research. Firstly, although DP-MSCs express markers of TMCs following the exposure of a combination of transcription factors, they have not acquired characteristic functional properties of TMCs. Secondly, high throughput analysis of cellular structure and function through cellpainting and scRNA-seq assays enabled the direct study of genetic perturbations at the single cell resolution. Overall, this work provides a framework for investigating the role of genes involved in the pathogenesis of glaucoma in both genetic and morphology.

Previous methods of generating TM-like cells have been successful by directly co-culturing induced pluripotent cells with primary human TMCs. As such it is clear that other factors secreted from TMCs may contribute to the differentiation to TM-like cells. These growth factors may include epidermal growth factor (EGF), hepatocyte growth factor (HGF), insulin like growth factor (IGF)-1, tumor necrosis factor (TNF) a, platelet-derived growth factor (PDGF)-AA, PDGF-BB, PDGF-AB, and basic fibroblast growth factor (FGF-2) [144]. As such, further work investigating additional growth factors which may be crucial in the maintenance of primary TMCs cultures and prolong the doubling time *in vitro*, should be undertaken. To follow-up previous research [135], we examined the expression level of the common markers, *MYOC, MGP, CHI3L1*, which were also implicated in the work of Sathiyanathan and colleagues [145]. In ongoing differentiation experiments of TMCs, additional specific markers for TMCs should be involved, which include CDH23, SPP1, F5, KCNAB1, FGF9, HEY1, and BDNF, as distinctions from TM-MSCs, cornea and sclera.

In regard to the CROP-seq experiments, this comprehensive transcriptomic and the morphological dataset of TMW cells represents the largest functional follow-up of genes implicated through GWAS to date. In the gene expression comparison, different cell types may be grouped according to their transcriptome patterns [143] and the influence of the non-normal distributions and outliers may be minimized. For the cell morphology, using the median value of each feature, and adding features' dispersion and covariances to the profiles may increase the hit rates and reliability in finding positive genes related to the disease.

9. REFERENCES

1. Kwon, Y. H., Fingert, J. H., Kuehn, M. H. & Alward, W. L. M. Primary Open-Angle Glaucoma. *New England Journal of Medicine* vol. 360 1113–1124 (2009).
2. Quigley, H. A. & Broman, A. T. The number of people with glaucoma worldwide in 2010 and 2020. *Br. J. Ophthalmol.* **90**, 262–267 (2006).
3. White, A., Goldberg, I. & Australian and New Zealand Glaucoma Interest Group and the Royal Australian and New Zealand College of Ophthalmologists. Guidelines for the collaborative care of glaucoma patients and suspects by ophthalmologists and optometrists in Australia. *Clin. Experiment. Ophthalmol.* **42**, 107–117 (2014).
4. Dirani, M. *et al.* Economic impact of primary open-angle glaucoma in Australia. *Clin. Experiment. Ophthalmol.* **39**, 623–632 (2011).
5. Weinreb, R. N., Aung, T. & Medeiros, F. A. The pathophysiology and treatment of glaucoma: a review. *JAMA* **311**, 1901–1911 (2014).
6. Fechtner, R. D. & Weinreb, R. N. Mechanisms of optic nerve damage in primary open angle glaucoma. *Surv. Ophthalmol.* **39**, 23–42 (1994).
7. Quigley, H. A. *et al.* Retrograde axonal transport of BDNF in retinal ganglion cells is blocked by acute IOP elevation in rats. *Invest. Ophthalmol. Vis. Sci.* **41**, 3460–3466 (2000).
8. Ko, M.-L., Peng, P.-H., Ma, M.-C., Ritch, R. & Chen, C.-F. Dynamic changes in reactive oxygen species and antioxidant levels in retinas in experimental glaucoma. *Free Radic. Biol. Med.* **39**, 365–373 (2005).
9. Hernandez, M. R. The optic nerve head in glaucoma: role of astrocytes in tissue remodeling. *Prog. Retin. Eye Res.* **19**, 297–321 (2000).
10. Nakazawa, T. *et al.* Tumor necrosis factor-alpha mediates oligodendrocyte death and delayed retinal ganglion cell loss in a mouse model of glaucoma. *J. Neurosci.* **26**, 12633–12641 (2006).
11. Ren, R. *et al.* Cerebrospinal fluid pressure in glaucoma: a prospective study. *Ophthalmology* **117**,

259–266 (2010).

12. Wang, N. *et al.* Orbital cerebrospinal fluid space in glaucoma: the Beijing intracranial and intraocular pressure (iCOP) study. *Ophthalmology* **119**, 2065–2073.e1 (2012).
13. Roy Chowdhury, U. & Fautsch, M. P. Intracranial Pressure and Its Relationship to Glaucoma: Current Understanding and Future Directions. *Med Hypothesis Discov Innov Ophthalmol* **4**, 71–80 (2015).
14. Stone, E. M. *et al.* Identification of a gene that causes primary open angle glaucoma. *Science* **275**, 668–670 (1997).
15. Rezaie, T. *et al.* Adult-onset primary open-angle glaucoma caused by mutations in optineurin. *Science* **295**, 1077–1079 (2002).
16. Fingert, J. H. Primary open-angle glaucoma genes. *Eye* **25**, 587–595 (2011).
17. Tamm, E. R. Myocilin and glaucoma: facts and ideas. *Prog. Retin. Eye Res.* **21**, 395–428 (2002).
18. Liu, Y. & Allingham, R. R. Major review: Molecular genetics of primary open-angle glaucoma. *Exp. Eye Res.* **160**, 62–84 (2017).
19. Cirulli, E. T. *et al.* Exome sequencing in amyotrophic lateral sclerosis identifies risk genes and pathways. *Science* **347**, 1436–1441 (2015).
20. Welter, D. *et al.* The NHGRI GWAS Catalog, a curated resource of SNP-trait associations. *Nucleic Acids Res.* **42**, D1001–6 (2014).
21. Thorleifsson, G. *et al.* Common variants near CAV1 and CAV2 are associated with primary open-angle glaucoma. *Nat. Genet.* **42**, 906–909 (2010).
22. Burdon, K. P. *et al.* Genome-wide association study identifies susceptibility loci for open angle glaucoma at TMCO1 and CDKN2B-AS1. *Nat. Genet.* **43**, 574–578 (2011).
23. Gharahkhani, P. *et al.* Common variants near ABCA1, AFAP1 and GMDS confer risk of primary open-angle glaucoma. *Nat. Genet.* **46**, 1120–1125 (2014).
24. Bailey, J. N. C. *et al.* Genome-wide association analysis identifies TXNRD2, ATXN2 and FOXC1 as susceptibility loci for primary open-angle glaucoma. *Nat. Genet.* **48**, 189–194 (2016).

25. Gu, X., Reagan, A. M., McClellan, M. E. & Elliott, M. H. Caveolins and caveolae in ocular physiology and pathophysiology. *Prog. Retin. Eye Res.* **56**, 84–106 (2017).

26. Gao, S. & Jakobs, T. C. Mice Homozygous for a Deletion in the Glaucoma Susceptibility Locus INK4 Show Increased Vulnerability of Retinal Ganglion Cells to Elevated Intraocular Pressure. *Am. J. Pathol.* **186**, 985–1005 (2016).

27. Cheng, C.-Y. *et al.* Association of common SIX6 polymorphisms with peripapillary retinal nerve fiber layer thickness: the Singapore Chinese Eye Study. *Invest. Ophthalmol. Vis. Sci.* **56**, 478–483 (2014).

28. Skowronska-Krawczyk, D. *et al.* P16INK4a Upregulation Mediated by SIX6 Defines Retinal Ganglion Cell Pathogenesis in Glaucoma. *Mol. Cell* **59**, 931–940 (2015).

29. Chen, Y. *et al.* Common variants near ABCA1 and in PMM2 are associated with primary open-angle glaucoma. *Nat. Genet.* **46**, 1115–1119 (2014).

30. Caprioli, J., Munemasa, Y., Kwong, J. M. K. & Piri, N. Overexpression of thioredoxins 1 and 2 increases retinal ganglion cell survival after pharmacologically induced oxidative stress, optic nerve transection, and in experimental glaucoma. *Trans. Am. Ophthalmol. Soc.* **107**, 161–165 (2009).

31. Gould, D. B., Smith, R. S. & John, S. W. M. Anterior segment development relevant to glaucoma. *Int. J. Dev. Biol.* **48**, 1015–1029 (2004).

32. Lattante, S. *et al.* Contribution of ATXN2 intermediary polyQ expansions in a spectrum of neurodegenerative disorders. *Neurology* **83**, 990–995 (2014).

33. MacGregor, S. *et al.* Genome-wide association study of intraocular pressure uncovers new pathways to glaucoma. *Nat. Genet.* **50**, 1067–1071 (2018).

34. Wiggs, J. L. & Pasquale, L. R. Genetics of glaucoma. *Hum. Mol. Genet.* **26**, R21–R27 (2017).

35. Fautsch, M. P. & Johnson, D. H. Aqueous humor outflow: what do we know? Where will it lead us? *Invest. Ophthalmol. Vis. Sci.* **47**, 4181–4187 (2006).

36. Inoue, T. & Tanihara, H. Rho-associated kinase inhibitors: a novel glaucoma therapy. *Prog.*

Retin. Eye Res. **37**, 1–12 (2013).

37. Flocks, M. The anatomy of the trabecular meshwork as seen in tangential section. *AMA Arch. Ophthalmol.* **56**, 708–718 (1956).
38. Tamm, E. R. The trabecular meshwork outflow pathways: structural and functional aspects. *Exp. Eye Res.* **88**, 648–655 (2009).
39. Mäepea, O. & Bill, A. Pressures in the juxtacanalicular tissue and Schlemm's canal in monkeys. *Exp. Eye Res.* **54**, 879–883 (1992).
40. Alvarado, J., Murphy, C. & Juster, R. Trabecular meshwork cellularity in primary open-angle glaucoma and nonglaucomatous normals. *Ophthalmology* **91**, 564–579 (1984).
41. Acott, T. S. & Kelley, M. J. Extracellular matrix in the trabecular meshwork. *Exp. Eye Res.* **86**, 543–561 (2008).
42. Faralli, J. A., Filla, M. S. & Peters, D. M. Role of Fibronectin in Primary Open Angle Glaucoma. *Cells* **8**, (2019).
43. Baleriola, J. *et al.* Apoptosis in the trabecular meshwork of glaucomatous patients. *Mol. Vis.* **14**, 1513–1516 (2008).
44. Li, J., Tripathi, B. J. & Tripathi, R. C. Modulation of pre-mRNA splicing and protein production of fibronectin by TGF-beta2 in porcine trabecular cells. *Invest. Ophthalmol. Vis. Sci.* **41**, 3437–3443 (2000).
45. Iyer, P., Maddala, R., Pattabiraman, P. P. & Rao, P. V. Connective tissue growth factor-mediated upregulation of neuromedin U expression in trabecular meshwork cells and its role in homeostasis of aqueous humor outflow. *Invest. Ophthalmol. Vis. Sci.* **53**, 4952–4962 (2012).
46. Junglas, B. *et al.* Connective tissue growth factor causes glaucoma by modifying the actin cytoskeleton of the trabecular meshwork. *Am. J. Pathol.* **180**, 2386–2403 (2012).
47. Hewitt, A. W., Mackey, D. A. & Craig, J. E. Myocilin allele-specific glaucoma phenotype database. *Hum. Mutat.* **29**, 207–211 (2008).
48. Wiggs, J. L., Del Bono, E. A., Schuman, J. S., Hutchinson, B. T. & Walton, D. S. Clinical

features of five pedigrees genetically linked to the juvenile glaucoma locus on chromosome 1q21-q31. *Ophthalmology* **102**, 1782–1789 (1995).

49. Fingert, J. H., Stone, E. M., Sheffield, V. C. & Alward, W. L. M. Myocilin glaucoma. *Surv. Ophthalmol.* **47**, 547–561 (2002).
50. Kim, B. S. *et al.* Targeted Disruption of the Myocilin Gene (Myoc) Suggests that Human Glaucoma-Causing Mutations Are Gain of Function. *Mol. Cell. Biol.* **21**, 7707–7713 (2001).
51. Gould, D. B. *et al.* Genetically increasing Myoc expression supports a necessary pathologic role of abnormal proteins in glaucoma. *Mol. Cell. Biol.* **24**, 9019–9025 (2004).
52. Zhou, Z. & Vollrath, D. A cellular assay distinguishes normal and mutant TIGR/myocilin protein. *Hum. Mol. Genet.* **8**, 2221–2228 (1999).
53. Donegan, R. K. *et al.* Structural basis for misfolding in myocilin-associated glaucoma. *Hum. Mol. Genet.* **24**, 2111–2124 (2015).
54. Donegan, R. K., Hill, S. E., Turnage, K. C., Orwig, S. D. & Lieberman, R. L. The glaucoma-associated olfactomedin domain of myocilin is a novel calcium binding protein. *J. Biol. Chem.* **287**, 43370–43377 (2012).
55. Jacobson, N. *et al.* Non-secretion of mutant proteins of the glaucoma gene myocilin in cultured trabecular meshwork cells and in aqueous humor. *Hum. Mol. Genet.* **10**, 117–125 (2001).
56. He, Y., Leung, K. W., Zhuo, Y.-H. & Ge, J. Pro370Leu mutant myocilin impairs mitochondrial functions in human trabecular meshwork cells. *Mol. Vis.* **15**, 815–825 (2009).
57. Boland, M. V. *et al.* Comparative effectiveness of treatments for open-angle glaucoma: a systematic review for the U.S. Preventive Services Task Force. *Ann. Intern. Med.* **158**, 271–279 (2013).
58. Glaucoma: diagnosis and management | Guidance | NICE.
59. Feng, Y., LoGrasso, P. V., Defert, O. & Li, R. Rho Kinase (ROCK) Inhibitors and Their Therapeutic Potential. *J. Med. Chem.* **59**, 2269–2300 (2016).
60. Tanihara, H. *et al.* Intra-ocular pressure-lowering effects of a Rho kinase inhibitor, ripasudil

(K-115), over 24 hours in primary open-angle glaucoma and ocular hypertension: a randomized, open-label, crossover study. *Acta Ophthalmol.* **93**, e254–60 (2015).

61. Izzotti, A., Saccà, S. C., Longobardi, M. & Cartiglia, C. Sensitivity of ocular anterior chamber tissues to oxidative damage and its relevance to the pathogenesis of glaucoma. *Invest. Ophthalmol. Vis. Sci.* **50**, 5251–5258 (2009).
62. Luna, C. *et al.* Resveratrol prevents the expression of glaucoma markers induced by chronic oxidative stress in trabecular meshwork cells. *Food Chem. Toxicol.* **47**, 198–204 (2009).
63. Tourtas, T., Birke, M. T., Kruse, F. E., Welge-Lüssen, U.-C. & Birke, K. Preventive effects of omega-3 and omega-6 Fatty acids on peroxide mediated oxidative stress responses in primary human trabecular meshwork cells. *PLoS One* **7**, e31340 (2012).
64. Zhao, J. *et al.* Oxidative stress in the trabecular meshwork (Review). *Int. J. Mol. Med.* **38**, 995–1002 (2016).
65. Welch, W. J. & Brown, C. R. Influence of molecular and chemical chaperones on protein folding. *Cell Stress Chaperones* **1**, 109–115 (1996).
66. Zode, G. S. *et al.* Reduction of ER stress via a chemical chaperone prevents disease phenotypes in a mouse model of primary open angle glaucoma. *J. Clin. Invest.* **121**, 3542–3553 (2011).
67. Zode, G. S. *et al.* Topical ocular sodium 4-phenylbutyrate rescues glaucoma in a myocilin mouse model of primary open-angle glaucoma. *Invest. Ophthalmol. Vis. Sci.* **53**, 1557–1565 (2012).
68. Weinreb, R. N. & Lindsey, J. D. The importance of models in glaucoma research. *J. Glaucoma* **14**, 302–304 (2005).
69. Yücel, Y. H., Kalichman, M. W., Mizisin, A. P., Powell, H. C. & Weinreb, R. N. Histomorphometric analysis of optic nerve changes in experimental glaucoma. *J. Glaucoma* **8**, 38–45 (1999).
70. Ju, W.-K. *et al.* Intraocular pressure elevation induces mitochondrial fission and triggers OPA1 release in glaucomatous optic nerve. *Invest. Ophthalmol. Vis. Sci.* **49**, 4903–4911 (2008).
71. Zhu, W. *et al.* Transplantation of iPSC-derived TM cells rescues glaucoma phenotypes in vivo.

Proc. Natl. Acad. Sci. U. S. A. **113**, E3492–500 (2016).

72. Polansky, J. R. & Alvarado, J. A. Isolation and evaluation of target cells in glaucoma research: hormone receptors and drug responses. *Curr. Eye Res.* **4**, 267–279 (1985).
73. Lindsey, J. D. & Weinreb, R. N. Survival and differentiation of purified retinal ganglion cells in a chemically defined microenvironment. *Invest. Ophthalmol. Vis. Sci.* **35**, 3640–3648 (1994).
74. Stamer, W. D., Seftor, R. E., Williams, S. K., Samaha, H. A. & Snyder, R. W. Isolation and culture of human trabecular meshwork cells by extracellular matrix digestion. *Curr. Eye Res.* **14**, 611–617 (1995).
75. Zhang, X., Clark, A. F. & Yorio, T. Interactions of endothelin-1 with dexamethasone in primary cultured human trabecular meshwork cells. *Invest. Ophthalmol. Vis. Sci.* **44**, 5301–5308 (2003).
76. Gottanka, J., Chan, D., Eichhorn, M., Lütjen-Drecoll, E. & Ethier, C. R. Effects of TGF-beta2 in perfused human eyes. *Invest. Ophthalmol. Vis. Sci.* **45**, 153–158 (2004).
77. Keller, K. E. *et al.* Consensus recommendations for trabecular meshwork cell isolation, characterization and culture. *Exp. Eye Res.* **171**, 164–173 (2018).
78. Cvekl, A. & Duncan, M. K. Genetic and epigenetic mechanisms of gene regulation during lens development. *Prog. Retin. Eye Res.* **26**, 555–597 (2007).
79. Johnston, M. C., Noden, D. M., Hazelton, R. D., Coulombre, J. L. & Coulombre, A. J. Origins of avian ocular and periocular tissues. *Exp. Eye Res.* **29**, 27–43 (1979).
80. Mori, M., Ghyselinck, N. B., Chambon, P. & Mark, M. Systematic immunolocalization of retinoid receptors in developing and adult mouse eyes. *Invest. Ophthalmol. Vis. Sci.* **42**, 1312–1318 (2001).
81. Matt, N. *et al.* Retinoic acid-dependent eye morphogenesis is orchestrated by neural crest cells. *Development* **132**, 4789–4800 (2005).
82. Altucci, L. & Gronemeyer, H. Nuclear receptors in cell life and death. *Trends Endocrinol. Metab.* **12**, 460–468 (2001).
83. Kidson, S. H., Kume, T., Deng, K., Winfrey, V. & Hogan, B. L. The forkhead/winged-helix gene,

Mf1, is necessary for the normal development of the cornea and formation of the anterior chamber in the mouse eye. *Dev. Biol.* **211**, 306–322 (1999).

84. Hogan, B. L. Bone morphogenetic proteins: multifunctional regulators of vertebrate development. *Genes Dev.* **10**, 1580–1594 (1996).
85. Chang, B. *et al.* Haploinsufficient Bmp4 ocular phenotypes include anterior segment dysgenesis with elevated intraocular pressure. *BMC Genet.* **2**, 18 (2001).
86. Ittner, L. M. *et al.* Compound developmental eye disorders following inactivation of TGFbeta signaling in neural-crest stem cells. *J. Biol.* **4**, 11 (2005).
87. Ding, Q. J. *et al.* Induction of trabecular meshwork cells from induced pluripotent stem cells. *Invest. Ophthalmol. Vis. Sci.* **55**, 7065–7072 (2014).
88. Xue, W., Comes, N. & Borrás, T. Presence of an established calcification marker in trabecular meshwork tissue of glaucoma donors. *Invest. Ophthalmol. Vis. Sci.* **48**, 3184–3194 (2007).
89. Mao, W. *et al.* Characterization of a spontaneously immortalized bovine trabecular meshwork cell line. *Exp. Eye Res.* **105**, 53–59 (2012).
90. Stamer, W. D. & Clark, A. F. The many faces of the trabecular meshwork cell. *Exp. Eye Res.* **158**, 112–123 (2017).
91. Polansky, J. R., Fauss, D. J. & Zimmerman, C. C. Regulation of TIGR/MYOC gene expression in human trabecular meshwork cells. *Eye* **14 (Pt 3B)**, 503–514 (2000).
92. Faralli, J. A., Clark, R. W., Filla, M. S. & Peters, D. M. NFATc1 activity regulates the expression of myocilin induced by dexamethasone. *Exp. Eye Res.* **130**, 9–16 (2015).
93. Koga, T. *et al.* Rho-associated protein kinase inhibitor, Y-27632, induces alterations in adhesion, contraction and motility in cultured human trabecular meshwork cells. *Exp. Eye Res.* **82**, 362–370 (2006).
94. Nakamura, Y. *et al.* Signaling mechanism of TGF-beta1-induced collagen contraction mediated by bovine trabecular meshwork cells. *Invest. Ophthalmol. Vis. Sci.* **43**, 3465–3472 (2002).
95. Wiedenheft, B., Sternberg, S. H. & Doudna, J. A. RNA-guided genetic silencing systems in

bacteria and archaea. *Nature* **482**, 331–338 (2012).

96. Bhaya, D., Davison, M. & Barrangou, R. CRISPR-Cas systems in bacteria and archaea: versatile small RNAs for adaptive defense and regulation. *Annu. Rev. Genet.* **45**, 273–297 (2011).
97. Jinek, M. *et al.* A programmable dual-RNA-guided DNA endonuclease in adaptive bacterial immunity. *Science* **337**, 816–821 (2012).
98. Terns, M. P. & Terns, R. M. CRISPR-based adaptive immune systems. *Current Opinion in Microbiology* vol. 14 321–327 (2011).
99. Komor, A. C., Badran, A. H. & Liu, D. R. CRISPR-Based Technologies for the Manipulation of Eukaryotic Genomes. *Cell* **168**, 20–36 (2017).
100. Sanjana, N. E. Genome-scale CRISPR pooled screens. *Anal. Biochem.* **532**, 95–99 (2017).
101. Iliakis, G. *et al.* Mechanisms of DNA double strand break repair and chromosome aberration formation. *Cytogenet. Genome Res.* **104**, 14–20 (2004).
102. Pardo, B., Gómez-González, B. & Aguilera, A. DNA repair in mammalian cells: DNA double-strand break repair: how to fix a broken relationship. *Cell. Mol. Life Sci.* **66**, 1039–1056 (2009).
103. Shalem, O., Sanjana, N. E. & Zhang, F. High-throughput functional genomics using CRISPR–Cas9. *Nat. Rev. Genet.* **16**, 299–311 (2015).
104. Chen, S. *et al.* Genome-wide CRISPR Screen in a Mouse Model of Tumor Growth and Metastasis. *Cell* vol. 160 1246–1260 (2015).
105. Shi, J. *et al.* Discovery of cancer drug targets by CRISPR-Cas9 screening of protein domains. *Nat. Biotechnol.* **33**, 661–667 (2015).
106. Parnas, O. *et al.* A Genome-wide CRISPR Screen in Primary Immune Cells to Dissect Regulatory Networks. *Cell* **162**, 675–686 (2015).
107. Zhou, Y. *et al.* High-throughput screening of a CRISPR/Cas9 library for functional genomics in human cells. *Nature* **509**, 487–491 (2014).
108. Hung, S. S. C. *et al.* AAV-Mediated CRISPR/Cas Gene Editing of Retinal Cells In Vivo. *Invest.*

Ophthalmol. Vis. Sci. **57**, 3470–3476 (2016).

109. Jain, A. *et al.* CRISPR-Cas9–based treatment of myocilin-associated glaucoma. *Proc. Natl. Acad. Sci. U. S. A.* **114**, 11199–11204 (2017).

110. Bray, M.-A. *et al.* Cell Painting, a high-content image-based assay for morphological profiling using multiplexed fluorescent dyes. *Nat. Protoc.* **11**, 1757–1774 (2016).

111. Gustafsdottir, S. M. *et al.* Multiplex cytological profiling assay to measure diverse cellular states. *PLoS One* **8**, e80999 (2013).

112. Singh, S. *et al.* Morphological Profiles of RNAi-Induced Gene Knockdown Are Highly Reproducible but Dominated by Seed Effects. *PLoS One* **10**, e0131370 (2015).

113. Tang, F. *et al.* mRNA-Seq whole-transcriptome analysis of a single cell. *Nat. Methods* **6**, 377–382 (2009).

114. Tanay, A. & Regev, A. Scaling single-cell genomics from phenomenology to mechanism. *Nature* **541**, 331–338 (2017).

115. Picelli, S. *et al.* Smart-seq2 for sensitive full-length transcriptome profiling in single cells. *Nat. Methods* **10**, 1096–1098 (2013).

116. Macosko, E. Z. *et al.* Highly Parallel Genome-wide Expression Profiling of Individual Cells Using Nanoliter Droplets. *Cell* **161**, 1202–1214 (2015).

117. Salomon, R. *et al.* Droplet-based single cell RNAseq tools: a practical guide. *Lab Chip* **19**, 1706–1727 (2019).

118. Hwang, B., Lee, J. H. & Bang, D. Single-cell RNA sequencing technologies and bioinformatics pipelines. *Exp. Mol. Med.* **50**, 96 (2018).

119. Kim, K.-T. *et al.* Single-cell mRNA sequencing identifies subclonal heterogeneity in anti-cancer drug responses of lung adenocarcinoma cells. *Genome Biol.* **16**, 127 (2015).

120. Smillie, C. S. *et al.* Intra- and Inter-cellular Rewiring of the Human Colon during Ulcerative Colitis. *Cell* **178**, 714–730.e22 (2019).

121. Lukowski, S. W., Lo, C. Y., Sharov, A. A. & Nguyen, Q. A single−cell transcriptome atlas of the

adult human retina. *EMBO J.* (2019).

122. Patel, G. *et al.* Molecular taxonomy of human ocular outflow tissues defined by single-cell transcriptomics. *Proc. Natl. Acad. Sci. U. S. A.* **117**, 12856–12867 (2020).
123. Datlinger, P. *et al.* Pooled CRISPR screening with single-cell transcriptome readout. *Nat. Methods* **14**, 297–301 (2017).
124. Datlinger, P. *et al.* Pooled CRISPR screening with single-cell transcriptome readout. *Nat. Methods* **14**, 297–301 (2017).
125. Sanjana, N. E., Shalem, O. & Zhang, F. Improved vectors and genome-wide libraries for CRISPR screening. *Nat. Methods* **11**, 783–784 (2014).
126. Gilbert, L. A. *et al.* CRISPR-mediated modular RNA-guided regulation of transcription in eukaryotes. *Cell* **154**, 442–451 (2013).
127. Datlinger, P. *et al.* Pooled CRISPR screening with single-cell transcriptome readout. *Nat. Methods* **14**, 297–301 (2017).
128. Platt, R. J. *et al.* CRISPR-Cas9 knockin mice for genome editing and cancer modeling. *Cell* **159**, 440–455 (2014).
129. Datlinger, P. *et al.* Pooled CRISPR screening with single-cell transcriptome readout. *Nat. Methods* **14**, 297–301 (2017).
130. Datlinger, P. *et al.* Pooled CRISPR screening with single-cell transcriptome readout. *Nat. Methods* **14**, 297–301 (2017).
131. Caicedo, J. C. *et al.* Data-analysis strategies for image-based cell profiling. *Nat. Methods* **14**, 849–863 (2017).
132. Huber, W., von Heydebreck, A., Sültmann, H., Poustka, A. & Vingron, M. Variance stabilization applied to microarray data calibration and to the quantification of differential expression. *Bioinformatics* **18 Suppl 1**, S96–104 (2002).
133. Durbin, B. P., Hardin, J. S., Hawkins, D. M. & Rocke, D. M. A variance-stabilizing transformation for gene-expression microarray data. *Bioinformatics* **18 Suppl 1**, S105–10 (2002).

134. Marsaglia, G., Marsaglia, J. & Others. Evaluating the anderson-darling distribution. *J. Stat. Softw.* **9**, 1–5 (2004).

135. McDonald, N. L. V. Effects of retinoic acid, TGF on the expression of PITX2 mesenchymal stem cells (Thesis for Bachelor of Biomedical Science Honours). (University of Tasmania, 2015).

136. Zhou, Y. *et al.* Metascape provides a biologist-oriented resource for the analysis of systems-level datasets. *Nat. Commun.* **10**, 1523 (2019).

137. Scheetz, T. E. *et al.* Glaucoma Risk Alleles in the Ocular Hypertension Treatment Study. *Ophthalmology* **123**, 2527–2536 (2016).

138. Fingert, J. H. *et al.* Copy number variations on chromosome 12q14 in patients with normal tension glaucoma. *Hum. Mol. Genet.* **20**, 2482–2494 (2011).

139. Acharya, M., Huang, L., Fleisch, V. C., Allison, W. T. & Walter, M. A. A complex regulatory network of transcription factors critical for ocular development and disease. *Hum. Mol. Genet.* **20**, 1610–1624 (2011).

140. Paylakhi, S. H. *et al.* FOXC1 in human trabecular meshwork cells is involved in regulatory pathway that includes miR-204, MEIS2, and ITGβ1. *Exp. Eye Res.* **111**, 112–121 (2013).

141. Končitíková, R. *et al.* Kinetic and structural analysis of human ALDH9A1. *Biosci. Rep.* **39**, (2019).

142. Khawaja, A. P. *et al.* Assessing the Association of Mitochondrial Genetic Variation With Primary Open-Angle Glaucoma Using Gene-Set Analyses. *Invest. Ophthalmol. Vis. Sci.* **57**, 5046–5052 (2016).

143. van Zyl, T. *et al.* Cell Atlas of Aqueous Humor Outflow Pathways in Eyes of Humans and Four Model Species Provides Insights into Glaucoma Pathogenesis. doi:10.1101/2020.02.04.933911.

144. Wordinger, R. J. *et al.* Cultured human trabecular meshwork cells express functional growth factor receptors. *Invest. Ophthalmol. Vis. Sci.* **39**, 1575–1589 (1998).

145. Sathiyanathan, P., Tay, C. Y. & Stanton, L. W. Transcriptome analysis for the identification of cellular markers related to trabecular meshwork differentiation. *BMC Genomics* **18**, 383 (2017).

10. APPENDIX

Appendix List 1. *Morphological features extracted from CellProfiler*

"Cell_AreaShape_Area"
"Cell_AreaShape_Compactness"
"Cell_AreaShape_Eccentricity"
"Cell_AreaShape_Extent"
"Cell_AreaShape_FormFactor"
"Cell_AreaShape_MajorAxisLength"
"Cell_AreaShape_MaxFeretDiameter"
"Cell_AreaShape_MaximumRadius"
"Cell_AreaShape_MeanRadius"
"Cell_AreaShape_MedianRadius"
"Cell_AreaShape_MinFeretDiameter"
"Cell_AreaShape_MinorAxisLength"
"Cell_AreaShape_Orientation"
"Cell_AreaShape_Perimeter"
"Cell_AreaShape_Solidity"
"Cell_AreaShape_Zernike_0_0"
"Cell_AreaShape_Zernike_1_1"
"Cell_AreaShape_Zernike_2_0"
"Cell_AreaShape_Zernike_2_2"
"Cell_AreaShape_Zernike_3_1"
"Cell_AreaShape_Zernike_3_3"
"Cell_AreaShape_Zernike_4_0"
"Cell_AreaShape_Zernike_4_2"
"Cell_AreaShape_Zernike_4_4"
"Cell_AreaShape_Zernike_5_1"
"Cell_AreaShape_Zernike_5_3"
"Cell_AreaShape_Zernike_5_5"
"Cell_AreaShape_Zernike_6_0"
"Cell_AreaShape_Zernike_6_2"
"Cell_AreaShape_Zernike_6_4"
"Cell_AreaShape_Zernike_6_6"
"Cell_AreaShape_Zernike_7_1"
"Cell_AreaShape_Zernike_7_3"
"Cell_AreaShape_Zernike_7_5"
"Cell_AreaShape_Zernike_7_7"
"Cell_AreaShape_Zernike_8_0"
"Cell_AreaShape_Zernike_8_2"
"Cell_AreaShape_Zernike_8_4"
"Cell_AreaShape_Zernike_8_6"
"Cell_AreaShape_Zernike_8_8"
"Cell_AreaShape_Zernike_9_1"
"Cell_AreaShape_Zernike_9_3"
"Cell_AreaShape_Zernike_9_5"
"Cell_AreaShape_Zernike_9_7"
"Cell_AreaShape_Zernike_9_9"
"Cell_Correlation_Correlation_corAGP_corRNA"
"Cell_Correlation_Correlation_corER_corAGP"
"Cell_Correlation_Correlation_corER_corMito"
"Cell_Correlation_Correlation_corER_corRNA"
"Cell_Correlation_Correlation_corMito_corAGP"
"Cell_Correlation_Correlation_corMito_corRNA"

"Cell_Correlation_Correlation_corNucleus_corAGP"
"Cell_Correlation_Correlation_corNucleus_corER"
"Cell_Correlation_Correlation_corNucleus_corMito"
"Cell_Correlation_Correlation_corNucleus_corRNA"
"Cell_Correlation_Costes_corAGP_corER"
"Cell_Correlation_Costes_corAGP_corMito"
"Cell_Correlation_Costes_corAGP_corNucleus"
"Cell_Correlation_Costes_corAGP_corRNA"
"Cell_Correlation_Costes_corER_corAGP"
"Cell_Correlation_Costes_corER_corMito"
"Cell_Correlation_Costes_corER_corNucleus"
"Cell_Correlation_Costes_corER_corRNA"
"Cell_Correlation_Costes_corMito_corAGP"
"Cell_Correlation_Costes_corMito_corER"
"Cell_Correlation_Costes_corMito_corNucleus"
"Cell_Correlation_Costes_corMito_corRNA"
"Cell_Correlation_Costes_corNucleus_corAGP"
"Cell_Correlation_Costes_corNucleus_corER"
"Cell_Correlation_Costes_corNucleus_corMito"
"Cell_Correlation_Costes_corNucleus_corRNA"
"Cell_Correlation_Costes_corRNA_corAGP"
"Cell_Correlation_Costes_corRNA_corER"
"Cell_Correlation_Costes_corRNA_corMito"
"Cell_Correlation_Costes_corRNA_corNucleus"
"Cell_Correlation_K_corAGP_corER"
"Cell_Correlation_K_corAGP_corMito"
"Cell_Correlation_K_corAGP_corNucleus"
"Cell_Correlation_K_corAGP_corRNA"
"Cell_Correlation_K_corER_corAGP"
"Cell_Correlation_K_corER_corMito"
"Cell_Correlation_K_corER_corNucleus"
"Cell_Correlation_K_corER_corRNA"
"Cell_Correlation_K_corMito_corAGP"
"Cell_Correlation_K_corMito_corER"
"Cell_Correlation_K_corMito_corNucleus"
"Cell_Correlation_K_corMito_corRNA"
"Cell_Correlation_K_corNucleus_corAGP"
"Cell_Correlation_K_corNucleus_corER"
"Cell_Correlation_K_corNucleus_corMito"
"Cell_Correlation_K_corNucleus_corRNA"
"Cell_Correlation_K_corRNA_corAGP"
"Cell_Correlation_K_corRNA_corER"
"Cell_Correlation_K_corRNA_corMito"
"Cell_Correlation_K_corRNA_corNucleus"
"Cell_Correlation_Manders_corAGP_corER"
"Cell_Correlation_Manders_corAGP_corMito"
"Cell_Correlation_Manders_corAGP_corNucleus"
"Cell_Correlation_Manders_corAGP_corRNA"
"Cell_Correlation_Manders_corER_corAGP"
"Cell_Correlation_Manders_corER_corMito"
"Cell_Correlation_Manders_corER_corNucleus"
"Cell_Correlation_Manders_corER_corRNA"
"Cell_Correlation_Manders_corMito_corAGP"
"Cell_Correlation_Manders_corMito_corER"
"Cell_Correlation_Manders_corMito_corNucleus"
"Cell_Correlation_Manders_corMito_corRNA"
"Cell_Correlation_Manders_corNucleus_corAGP"
"Cell_Correlation_Manders_corNucleus_corER"
"Cell_Correlation_Manders_corNucleus_corMito"
"Cell_Correlation_Manders_corNucleus_corRNA"
"Cell_Correlation_Manders_corRNA_corAGP"
"Cell_Correlation_Manders_corRNA_corER"

"Cell_Correlation_Manders_corRNA_corMito"
"Cell_Correlation_Manders_corRNA_corNucleus"
"Cell_Correlation_Overlap_corAGP_corRNA"
"Cell_Correlation_Overlap_corER_corAGP"
"Cell_Correlation_Overlap_corER_corMito"
"Cell_Correlation_Overlap_corER_corRNA"
"Cell_Correlation_Overlap_corMito_corAGP"
"Cell_Correlation_Overlap_corMito_corRNA"
"Cell_Correlation_Overlap_corNucleus_corAGP"
"Cell_Correlation_Overlap_corNucleus_corER"
"Cell_Correlation_Overlap_corNucleus_corMito"
"Cell_Correlation_Overlap_corNucleus_corRNA"
"Cell_Correlation_RWC_corAGP_corER"
"Cell_Correlation_RWC_corAGP_corMito"
"Cell_Correlation_RWC_corAGP_corNucleus"
"Cell_Correlation_RWC_corAGP_corRNA"
"Cell_Correlation_RWC_corER_corAGP"
"Cell_Correlation_RWC_corER_corMito"
"Cell_Correlation_RWC_corER_corNucleus"
"Cell_Correlation_RWC_corER_corRNA"
"Cell_Correlation_RWC_corMito_corAGP"
"Cell_Correlation_RWC_corMito_corER"
"Cell_Correlation_RWC_corMito_corNucleus"
"Cell_Correlation_RWC_corMito_corRNA"
"Cell_Correlation_RWC_corNucleus_corAGP"
"Cell_Correlation_RWC_corNucleus_corER"
"Cell_Correlation_RWC_corNucleus_corMito"
"Cell_Correlation_RWC_corNucleus_corRNA"
"Cell_Correlation_RWC_corRNA_corAGP"
"Cell_Correlation_RWC_corRNA_corER"
"Cell_Correlation_RWC_corRNA_corMito"
"Cell_Correlation_RWC_corRNA_corNucleus"
"Cell_Granularity_10_corAGP"
"Cell_Granularity_10_corER"
"Cell_Granularity_10_corMito"
"Cell_Granularity_10_corRNA"
"Cell_Granularity_11_corAGP"
"Cell_Granularity_11_corER"
"Cell_Granularity_11_corMito"
"Cell_Granularity_11_corRNA"
"Cell_Granularity_12_corAGP"
"Cell_Granularity_12_corER"
"Cell_Granularity_12_corMito"
"Cell_Granularity_12_corRNA"
"Cell_Granularity_13_corAGP"
"Cell_Granularity_13_corER"
"Cell_Granularity_13_corMito"
"Cell_Granularity_13_corRNA"
"Cell_Granularity_14_corAGP"
"Cell_Granularity_14_corER"
"Cell_Granularity_14_corMito"
"Cell_Granularity_14_corRNA"
"Cell_Granularity_15_corAGP"
"Cell_Granularity_15_corER"
"Cell_Granularity_15_corMito"
"Cell_Granularity_15_corRNA"
"Cell_Granularity_16_corAGP"
"Cell_Granularity_16_corER"
"Cell_Granularity_16_corMito"
"Cell_Granularity_16_corRNA"
"Cell_Granularity_1_corAGP"
"Cell_Granularity_1_corER"

"Cell_Granularity_1_corMito"
"Cell_Granularity_1_corRNA"
"Cell_Granularity_2_corAGP"
"Cell_Granularity_2_corER"
"Cell_Granularity_2_corMito"
"Cell_Granularity_2_corRNA"
"Cell_Granularity_3_corAGP"
"Cell_Granularity_3_corER"
"Cell_Granularity_3_corMito"
"Cell_Granularity_3_corRNA"
"Cell_Granularity_4_corAGP"
"Cell_Granularity_4_corER"
"Cell_Granularity_4_corMito"
"Cell_Granularity_4_corRNA"
"Cell_Granularity_5_corAGP"
"Cell_Granularity_5_corER"
"Cell_Granularity_5_corMito"
"Cell_Granularity_5_corRNA"
"Cell_Granularity_6_corAGP"
"Cell_Granularity_6_corER"
"Cell_Granularity_6_corMito"
"Cell_Granularity_6_corRNA"
"Cell_Granularity_7_corAGP"
"Cell_Granularity_7_corER"
"Cell_Granularity_7_corMito"
"Cell_Granularity_7_corRNA"
"Cell_Granularity_8_corAGP"
"Cell_Granularity_8_corER"
"Cell_Granularity_8_corMito"
"Cell_Granularity_8_corRNA"
"Cell_Granularity_9_corAGP"
"Cell_Granularity_9_corER"
"Cell_Granularity_9_corMito"
"Cell_Granularity_9_corRNA"
"Cell_Intensity_IntegratedIntensityEdge_corAGP"
"Cell_Intensity_IntegratedIntensityEdge_corER"
"Cell_Intensity_IntegratedIntensityEdge_corMito"
"Cell_Intensity_IntegratedIntensityEdge_corNucleus"
"Cell_Intensity_IntegratedIntensityEdge_corRNA"
"Cell_Intensity_IntegratedIntensity_corAGP"
"Cell_Intensity_IntegratedIntensity_corER"
"Cell_Intensity_IntegratedIntensity_corMito"
"Cell_Intensity_IntegratedIntensity_corNucleus"
"Cell_Intensity_IntegratedIntensity_corRNA"
"Cell_Intensity_LowerQuartileIntensity_corAGP"
"Cell_Intensity_LowerQuartileIntensity_corER"
"Cell_Intensity_LowerQuartileIntensity_corMito"
"Cell_Intensity_LowerQuartileIntensity_corNucleus"
"Cell_Intensity_LowerQuartileIntensity_corRNA"
"Cell_Intensity_MADIntensity_corAGP"
"Cell_Intensity_MADIntensity_corER"
"Cell_Intensity_MADIntensity_corMito"
"Cell_Intensity_MADIntensity_corNucleus"
"Cell_Intensity_MADIntensity_corRNA"
"Cell_Intensity_MassDisplacement_corAGP"
"Cell_Intensity_MassDisplacement_corER"
"Cell_Intensity_MassDisplacement_corMito"
"Cell_Intensity_MassDisplacement_corNucleus"
"Cell_Intensity_MassDisplacement_corRNA"
"Cell_Intensity_MaxIntensityEdge_corAGP"
"Cell_Intensity_MaxIntensityEdge_corER"
"Cell_Intensity_MaxIntensityEdge_corMito"

"Cell_Intensity_MaxIntensityEdge_corNucleus"
"Cell_Intensity_MaxIntensityEdge_corRNA"
"Cell_Intensity_MaxIntensity_corAGP"
"Cell_Intensity_MaxIntensity_corER"
"Cell_Intensity_MaxIntensity_corMito"
"Cell_Intensity_MaxIntensity_corNucleus"
"Cell_Intensity_MaxIntensity_corRNA"
"Cell_Intensity_MeanIntensityEdge_corAGP"
"Cell_Intensity_MeanIntensityEdge_corER"
"Cell_Intensity_MeanIntensityEdge_corMito"
"Cell_Intensity_MeanIntensityEdge_corNucleus"
"Cell_Intensity_MeanIntensityEdge_corRNA"
"Cell_Intensity_MeanIntensity_corAGP"
"Cell_Intensity_MeanIntensity_corER"
"Cell_Intensity_MeanIntensity_corMito"
"Cell_Intensity_MeanIntensity_corNucleus"
"Cell_Intensity_MeanIntensity_corRNA"
"Cell_Intensity_MedianIntensity_corAGP"
"Cell_Intensity_MedianIntensity_corER"
"Cell_Intensity_MedianIntensity_corMito"
"Cell_Intensity_MedianIntensity_corNucleus"
"Cell_Intensity_MedianIntensity_corRNA"
"Cell_Intensity_MinIntensityEdge_corAGP"
"Cell_Intensity_MinIntensityEdge_corER"
"Cell_Intensity_MinIntensityEdge_corMito"
"Cell_Intensity_MinIntensityEdge_corNucleus"
"Cell_Intensity_MinIntensityEdge_corRNA"
"Cell_Intensity_MinIntensity_corAGP"
"Cell_Intensity_MinIntensity_corER"
"Cell_Intensity_MinIntensity_corMito"
"Cell_Intensity_MinIntensity_corNucleus"
"Cell_Intensity_MinIntensity_corRNA"
"Cell_Intensity_StdIntensityEdge_corAGP"
"Cell_Intensity_StdIntensityEdge_corER"
"Cell_Intensity_StdIntensityEdge_corMito"
"Cell_Intensity_StdIntensityEdge_corNucleus"
"Cell_Intensity_StdIntensityEdge_corRNA"
"Cell_Intensity_StdIntensity_corAGP"
"Cell_Intensity_StdIntensity_corER"
"Cell_Intensity_StdIntensity_corMito"
"Cell_Intensity_StdIntensity_corNucleus"
"Cell_Intensity_StdIntensity_corRNA"
"Cell_Intensity_UpperQuartileIntensity_corAGP"
"Cell_Intensity_UpperQuartileIntensity_corER"
"Cell_Intensity_UpperQuartileIntensity_corMito"
"Cell_Intensity_UpperQuartileIntensity_corNucleus"
"Cell_Intensity_UpperQuartileIntensity_corRNA"
"Cell_Neighbors_AngleBetweenNeighbors_5"
"Cell_Neighbors_AngleBetweenNeighbors_Adjacent"
"Cell_Neighbors_FirstClosestDistance_5"
"Cell_Neighbors_FirstClosestDistance_Adjacent"
"Cell_Neighbors_FirstClosestObjectNumber_5"
"Cell_Neighbors_FirstClosestObjectNumber_Adjacent"
"Cell_Neighbors_NumberOfNeighbors_5"
"Cell_Neighbors_NumberOfNeighbors_Adjacent"
"Cell_Neighbors_PercentTouching_5"
"Cell_Neighbors_PercentTouching_Adjacent"
"Cell_Neighbors_SecondClosestDistance_5"
"Cell_Neighbors_SecondClosestDistance_Adjacent"
"Cell_Neighbors_SecondClosestObjectNumber_5"
"Cell_Neighbors_SecondClosestObjectNumber_Adjacent"
"Cell_RadialDistribution_FracAtD_corAGP_1of4"

"Cell_RadialDistribution_FracAtD_corAGP_2of4"
"Cell_RadialDistribution_FracAtD_corAGP_3of4"
"Cell_RadialDistribution_FracAtD_corAGP_4of4"
"Cell_RadialDistribution_FracAtD_corER_1of4"
"Cell_RadialDistribution_FracAtD_corER_2of4"
"Cell_RadialDistribution_FracAtD_corER_3of4"
"Cell_RadialDistribution_FracAtD_corER_4of4"
"Cell_RadialDistribution_FracAtD_corMito_1of4"
"Cell_RadialDistribution_FracAtD_corMito_2of4"
"Cell_RadialDistribution_FracAtD_corMito_3of4"
"Cell_RadialDistribution_FracAtD_corMito_4of4"
"Cell_RadialDistribution_FracAtD_corNucleus_1of4"
"Cell_RadialDistribution_FracAtD_corNucleus_2of4"
"Cell_RadialDistribution_FracAtD_corNucleus_3of4"
"Cell_RadialDistribution_FracAtD_corNucleus_4of4"
"Cell_RadialDistribution_FracAtD_corRNA_1of4"
"Cell_RadialDistribution_FracAtD_corRNA_2of4"
"Cell_RadialDistribution_FracAtD_corRNA_3of4"
"Cell_RadialDistribution_FracAtD_corRNA_4of4"
"Cell_RadialDistribution_MeanFrac_corAGP_1of4"
"Cell_RadialDistribution_MeanFrac_corAGP_2of4"
"Cell_RadialDistribution_MeanFrac_corAGP_3of4"
"Cell_RadialDistribution_MeanFrac_corAGP_4of4"
"Cell_RadialDistribution_MeanFrac_corER_1of4"
"Cell_RadialDistribution_MeanFrac_corER_2of4"
"Cell_RadialDistribution_MeanFrac_corER_3of4"
"Cell_RadialDistribution_MeanFrac_corER_4of4"
"Cell_RadialDistribution_MeanFrac_corMito_1of4"
"Cell_RadialDistribution_MeanFrac_corMito_2of4"
"Cell_RadialDistribution_MeanFrac_corMito_3of4"
"Cell_RadialDistribution_MeanFrac_corMito_4of4"
"Cell_RadialDistribution_MeanFrac_corNucleus_1of4"
"Cell_RadialDistribution_MeanFrac_corNucleus_2of4"
"Cell_RadialDistribution_MeanFrac_corNucleus_3of4"
"Cell_RadialDistribution_MeanFrac_corNucleus_4of4"
"Cell_RadialDistribution_MeanFrac_corRNA_1of4"
"Cell_RadialDistribution_MeanFrac_corRNA_2of4"
"Cell_RadialDistribution_MeanFrac_corRNA_3of4"
"Cell_RadialDistribution_MeanFrac_corRNA_4of4"
"Cell_RadialDistribution_RadialCV_corAGP_1of4"
"Cell_RadialDistribution_RadialCV_corAGP_2of4"
"Cell_RadialDistribution_RadialCV_corAGP_3of4"
"Cell_RadialDistribution_RadialCV_corAGP_4of4"
"Cell_RadialDistribution_RadialCV_corER_1of4"
"Cell_RadialDistribution_RadialCV_corER_2of4"
"Cell_RadialDistribution_RadialCV_corER_3of4"
"Cell_RadialDistribution_RadialCV_corER_4of4"
"Cell_RadialDistribution_RadialCV_corMito_1of4"
"Cell_RadialDistribution_RadialCV_corMito_2of4"
"Cell_RadialDistribution_RadialCV_corMito_3of4"
"Cell_RadialDistribution_RadialCV_corMito_4of4"
"Cell_RadialDistribution_RadialCV_corNucleus_1of4"
"Cell_RadialDistribution_RadialCV_corNucleus_2of4"
"Cell_RadialDistribution_RadialCV_corNucleus_3of4"
"Cell_RadialDistribution_RadialCV_corNucleus_4of4"
"Cell_RadialDistribution_RadialCV_corRNA_1of4"
"Cell_RadialDistribution_RadialCV_corRNA_2of4"
"Cell_RadialDistribution_RadialCV_corRNA_3of4"
"Cell_RadialDistribution_RadialCV_corRNA_4of4"
"Cytoplasm_AreaShape_Area"
"Cytoplasm_AreaShape_Compactness"
"Cytoplasm_AreaShape_Eccentricity"

"Cytoplasm_AreaShape_Extent"
"Cytoplasm_AreaShape_FormFactor"
"Cytoplasm_AreaShape_MajorAxisLength"
"Cytoplasm_AreaShape_MaxFeretDiameter"
"Cytoplasm_AreaShape_MaximumRadius"
"Cytoplasm_AreaShape_MeanRadius"
"Cytoplasm_AreaShape_MedianRadius"
"Cytoplasm_AreaShape_MinFeretDiameter"
"Cytoplasm_AreaShape_MinorAxisLength"
"Cytoplasm_AreaShape_Orientation"
"Cytoplasm_AreaShape_Perimeter"
"Cytoplasm_AreaShape_Solidity"
"Cytoplasm_AreaShape_Zernike_0_0"
"Cytoplasm_AreaShape_Zernike_1_1"
"Cytoplasm_AreaShape_Zernike_2_0"
"Cytoplasm_AreaShape_Zernike_2_2"
"Cytoplasm_AreaShape_Zernike_3_1"
"Cytoplasm_AreaShape_Zernike_3_3"
"Cytoplasm_AreaShape_Zernike_4_0"
"Cytoplasm_AreaShape_Zernike_4_2"
"Cytoplasm_AreaShape_Zernike_4_4"
"Cytoplasm_AreaShape_Zernike_5_1"
"Cytoplasm_AreaShape_Zernike_5_3"
"Cytoplasm_AreaShape_Zernike_5_5"
"Cytoplasm_AreaShape_Zernike_6_0"
"Cytoplasm_AreaShape_Zernike_6_2"
"Cytoplasm_AreaShape_Zernike_6_4"
"Cytoplasm_AreaShape_Zernike_6_6"
"Cytoplasm_AreaShape_Zernike_7_1"
"Cytoplasm_AreaShape_Zernike_7_3"
"Cytoplasm_AreaShape_Zernike_7_5"
"Cytoplasm_AreaShape_Zernike_7_7"
"Cytoplasm_AreaShape_Zernike_8_0"
"Cytoplasm_AreaShape_Zernike_8_2"
"Cytoplasm_AreaShape_Zernike_8_4"
"Cytoplasm_AreaShape_Zernike_8_6"
"Cytoplasm_AreaShape_Zernike_8_8"
"Cytoplasm_AreaShape_Zernike_9_1"
"Cytoplasm_AreaShape_Zernike_9_3"
"Cytoplasm_AreaShape_Zernike_9_5"
"Cytoplasm_AreaShape_Zernike_9_7"
"Cytoplasm_AreaShape_Zernike_9_9"
"Cytoplasm_Correlation_Correlation_corAGP_corRNA"
"Cytoplasm_Correlation_Correlation_corER_corAGP"
"Cytoplasm_Correlation_Correlation_corER_corMito"
"Cytoplasm_Correlation_Correlation_corER_corRNA"
"Cytoplasm_Correlation_Correlation_corMito_corAGP"
"Cytoplasm_Correlation_Correlation_corMito_corRNA"
"Cytoplasm_Correlation_Correlation_corNucleus_corAGP"
"Cytoplasm_Correlation_Correlation_corNucleus_corER"
"Cytoplasm_Correlation_Correlation_corNucleus_corMito"
"Cytoplasm_Correlation_Correlation_corNucleus_corRNA"
"Cytoplasm_Correlation_Costes_corAGP_corER"
"Cytoplasm_Correlation_Costes_corAGP_corMito"
"Cytoplasm_Correlation_Costes_corAGP_corNucleus"
"Cytoplasm_Correlation_Costes_corAGP_corRNA"
"Cytoplasm_Correlation_Costes_corER_corAGP"
"Cytoplasm_Correlation_Costes_corER_corMito"
"Cytoplasm_Correlation_Costes_corER_corNucleus"
"Cytoplasm_Correlation_Costes_corER_corRNA"
"Cytoplasm_Correlation_Costes_corMito_corAGP"
"Cytoplasm_Correlation_Costes_corMito_corER"

"Cytoplasm_Correlation_Costes_corMito_corNucleus"
"Cytoplasm_Correlation_Costes_corMito_corRNA"
"Cytoplasm_Correlation_Costes_corNucleus_corAGP"
"Cytoplasm_Correlation_Costes_corNucleus_corER"
"Cytoplasm_Correlation_Costes_corNucleus_corMito"
"Cytoplasm_Correlation_Costes_corNucleus_corRNA"
"Cytoplasm_Correlation_Costes_corRNA_corAGP"
"Cytoplasm_Correlation_Costes_corRNA_corER"
"Cytoplasm_Correlation_Costes_corRNA_corMito"
"Cytoplasm_Correlation_Costes_corRNA_corNucleus"
"Cytoplasm_Correlation_K_corAGP_corER"
"Cytoplasm_Correlation_K_corAGP_corMito"
"Cytoplasm_Correlation_K_corAGP_corNucleus"
"Cytoplasm_Correlation_K_corAGP_corRNA"
"Cytoplasm_Correlation_K_corER_corAGP"
"Cytoplasm_Correlation_K_corER_corMito"
"Cytoplasm_Correlation_K_corER_corNucleus"
"Cytoplasm_Correlation_K_corER_corRNA"
"Cytoplasm_Correlation_K_corMito_corAGP"
"Cytoplasm_Correlation_K_corMito_corER"
"Cytoplasm_Correlation_K_corMito_corNucleus"
"Cytoplasm_Correlation_K_corMito_corRNA"
"Cytoplasm_Correlation_K_corNucleus_corAGP"
"Cytoplasm_Correlation_K_corNucleus_corER"
"Cytoplasm_Correlation_K_corNucleus_corMito"
"Cytoplasm_Correlation_K_corNucleus_corRNA"
"Cytoplasm_Correlation_K_corRNA_corAGP"
"Cytoplasm_Correlation_K_corRNA_corER"
"Cytoplasm_Correlation_K_corRNA_corMito"
"Cytoplasm_Correlation_K_corRNA_corNucleus"
"Cytoplasm_Correlation_Manders_corAGP_corER"
"Cytoplasm_Correlation_Manders_corAGP_corMito"
"Cytoplasm_Correlation_Manders_corAGP_corNucleus"
"Cytoplasm_Correlation_Manders_corAGP_corRNA"
"Cytoplasm_Correlation_Manders_corER_corAGP"
"Cytoplasm_Correlation_Manders_corER_corMito"
"Cytoplasm_Correlation_Manders_corER_corNucleus"
"Cytoplasm_Correlation_Manders_corER_corRNA"
"Cytoplasm_Correlation_Manders_corMito_corAGP"
"Cytoplasm_Correlation_Manders_corMito_corER"
"Cytoplasm_Correlation_Manders_corMito_corNucleus"
"Cytoplasm_Correlation_Manders_corMito_corRNA"
"Cytoplasm_Correlation_Manders_corNucleus_corAGP"
"Cytoplasm_Correlation_Manders_corNucleus_corER"
"Cytoplasm_Correlation_Manders_corNucleus_corMito"
"Cytoplasm_Correlation_Manders_corNucleus_corRNA"
"Cytoplasm_Correlation_Manders_corRNA_corAGP"
"Cytoplasm_Correlation_Manders_corRNA_corER"
"Cytoplasm_Correlation_Manders_corRNA_corMito"
"Cytoplasm_Correlation_Manders_corRNA_corNucleus"
"Cytoplasm_Correlation_Overlap_corAGP_corRNA"
"Cytoplasm_Correlation_Overlap_corER_corAGP"
"Cytoplasm_Correlation_Overlap_corER_corMito"
"Cytoplasm_Correlation_Overlap_corER_corRNA"
"Cytoplasm_Correlation_Overlap_corMito_corAGP"
"Cytoplasm_Correlation_Overlap_corMito_corRNA"
"Cytoplasm_Correlation_Overlap_corNucleus_corAGP"
"Cytoplasm_Correlation_Overlap_corNucleus_corER"
"Cytoplasm_Correlation_Overlap_corNucleus_corMito"
"Cytoplasm_Correlation_Overlap_corNucleus_corRNA"
"Cytoplasm_Correlation_RWC_corAGP_corER"
"Cytoplasm_Correlation_RWC_corAGP_corMito"

"Cytoplasm_Correlation_RWC_corAGP_corNucleus"
"Cytoplasm_Correlation_RWC_corAGP_corRNA"
"Cytoplasm_Correlation_RWC_corER_corAGP"
"Cytoplasm_Correlation_RWC_corER_corMito"
"Cytoplasm_Correlation_RWC_corER_corNucleus"
"Cytoplasm_Correlation_RWC_corER_corRNA"
"Cytoplasm_Correlation_RWC_corMito_corAGP"
"Cytoplasm_Correlation_RWC_corMito_corER"
"Cytoplasm_Correlation_RWC_corMito_corNucleus"
"Cytoplasm_Correlation_RWC_corMito_corRNA"
"Cytoplasm_Correlation_RWC_corNucleus_corAGP"
"Cytoplasm_Correlation_RWC_corNucleus_corER"
"Cytoplasm_Correlation_RWC_corNucleus_corMito"
"Cytoplasm_Correlation_RWC_corNucleus_corRNA"
"Cytoplasm_Correlation_RWC_corRNA_corAGP"
"Cytoplasm_Correlation_RWC_corRNA_corER"
"Cytoplasm_Correlation_RWC_corRNA_corMito"
"Cytoplasm_Correlation_RWC_corRNA_corNucleus"
"Cytoplasm_Granularity_10_corAGP"
"Cytoplasm_Granularity_10_corER"
"Cytoplasm_Granularity_10_corMito"
"Cytoplasm_Granularity_10_corRNA"
"Cytoplasm_Granularity_11_corAGP"
"Cytoplasm_Granularity_11_corER"
"Cytoplasm_Granularity_11_corMito"
"Cytoplasm_Granularity_11_corRNA"
"Cytoplasm_Granularity_12_corAGP"
"Cytoplasm_Granularity_12_corER"
"Cytoplasm_Granularity_12_corMito"
"Cytoplasm_Granularity_12_corRNA"
"Cytoplasm_Granularity_13_corAGP"
"Cytoplasm_Granularity_13_corER"
"Cytoplasm_Granularity_13_corMito"
"Cytoplasm_Granularity_13_corRNA"
"Cytoplasm_Granularity_14_corAGP"
"Cytoplasm_Granularity_14_corER"
"Cytoplasm_Granularity_14_corMito"
"Cytoplasm_Granularity_14_corRNA"
"Cytoplasm_Granularity_15_corAGP"
"Cytoplasm_Granularity_15_corER"
"Cytoplasm_Granularity_15_corMito"
"Cytoplasm_Granularity_15_corRNA"
"Cytoplasm_Granularity_16_corAGP"
"Cytoplasm_Granularity_16_corER"
"Cytoplasm_Granularity_16_corMito"
"Cytoplasm_Granularity_16_corRNA"
"Cytoplasm_Granularity_1_corAGP"
"Cytoplasm_Granularity_1_corER"
"Cytoplasm_Granularity_1_corMito"
"Cytoplasm_Granularity_1_corRNA"
"Cytoplasm_Granularity_2_corAGP"
"Cytoplasm_Granularity_2_corER"
"Cytoplasm_Granularity_2_corMito"
"Cytoplasm_Granularity_2_corRNA"
"Cytoplasm_Granularity_3_corAGP"
"Cytoplasm_Granularity_3_corER"
"Cytoplasm_Granularity_3_corMito"
"Cytoplasm_Granularity_3_corRNA"
"Cytoplasm_Granularity_4_corAGP"
"Cytoplasm_Granularity_4_corER"
"Cytoplasm_Granularity_4_corMito"
"Cytoplasm_Granularity_4_corRNA"

"Cytoplasm_Granularity_5_corAGP"
"Cytoplasm_Granularity_5_corER"
"Cytoplasm_Granularity_5_corMito"
"Cytoplasm_Granularity_5_corRNA"
"Cytoplasm_Granularity_6_corAGP"
"Cytoplasm_Granularity_6_corER"
"Cytoplasm_Granularity_6_corMito"
"Cytoplasm_Granularity_6_corRNA"
"Cytoplasm_Granularity_7_corAGP"
"Cytoplasm_Granularity_7_corER"
"Cytoplasm_Granularity_7_corMito"
"Cytoplasm_Granularity_7_corRNA"
"Cytoplasm_Granularity_8_corAGP"
"Cytoplasm_Granularity_8_corER"
"Cytoplasm_Granularity_8_corMito"
"Cytoplasm_Granularity_8_corRNA"
"Cytoplasm_Granularity_9_corAGP"
"Cytoplasm_Granularity_9_corER"
"Cytoplasm_Granularity_9_corMito"
"Cytoplasm_Granularity_9_corRNA"
"Cytoplasm_Intensity_IntegratedIntensityEdge_corAGP"
"Cytoplasm_Intensity_IntegratedIntensityEdge_corER"
"Cytoplasm_Intensity_IntegratedIntensityEdge_corMito"
"Cytoplasm_Intensity_IntegratedIntensityEdge_corNucleus"
"Cytoplasm_Intensity_IntegratedIntensityEdge_corRNA"
"Cytoplasm_Intensity_IntegratedIntensity_corAGP"
"Cytoplasm_Intensity_IntegratedIntensity_corER"
"Cytoplasm_Intensity_IntegratedIntensity_corMito"
"Cytoplasm_Intensity_IntegratedIntensity_corNucleus"
"Cytoplasm_Intensity_IntegratedIntensity_corRNA"
"Cytoplasm_Intensity_LowerQuartileIntensity_corAGP"
"Cytoplasm_Intensity_LowerQuartileIntensity_corER"
"Cytoplasm_Intensity_LowerQuartileIntensity_corMito"
"Cytoplasm_Intensity_LowerQuartileIntensity_corNucleus"
"Cytoplasm_Intensity_LowerQuartileIntensity_corRNA"
"Cytoplasm_Intensity_MADIntensity_corAGP"
"Cytoplasm_Intensity_MADIntensity_corER"
"Cytoplasm_Intensity_MADIntensity_corMito"
"Cytoplasm_Intensity_MADIntensity_corNucleus"
"Cytoplasm_Intensity_MADIntensity_corRNA"
"Cytoplasm_Intensity_MassDisplacement_corAGP"
"Cytoplasm_Intensity_MassDisplacement_corER"
"Cytoplasm_Intensity_MassDisplacement_corMito"
"Cytoplasm_Intensity_MassDisplacement_corNucleus"
"Cytoplasm_Intensity_MassDisplacement_corRNA"
"Cytoplasm_Intensity_MaxIntensityEdge_corAGP"
"Cytoplasm_Intensity_MaxIntensityEdge_corER"
"Cytoplasm_Intensity_MaxIntensityEdge_corMito"
"Cytoplasm_Intensity_MaxIntensityEdge_corNucleus"
"Cytoplasm_Intensity_MaxIntensityEdge_corRNA"
"Cytoplasm_Intensity_MaxIntensity_corAGP"
"Cytoplasm_Intensity_MaxIntensity_corER"
"Cytoplasm_Intensity_MaxIntensity_corMito"
"Cytoplasm_Intensity_MaxIntensity_corNucleus"
"Cytoplasm_Intensity_MaxIntensity_corRNA"
"Cytoplasm_Intensity_MeanIntensityEdge_corAGP"
"Cytoplasm_Intensity_MeanIntensityEdge_corER"
"Cytoplasm_Intensity_MeanIntensityEdge_corMito"
"Cytoplasm_Intensity_MeanIntensityEdge_corNucleus"
"Cytoplasm_Intensity_MeanIntensityEdge_corRNA"
"Cytoplasm_Intensity_MeanIntensity_corAGP"
"Cytoplasm_Intensity_MeanIntensity_corER"

"Cytoplasm_Intensity_MeanIntensity_corMito"
"Cytoplasm_Intensity_MeanIntensity_corNucleus"
"Cytoplasm_Intensity_MeanIntensity_corRNA"
"Cytoplasm_Intensity_MedianIntensity_corAGP"
"Cytoplasm_Intensity_MedianIntensity_corER"
"Cytoplasm_Intensity_MedianIntensity_corMito"
"Cytoplasm_Intensity_MedianIntensity_corNucleus"
"Cytoplasm_Intensity_MedianIntensity_corRNA"
"Cytoplasm_Intensity_MinIntensityEdge_corAGP"
"Cytoplasm_Intensity_MinIntensityEdge_corER"
"Cytoplasm_Intensity_MinIntensityEdge_corMito"
"Cytoplasm_Intensity_MinIntensityEdge_corNucleus"
"Cytoplasm_Intensity_MinIntensityEdge_corRNA"
"Cytoplasm_Intensity_MinIntensity_corAGP"
"Cytoplasm_Intensity_MinIntensity_corER"
"Cytoplasm_Intensity_MinIntensity_corMito"
"Cytoplasm_Intensity_MinIntensity_corNucleus"
"Cytoplasm_Intensity_MinIntensity_corRNA"
"Cytoplasm_Intensity_StdIntensityEdge_corAGP"
"Cytoplasm_Intensity_StdIntensityEdge_corER"
"Cytoplasm_Intensity_StdIntensityEdge_corMito"
"Cytoplasm_Intensity_StdIntensityEdge_corNucleus"
"Cytoplasm_Intensity_StdIntensityEdge_corRNA"
"Cytoplasm_Intensity_StdIntensity_corAGP"
"Cytoplasm_Intensity_StdIntensity_corER"
"Cytoplasm_Intensity_StdIntensity_corMito"
"Cytoplasm_Intensity_StdIntensity_corNucleus"
"Cytoplasm_Intensity_StdIntensity_corRNA"
"Cytoplasm_Intensity_UpperQuartileIntensity_corAGP"
"Cytoplasm_Intensity_UpperQuartileIntensity_corER"
"Cytoplasm_Intensity_UpperQuartileIntensity_corMito"
"Cytoplasm_Intensity_UpperQuartileIntensity_corNucleus"
"Cytoplasm_Intensity_UpperQuartileIntensity_corRNA"
"Cytoplasm_RadialDistribution_FracAtD_corAGP_1of4"
"Cytoplasm_RadialDistribution_FracAtD_corAGP_2of4"
"Cytoplasm_RadialDistribution_FracAtD_corAGP_3of4"
"Cytoplasm_RadialDistribution_FracAtD_corAGP_4of4"
"Cytoplasm_RadialDistribution_FracAtD_corER_1of4"
"Cytoplasm_RadialDistribution_FracAtD_corER_2of4"
"Cytoplasm_RadialDistribution_FracAtD_corER_3of4"
"Cytoplasm_RadialDistribution_FracAtD_corER_4of4"
"Cytoplasm_RadialDistribution_FracAtD_corMito_1of4"
"Cytoplasm_RadialDistribution_FracAtD_corMito_2of4"
"Cytoplasm_RadialDistribution_FracAtD_corMito_3of4"
"Cytoplasm_RadialDistribution_FracAtD_corMito_4of4"
"Cytoplasm_RadialDistribution_FracAtD_corNucleus_1of4"
"Cytoplasm_RadialDistribution_FracAtD_corNucleus_2of4"
"Cytoplasm_RadialDistribution_FracAtD_corNucleus_3of4"
"Cytoplasm_RadialDistribution_FracAtD_corNucleus_4of4"
"Cytoplasm_RadialDistribution_FracAtD_corRNA_1of4"
"Cytoplasm_RadialDistribution_FracAtD_corRNA_2of4"
"Cytoplasm_RadialDistribution_FracAtD_corRNA_3of4"
"Cytoplasm_RadialDistribution_FracAtD_corRNA_4of4"
"Cytoplasm_RadialDistribution_MeanFrac_corAGP_1of4"
"Cytoplasm_RadialDistribution_MeanFrac_corAGP_2of4"
"Cytoplasm_RadialDistribution_MeanFrac_corAGP_3of4"
"Cytoplasm_RadialDistribution_MeanFrac_corAGP_4of4"
"Cytoplasm_RadialDistribution_MeanFrac_corER_1of4"
"Cytoplasm_RadialDistribution_MeanFrac_corER_2of4"
"Cytoplasm_RadialDistribution_MeanFrac_corER_3of4"
"Cytoplasm_RadialDistribution_MeanFrac_corER_4of4"
"Cytoplasm_RadialDistribution_MeanFrac_corMito_1of4"

"Cytoplasm_RadialDistribution_MeanFrac_corMito_2of4"
"Cytoplasm_RadialDistribution_MeanFrac_corMito_3of4"
"Cytoplasm_RadialDistribution_MeanFrac_corMito_4of4"
"Cytoplasm_RadialDistribution_MeanFrac_corNucleus_1of4"
"Cytoplasm_RadialDistribution_MeanFrac_corNucleus_2of4"
"Cytoplasm_RadialDistribution_MeanFrac_corNucleus_3of4"
"Cytoplasm_RadialDistribution_MeanFrac_corNucleus_4of4"
"Cytoplasm_RadialDistribution_MeanFrac_corRNA_1of4"
"Cytoplasm_RadialDistribution_MeanFrac_corRNA_2of4"
"Cytoplasm_RadialDistribution_MeanFrac_corRNA_3of4"
"Cytoplasm_RadialDistribution_MeanFrac_corRNA_4of4"
"Cytoplasm_RadialDistribution_RadialCV_corAGP_1of4"
"Cytoplasm_RadialDistribution_RadialCV_corAGP_2of4"
"Cytoplasm_RadialDistribution_RadialCV_corAGP_3of4"
"Cytoplasm_RadialDistribution_RadialCV_corAGP_4of4"
"Cytoplasm_RadialDistribution_RadialCV_corER_1of4"
"Cytoplasm_RadialDistribution_RadialCV_corER_2of4"
"Cytoplasm_RadialDistribution_RadialCV_corER_3of4"
"Cytoplasm_RadialDistribution_RadialCV_corER_4of4"
"Cytoplasm_RadialDistribution_RadialCV_corMito_1of4"
"Cytoplasm_RadialDistribution_RadialCV_corMito_2of4"
"Cytoplasm_RadialDistribution_RadialCV_corMito_3of4"
"Cytoplasm_RadialDistribution_RadialCV_corMito_4of4"
"Cytoplasm_RadialDistribution_RadialCV_corNucleus_1of4"
"Cytoplasm_RadialDistribution_RadialCV_corNucleus_2of4"
"Cytoplasm_RadialDistribution_RadialCV_corNucleus_3of4"
"Cytoplasm_RadialDistribution_RadialCV_corNucleus_4of4"
"Cytoplasm_RadialDistribution_RadialCV_corRNA_1of4"
"Cytoplasm_RadialDistribution_RadialCV_corRNA_2of4"
"Cytoplasm_RadialDistribution_RadialCV_corRNA_3of4"
"Cytoplasm_RadialDistribution_RadialCV_corRNA_4of4"
"Nuclei_AreaShape_Area"
"Nuclei_AreaShape_Compactness"
"Nuclei_AreaShape_Eccentricity"
"Nuclei_AreaShape_Extent"
"Nuclei_AreaShape_FormFactor"
"Nuclei_AreaShape_MajorAxisLength"
"Nuclei_AreaShape_MaxFeretDiameter"
"Nuclei_AreaShape_MaximumRadius"
"Nuclei_AreaShape_MeanRadius"
"Nuclei_AreaShape_MedianRadius"
"Nuclei_AreaShape_MinFeretDiameter"
"Nuclei_AreaShape_MinorAxisLength"
"Nuclei_AreaShape_Orientation"
"Nuclei_AreaShape_Perimeter"
"Nuclei_AreaShape_Solidity"
"Nuclei_AreaShape_Zernike_0_0"
"Nuclei_AreaShape_Zernike_1_1"
"Nuclei_AreaShape_Zernike_2_0"
"Nuclei_AreaShape_Zernike_2_2"
"Nuclei_AreaShape_Zernike_3_1"
"Nuclei_AreaShape_Zernike_3_3"
"Nuclei_AreaShape_Zernike_4_0"
"Nuclei_AreaShape_Zernike_4_2"
"Nuclei_AreaShape_Zernike_4_4"
"Nuclei_AreaShape_Zernike_5_1"
"Nuclei_AreaShape_Zernike_5_3"
"Nuclei_AreaShape_Zernike_5_5"
"Nuclei_AreaShape_Zernike_6_0"
"Nuclei_AreaShape_Zernike_6_2"
"Nuclei_AreaShape_Zernike_6_4"
"Nuclei_AreaShape_Zernike_6_6"

"Nuclei_AreaShape_Zernike_7_1"
"Nuclei_AreaShape_Zernike_7_3"
"Nuclei_AreaShape_Zernike_7_5"
"Nuclei_AreaShape_Zernike_7_7"
"Nuclei_AreaShape_Zernike_8_0"
"Nuclei_AreaShape_Zernike_8_2"
"Nuclei_AreaShape_Zernike_8_4"
"Nuclei_AreaShape_Zernike_8_6"
"Nuclei_AreaShape_Zernike_8_8"
"Nuclei_AreaShape_Zernike_9_1"
"Nuclei_AreaShape_Zernike_9_3"
"Nuclei_AreaShape_Zernike_9_5"
"Nuclei_AreaShape_Zernike_9_7"
"Nuclei_AreaShape_Zernike_9_9"
"Nuclei_Correlation_Correlation_corAGP_corRNA"
"Nuclei_Correlation_Correlation_corER_corAGP"
"Nuclei_Correlation_Correlation_corER_corMito"
"Nuclei_Correlation_Correlation_corER_corRNA"
"Nuclei_Correlation_Correlation_corMito_corAGP"
"Nuclei_Correlation_Correlation_corMito_corRNA"
"Nuclei_Correlation_Correlation_corNucleus_corAGP"
"Nuclei_Correlation_Correlation_corNucleus_corER"
"Nuclei_Correlation_Correlation_corNucleus_corMito"
"Nuclei_Correlation_Correlation_corNucleus_corRNA"
"Nuclei_Correlation_Costes_corAGP_corER"
"Nuclei_Correlation_Costes_corAGP_corMito"
"Nuclei_Correlation_Costes_corAGP_corNucleus"
"Nuclei_Correlation_Costes_corAGP_corRNA"
"Nuclei_Correlation_Costes_corER_corAGP"
"Nuclei_Correlation_Costes_corER_corMito"
"Nuclei_Correlation_Costes_corER_corNucleus"
"Nuclei_Correlation_Costes_corER_corRNA"
"Nuclei_Correlation_Costes_corMito_corAGP"
"Nuclei_Correlation_Costes_corMito_corER"
"Nuclei_Correlation_Costes_corMito_corNucleus"
"Nuclei_Correlation_Costes_corMito_corRNA"
"Nuclei_Correlation_Costes_corNucleus_corAGP"
"Nuclei_Correlation_Costes_corNucleus_corER"
"Nuclei_Correlation_Costes_corNucleus_corMito"
"Nuclei_Correlation_Costes_corNucleus_corRNA"
"Nuclei_Correlation_Costes_corRNA_corAGP"
"Nuclei_Correlation_Costes_corRNA_corER"
"Nuclei_Correlation_Costes_corRNA_corMito"
"Nuclei_Correlation_Costes_corRNA_corNucleus"
"Nuclei_Correlation_K_corAGP_corER"
"Nuclei_Correlation_K_corAGP_corMito"
"Nuclei_Correlation_K_corAGP_corNucleus"
"Nuclei_Correlation_K_corAGP_corRNA"
"Nuclei_Correlation_K_corER_corAGP"
"Nuclei_Correlation_K_corER_corMito"
"Nuclei_Correlation_K_corER_corNucleus"
"Nuclei_Correlation_K_corER_corRNA"
"Nuclei_Correlation_K_corMito_corAGP"
"Nuclei_Correlation_K_corMito_corER"
"Nuclei_Correlation_K_corMito_corNucleus"
"Nuclei_Correlation_K_corMito_corRNA"
"Nuclei_Correlation_K_corNucleus_corAGP"
"Nuclei_Correlation_K_corNucleus_corER"
"Nuclei_Correlation_K_corNucleus_corMito"
"Nuclei_Correlation_K_corNucleus_corRNA"
"Nuclei_Correlation_K_corRNA_corAGP"
"Nuclei_Correlation_K_corRNA_corER"

"Nuclei_Correlation_K_corRNA_corMito"
"Nuclei_Correlation_K_corRNA_corNucleus"
"Nuclei_Correlation_Manders_corAGP_corER"
"Nuclei_Correlation_Manders_corAGP_corMito"
"Nuclei_Correlation_Manders_corAGP_corNucleus"
"Nuclei_Correlation_Manders_corAGP_corRNA"
"Nuclei_Correlation_Manders_corER_corAGP"
"Nuclei_Correlation_Manders_corER_corMito"
"Nuclei_Correlation_Manders_corER_corNucleus"
"Nuclei_Correlation_Manders_corER_corRNA"
"Nuclei_Correlation_Manders_corMito_corAGP"
"Nuclei_Correlation_Manders_corMito_corER"
"Nuclei_Correlation_Manders_corMito_corNucleus"
"Nuclei_Correlation_Manders_corMito_corRNA"
"Nuclei_Correlation_Manders_corNucleus_corAGP"
"Nuclei_Correlation_Manders_corNucleus_corER"
"Nuclei_Correlation_Manders_corNucleus_corMito"
"Nuclei_Correlation_Manders_corNucleus_corRNA"
"Nuclei_Correlation_Manders_corRNA_corAGP"
"Nuclei_Correlation_Manders_corRNA_corER"
"Nuclei_Correlation_Manders_corRNA_corMito"
"Nuclei_Correlation_Manders_corRNA_corNucleus"
"Nuclei_Correlation_Overlap_corAGP_corRNA"
"Nuclei_Correlation_Overlap_corER_corAGP"
"Nuclei_Correlation_Overlap_corER_corMito"
"Nuclei_Correlation_Overlap_corER_corRNA"
"Nuclei_Correlation_Overlap_corMito_corAGP"
"Nuclei_Correlation_Overlap_corMito_corRNA"
"Nuclei_Correlation_Overlap_corNucleus_corAGP"
"Nuclei_Correlation_Overlap_corNucleus_corER"
"Nuclei_Correlation_Overlap_corNucleus_corMito"
"Nuclei_Correlation_Overlap_corNucleus_corRNA"
"Nuclei_Correlation_RWC_corAGP_corER"
"Nuclei_Correlation_RWC_corAGP_corMito"
"Nuclei_Correlation_RWC_corAGP_corNucleus"
"Nuclei_Correlation_RWC_corAGP_corRNA"
"Nuclei_Correlation_RWC_corER_corAGP"
"Nuclei_Correlation_RWC_corER_corMito"
"Nuclei_Correlation_RWC_corER_corNucleus"
"Nuclei_Correlation_RWC_corER_corRNA"
"Nuclei_Correlation_RWC_corMito_corAGP"
"Nuclei_Correlation_RWC_corMito_corER"
"Nuclei_Correlation_RWC_corMito_corNucleus"
"Nuclei_Correlation_RWC_corMito_corRNA"
"Nuclei_Correlation_RWC_corNucleus_corAGP"
"Nuclei_Correlation_RWC_corNucleus_corER"
"Nuclei_Correlation_RWC_corNucleus_corMito"
"Nuclei_Correlation_RWC_corNucleus_corRNA"
"Nuclei_Correlation_RWC_corRNA_corAGP"
"Nuclei_Correlation_RWC_corRNA_corER"
"Nuclei_Correlation_RWC_corRNA_corMito"
"Nuclei_Correlation_RWC_corRNA_corNucleus"
"Nuclei_Granularity_10_corAGP"
"Nuclei_Granularity_10_corER"
"Nuclei_Granularity_10_corMito"
"Nuclei_Granularity_10_corRNA"
"Nuclei_Granularity_11_corAGP"
"Nuclei_Granularity_11_corER"
"Nuclei_Granularity_11_corMito"
"Nuclei_Granularity_11_corRNA"
"Nuclei_Granularity_12_corAGP"
"Nuclei_Granularity_12_corER"

"Nuclei_Granularity_12_corMito"
"Nuclei_Granularity_12_corRNA"
"Nuclei_Granularity_13_corAGP"
"Nuclei_Granularity_13_corER"
"Nuclei_Granularity_13_corMito"
"Nuclei_Granularity_13_corRNA"
"Nuclei_Granularity_14_corAGP"
"Nuclei_Granularity_14_corER"
"Nuclei_Granularity_14_corMito"
"Nuclei_Granularity_14_corRNA"
"Nuclei_Granularity_15_corAGP"
"Nuclei_Granularity_15_corER"
"Nuclei_Granularity_15_corMito"
"Nuclei_Granularity_15_corRNA"
"Nuclei_Granularity_16_corAGP"
"Nuclei_Granularity_16_corER"
"Nuclei_Granularity_16_corMito"
"Nuclei_Granularity_16_corRNA"
"Nuclei_Granularity_1_corAGP"
"Nuclei_Granularity_1_corER"
"Nuclei_Granularity_1_corMito"
"Nuclei_Granularity_1_corRNA"
"Nuclei_Granularity_2_corAGP"
"Nuclei_Granularity_2_corER"
"Nuclei_Granularity_2_corMito"
"Nuclei_Granularity_2_corRNA"
"Nuclei_Granularity_3_corAGP"
"Nuclei_Granularity_3_corER"
"Nuclei_Granularity_3_corMito"
"Nuclei_Granularity_3_corRNA"
"Nuclei_Granularity_4_corAGP"
"Nuclei_Granularity_4_corER"
"Nuclei_Granularity_4_corMito"
"Nuclei_Granularity_4_corRNA"
"Nuclei_Granularity_5_corAGP"
"Nuclei_Granularity_5_corER"
"Nuclei_Granularity_5_corMito"
"Nuclei_Granularity_5_corRNA"
"Nuclei_Granularity_6_corAGP"
"Nuclei_Granularity_6_corER"
"Nuclei_Granularity_6_corMito"
"Nuclei_Granularity_6_corRNA"
"Nuclei_Granularity_7_corAGP"
"Nuclei_Granularity_7_corER"
"Nuclei_Granularity_7_corMito"
"Nuclei_Granularity_7_corRNA"
"Nuclei_Granularity_8_corAGP"
"Nuclei_Granularity_8_corER"
"Nuclei_Granularity_8_corMito"
"Nuclei_Granularity_8_corRNA"
"Nuclei_Granularity_9_corAGP"
"Nuclei_Granularity_9_corER"
"Nuclei_Granularity_9_corMito"
"Nuclei_Granularity_9_corRNA"
"Nuclei_Intensity_IntegratedIntensityEdge_corAGP"
"Nuclei_Intensity_IntegratedIntensityEdge_corER"
"Nuclei_Intensity_IntegratedIntensityEdge_corMito"
"Nuclei_Intensity_IntegratedIntensityEdge_corNucleus"
"Nuclei_Intensity_IntegratedIntensityEdge_corRNA"
"Nuclei_Intensity_IntegratedIntensity_corAGP"
"Nuclei_Intensity_IntegratedIntensity_corER"
"Nuclei_Intensity_IntegratedIntensity_corMito"

"Nuclei_Intensity_IntegratedIntensity_corNucleus"
"Nuclei_Intensity_IntegratedIntensity_corRNA"
"Nuclei_Intensity_LowerQuartileIntensity_corAGP"
"Nuclei_Intensity_LowerQuartileIntensity_corER"
"Nuclei_Intensity_LowerQuartileIntensity_corMito"
"Nuclei_Intensity_LowerQuartileIntensity_corNucleus"
"Nuclei_Intensity_LowerQuartileIntensity_corRNA"
"Nuclei_Intensity_MADIntensity_corAGP"
"Nuclei_Intensity_MADIntensity_corER"
"Nuclei_Intensity_MADIntensity_corMito"
"Nuclei_Intensity_MADIntensity_corNucleus"
"Nuclei_Intensity_MADIntensity_corRNA"
"Nuclei_Intensity_MassDisplacement_corAGP"
"Nuclei_Intensity_MassDisplacement_corER"
"Nuclei_Intensity_MassDisplacement_corMito"
"Nuclei_Intensity_MassDisplacement_corNucleus"
"Nuclei_Intensity_MassDisplacement_corRNA"
"Nuclei_Intensity_MaxIntensityEdge_corAGP"
"Nuclei_Intensity_MaxIntensityEdge_corER"
"Nuclei_Intensity_MaxIntensityEdge_corMito"
"Nuclei_Intensity_MaxIntensityEdge_corNucleus"
"Nuclei_Intensity_MaxIntensityEdge_corRNA"
"Nuclei_Intensity_MaxIntensity_corAGP"
"Nuclei_Intensity_MaxIntensity_corER"
"Nuclei_Intensity_MaxIntensity_corMito"
"Nuclei_Intensity_MaxIntensity_corNucleus"
"Nuclei_Intensity_MaxIntensity_corRNA"
"Nuclei_Intensity_MeanIntensityEdge_corAGP"
"Nuclei_Intensity_MeanIntensityEdge_corER"
"Nuclei_Intensity_MeanIntensityEdge_corMito"
"Nuclei_Intensity_MeanIntensityEdge_corNucleus"
"Nuclei_Intensity_MeanIntensityEdge_corRNA"
"Nuclei_Intensity_MeanIntensity_corAGP"
"Nuclei_Intensity_MeanIntensity_corER"
"Nuclei_Intensity_MeanIntensity_corMito"
"Nuclei_Intensity_MeanIntensity_corNucleus"
"Nuclei_Intensity_MeanIntensity_corRNA"
"Nuclei_Intensity_MedianIntensity_corAGP"
"Nuclei_Intensity_MedianIntensity_corER"
"Nuclei_Intensity_MedianIntensity_corMito"
"Nuclei_Intensity_MedianIntensity_corNucleus"
"Nuclei_Intensity_MedianIntensity_corRNA"
"Nuclei_Intensity_MinIntensityEdge_corAGP"
"Nuclei_Intensity_MinIntensityEdge_corER"
"Nuclei_Intensity_MinIntensityEdge_corMito"
"Nuclei_Intensity_MinIntensityEdge_corNucleus"
"Nuclei_Intensity_MinIntensityEdge_corRNA"
"Nuclei_Intensity_MinIntensity_corAGP"
"Nuclei_Intensity_MinIntensity_corER"
"Nuclei_Intensity_MinIntensity_corMito"
"Nuclei_Intensity_MinIntensity_corNucleus"
"Nuclei_Intensity_MinIntensity_corRNA"
"Nuclei_Intensity_StdIntensityEdge_corAGP"
"Nuclei_Intensity_StdIntensityEdge_corER"
"Nuclei_Intensity_StdIntensityEdge_corMito"
"Nuclei_Intensity_StdIntensityEdge_corNucleus"
"Nuclei_Intensity_StdIntensityEdge_corRNA"
"Nuclei_Intensity_StdIntensity_corAGP"
"Nuclei_Intensity_StdIntensity_corER"
"Nuclei_Intensity_StdIntensity_corMito"
"Nuclei_Intensity_StdIntensity_corNucleus"
"Nuclei_Intensity_StdIntensity_corRNA"

"Nuclei_Intensity_UpperQuartileIntensity_corAGP"
"Nuclei_Intensity_UpperQuartileIntensity_corER"
"Nuclei_Intensity_UpperQuartileIntensity_corMito"
"Nuclei_Intensity_UpperQuartileIntensity_corNucleus"
"Nuclei_Intensity_UpperQuartileIntensity_corRNA"
"Nuclei_Neighbors_AngleBetweenNeighbors_1"
"Nuclei_Neighbors_FirstClosestDistance_1"
"Nuclei_Neighbors_FirstClosestObjectNumber_1"
"Nuclei_Neighbors_NumberOfNeighbors_1"
"Nuclei_Neighbors_PercentTouching_1"
"Nuclei_Neighbors_SecondClosestDistance_1"
"Nuclei_Neighbors_SecondClosestObjectNumber_1"
"Nuclei_RadialDistribution_FracAtD_corAGP_1of4"
"Nuclei_RadialDistribution_FracAtD_corAGP_2of4"
"Nuclei_RadialDistribution_FracAtD_corAGP_3of4"
"Nuclei_RadialDistribution_FracAtD_corAGP_4of4"
"Nuclei_RadialDistribution_FracAtD_corER_1of4"
"Nuclei_RadialDistribution_FracAtD_corER_2of4"
"Nuclei_RadialDistribution_FracAtD_corER_3of4"
"Nuclei_RadialDistribution_FracAtD_corER_4of4"
"Nuclei_RadialDistribution_FracAtD_corMito_1of4"
"Nuclei_RadialDistribution_FracAtD_corMito_2of4"
"Nuclei_RadialDistribution_FracAtD_corMito_3of4"
"Nuclei_RadialDistribution_FracAtD_corMito_4of4"
"Nuclei_RadialDistribution_FracAtD_corNucleus_1of4"
"Nuclei_RadialDistribution_FracAtD_corNucleus_2of4"
"Nuclei_RadialDistribution_FracAtD_corNucleus_3of4"
"Nuclei_RadialDistribution_FracAtD_corNucleus_4of4"
"Nuclei_RadialDistribution_FracAtD_corRNA_1of4"
"Nuclei_RadialDistribution_FracAtD_corRNA_2of4"
"Nuclei_RadialDistribution_FracAtD_corRNA_3of4"
"Nuclei_RadialDistribution_FracAtD_corRNA_4of4"
"Nuclei_RadialDistribution_MeanFrac_corAGP_1of4"
"Nuclei_RadialDistribution_MeanFrac_corAGP_2of4"
"Nuclei_RadialDistribution_MeanFrac_corAGP_3of4"
"Nuclei_RadialDistribution_MeanFrac_corAGP_4of4"
"Nuclei_RadialDistribution_MeanFrac_corER_1of4"
"Nuclei_RadialDistribution_MeanFrac_corER_2of4"
"Nuclei_RadialDistribution_MeanFrac_corER_3of4"
"Nuclei_RadialDistribution_MeanFrac_corER_4of4"
"Nuclei_RadialDistribution_MeanFrac_corMito_1of4"
"Nuclei_RadialDistribution_MeanFrac_corMito_2of4"
"Nuclei_RadialDistribution_MeanFrac_corMito_3of4"
"Nuclei_RadialDistribution_MeanFrac_corMito_4of4"
"Nuclei_RadialDistribution_MeanFrac_corNucleus_1of4"
"Nuclei_RadialDistribution_MeanFrac_corNucleus_2of4"
"Nuclei_RadialDistribution_MeanFrac_corNucleus_3of4"
"Nuclei_RadialDistribution_MeanFrac_corNucleus_4of4"
"Nuclei_RadialDistribution_MeanFrac_corRNA_1of4"
"Nuclei_RadialDistribution_MeanFrac_corRNA_2of4"
"Nuclei_RadialDistribution_MeanFrac_corRNA_3of4"
"Nuclei_RadialDistribution_MeanFrac_corRNA_4of4"
"Nuclei_RadialDistribution_RadialCV_corAGP_1of4"
"Nuclei_RadialDistribution_RadialCV_corAGP_2of4"
"Nuclei_RadialDistribution_RadialCV_corAGP_3of4"
"Nuclei_RadialDistribution_RadialCV_corAGP_4of4"
"Nuclei_RadialDistribution_RadialCV_corER_1of4"
"Nuclei_RadialDistribution_RadialCV_corER_2of4"
"Nuclei_RadialDistribution_RadialCV_corER_3of4"
"Nuclei_RadialDistribution_RadialCV_corER_4of4"
"Nuclei_RadialDistribution_RadialCV_corMito_1of4"
"Nuclei_RadialDistribution_RadialCV_corMito_2of4"

"Nuclei_RadialDistribution_RadialCV_corMito_3of4"
"Nuclei_RadialDistribution_RadialCV_corMito_4of4"
"Nuclei_RadialDistribution_RadialCV_corNucleus_1of4"
"Nuclei_RadialDistribution_RadialCV_corNucleus_2of4"
"Nuclei_RadialDistribution_RadialCV_corNucleus_3of4"
"Nuclei_RadialDistribution_RadialCV_corNucleus_4of4"
"Nuclei_RadialDistribution_RadialCV_corRNA_1of4"
"Nuclei_RadialDistribution_RadialCV_corRNA_2of4"
"Nuclei_RadialDistribution_RadialCV_corRNA_3of4"
"Nuclei_RadialDistribution_RadialCV_corRNA_4of4"

Appendix Table. 1 *Non-standard abbreviations*

Abbreviation	Full name
BMP4	bone morphogenetic protein 4
BSA	Bovine Serum Albumin
CRISPR	clustered regularly interspaced short palindromic repeats
CROP-seq	CRISPR droplet sequencing
DEGs	differentially expressed genes
DP-MSCs	dental pulp-Mesenchymal stem cells
ECM	extracellular matrix
ELISA	Enzyme-linked immunosorbent assay
ER	endoplasmic reticulum
FACS	fluorescence activated cell sorting
FBS	fetal bovine serum
GWAS	genome-wide association studies
HDR	homology-directed repair
HNDF	human neonatal dermal fibroblast
IOP	Intraocular pressure
JCT	juxtacanalicular tissue
MSCs	mesenchymal stem cells
NGS	next generation sequencing
NHEJ	non-homologous end joining
NTG	normal-tension glaucoma
PBA	sodium 4-phenylbutyrate
PBS	phosphate-buffered saline
POAG	Primary open-angle glaucoma
POM	periocular mesenchyme
RA	retinoic acid
RAR	retinoic acid receptor
RGCs	retinal ganglion cells
RNAi	RNA interference
ROCK	Rho kinase
ROS	reactive oxygen species
RXR	retinoid X receptor
scRNA-seq	single-cell RNA sequencing
sgRNAs	single-guide RNAs
SNPs	single nucleotide polymorphisms
SpCas9	*Streptococcus pyogenes* Cas9
TGF-β2	transforming growth factor-β2
TM	trabecular meshwork
TMCs	trabecular meshwork cells
TNF-α	tumor necrosis factor α
UMI	unique molecular identifier
WGA	Wheat Germ Agglutinin

Appendix Table. 2 *Gene name abbreviations for genes selected for CRISPR/Cas knockout*

Abbreviation	Full name
ABCA1	ATP binding cassette subfamily A member 1
ABO	ABO, alpha 1-3-N-acetylgalactosaminyltransferase and alpha 1-3-galactosyltransferase
ADAMTS6	ADAM metallopeptidase with thrombospondin type 1 motif 6
AFAP1	actin filament associated protein 1
ALDH9A1	aldehyde dehydrogenase 9 family member A1
ANAPC1	anaphase promoting complex subunit 1
ANGPT1	angiopoietin 1
ANGPT2	angiopoietin 2
ANGPTL2	angiopoietin like 2
ANKH	ANKH inorganic pyrophosphate transport regulator
ANTXR1	ANTXR cell adhesion molecule 1
ARHGEF12	Rho guanine nucleotide exchange factor 12
ATXN2	ataxin 2
BCAS3	BCAS3 microtubule associated cell migration factor
CAPZA1	capping actin protein of muscle Z-line subunit alpha 1
CAV1	caveolin 1
CAV2	caveolin 2
CDH11	cadherin 11
COL24A1	collagen type XXIV alpha 1 chain
CTTNBP2	cortactin binding protein 2
CYP1B1	cytochrome P450 family 1 subfamily B member 1
DGKG	diacylglycerol kinase gamma
EFEMP1	EGF containing fibulin extracellular matrix protein 1
EMCN	endomucin
EMID1	EMI domain containing 1
ETS1	ETS proto-oncogene 1, transcription factor
FBXO32	F-box protein 32
FER	FER tyrosine kinase

FERMT2	fermitin family member 2
FMNL2	formin like 2
FNDC3B	fibronectin type III domain containing 3B
FOXC1	forkhead box C1
GAS7	growth arrest specific 7
GMDS	GDP-mannose 4,6-dehydratase
GNB1L	G protein subunit beta 1 like
KALRN	kalirin RhoGEF kinase
KREMEN1	kringle containing transmembrane protein 1
LMO7	LIM domain 7
LMX1B	LIM homeobox transcription factor 1 beta
LTBP2	latent transforming growth factor beta binding protein 2
ME3	malic enzyme 3
MECOM	MDS1 and EVI1 complex locus
MYOC	myocilin
MYOF	myoferlin
PARD3B	par-3 family cell polarity regulator beta
PDE7B	phosphodiesterase 7B
PKHD1	PKHD1 ciliary IPT domain containing fibrocystin/polyductin
PLEKHA7	pleckstrin homology domain containing A7
PRSS23	serine protease 23
PTPRJ	protein tyrosine phosphatase receptor type J
RALGPS1	Ral GEF with PH domain and SH3 binding motif 1
RUNX2	RUNX family transcription factor 2
SPTBN1	spectrin beta, non-erythrocytic 1
TEK	TEK receptor tyrosine kinase
TES	testin LIM domain protein
TEX41	testis expressed 41
TIMP3	TIMP metallopeptidase inhibitor 3
TMCO1	transmembrane and coiled-coil domains 1
TNS1	tensin 1
TRIOBP	TRIO and F-actin binding protein

TXNRD2	thioredoxin reductase 2
ZNF280D	zinc finger protein 280D

Appendix Table. 3 *Gene name abbreviations identified through CROP-seq*

Abbreviation	Full name
TAC1	tachykinin precursor 1
IL1RN	interleukin 1 receptor antagonist
MMP10	matrix metallopeptidase 10
OASL	2'-5'-oligoadenylate synthetase like
RSAD2	radical S-adenosyl methionine domain containing 2
PRG4	proteoglycan 4
IFI44L	interferon induced protein 44 like
PRSS35	serine protease 35
CMPK2	cytidine/uridine monophosphate kinase 2
MX1	MX dynamin like GTPase 1
IFIT1	interferon induced protein with tetratricopeptide repeats 1
OAS1	2'-5'-oligoadenylate synthetase 1
ISG15	ISG15 ubiquitin like modifier
MX2	MX dynamin like GTPase 2
IFI6	interferon alpha inducible protein 6
FYB1	FYN binding protein 1
CRYGS	crystallin gamma S
IFI27	interferon alpha inducible protein 27
IFIT3	interferon induced protein with tetratricopeptide repeats 3
BST2	bone marrow stromal cell antigen 2
IFIH1	interferon induced with helicase C domain 1
OAS2	2'-5'-oligoadenylate synthetase 2
IFITM1	interferon induced transmembrane protein 1
USP18	ubiquitin specific peptidase 18
HERC5	HECT and RLD domain containing E3 ubiquitin protein ligase 5
RTP4	receptor transporter protein 4
CCDC33	coiled-coil domain containing 33
KCNK3	potassium two pore domain channel subfamily K member 3
C3orf80	chromosome 3 open reading frame 80

KIT	KIT proto-oncogene, receptor tyrosine kinase
PTPRE	protein tyrosine phosphatase receptor type E
LDLRAD4	low density lipoprotein receptor class A domain containing 4
MGARP	mitochondria localized glutamic acid rich protein
OAS3	2'-5'-oligoadenylate synthetase 3
SLC16A6	solute carrier family 16 member 6
ALDH1A1	aldehyde dehydrogenase 1 family member A1
RNF128	ring finger protein 128
CCL3L1	C-C motif chemokine ligand 3 like 1
ADGRG1	adhesion G protein-coupled receptor G1
LGALS9	galectin 9
TSPAN15	tetraspanin 15
MMP1	matrix metallopeptidase 1
AQP3	aquaporin 3 (Gill blood group)
GPR68	G protein-coupled receptor 68
PTHLH	parathyroid hormone like hormone
XAF1	XIAP associated factor 1
MYOZ1	myozenin 1
HERC6	HECT and RLD domain containing E3 ubiquitin protein ligase family member 6
IRF7	interferon regulatory factor 7
RASL11B	RAS like family 11 member B
PKIB	cAMP-dependent protein kinase inhibitor beta
LCE1C	late cornified envelope 1C
CD70	CD70 molecule
HS3ST2	heparan sulfate-glucosamine 3-sulfotransferase 2
RSPO2	R-spondin 2
TNFSF11	TNF superfamily member 11
LYPD6B	LY6/PLAUR domain containing 6B
LAMC3	laminin subunit gamma 3
MGP	matrix Gla protein
SPP1	secreted phosphoprotein 1
NEFL	neurofilament light

CXCL11	C-X-C motif chemokine ligand 11
PI16	peptidase inhibitor 16
NOX4	NADPH oxidase 4
F2RL1	F2R like trypsin receptor 1
PLXNA4	plexin A4
NPPC	natriuretic peptide C
CCL5	C-C motif chemokine ligand 5
PLXDC1	plexin domain containing 1
CXADR	CXADR Ig-like cell adhesion molecule
CXCL1	C-X-C motif chemokine ligand 1
LRFN5	leucine rich repeat and fibronectin type III domain containing 5
LCE2A	late cornified envelope 2A
GRIN2A	glutamate ionotropic receptor NMDA type subunit 2A
EPHB1	EPH receptor B1
EFEMP1	EGF containing fibulin extracellular matrix protein 1
MT1G	metallothionein 1G
LYPD3	LY6/PLAUR domain containing 3
GPRC5A	G protein-coupled receptor class C group 5 member A
CCL2	C-C motif chemokine ligand 2
SEMA7A	semaphorin 7A (John Milton Hagen blood group)
PIP	prolactin induced protein
CXCL6	C-X-C motif chemokine ligand 6
TAGLN3	transgelin 3
CST1	cystatin SN
APOE	apolipoprotein E
IL1B	interleukin 1 beta
SYTL5	synaptotagmin like 5
ATP6V0D2	ATPase H+ transporting V0 subunit d2
DPT	dermatopontin
PTGDR	prostaglandin D2 receptor
NFATC2	nuclear factor of activated T cells 2
IFITM10	interferon induced transmembrane protein 10

SLITRK6	SLIT and NTRK like family member 6
LCE3D	late cornified envelope 3D
CHODL	chondrolectin
PLD5	phospholipase D family member 5
C11orf96	chromosome 11 open reading frame 96
IVL	involucrin
CLCA2	chloride channel accessory 2
IL1A	interleukin 1 alpha
RANBP3L	RAN binding protein 3 like
RRAD	RRAD, Ras related glycolysis inhibitor and calcium channel regulator
RASD2	RASD family member 2
ANGPTL1	angiopoietin like 1
SHISAL2B	shisa like 2B
PRDM1	PR/SET domain 1
KYNU	kynureninase
USP53	ubiquitin specific peptidase 53
GAB3	GRB2 associated binding protein 3
RSPO3	R-spondin 3
DDX58	DExD/H-box helicase 58
IFIT2	interferon induced protein with tetratricopeptide repeats 2
ICOSLG	inducible T cell costimulator ligand
NKX2-2	NK2 homeobox 2
PIEZO2	piezo type mechanosensitive ion channel component 2
MMP3	matrix metallopeptidase 3
IGFL3	IGF like family member 3
TBX21	T-box transcription factor 21
PMCH	pro-melanin concentrating hormone
RARRES2	retinoic acid receptor responder 2
LCE2C	late cornified envelope 2C
EGR2	early growth response 2
CSF2	colony stimulating factor 2
TTR	transthyretin

STATH	statherin
MYOC	myocilin
CCL8	C-C motif chemokine ligand 8
CORIN	corin, serine peptidase
HS6ST3	heparan sulfate 6-O-sulfotransferase 3
PTPRR	protein tyrosine phosphatase receptor type R
NR0B1	nuclear receptor subfamily 0 group B member 1
SCUBE3	signal peptide, CUB domain and EGF like domain containing 3
BCAN	brevican
SCG5	secretogranin V
OLFML1	olfactomedin like 1
GRB14	growth factor receptor bound protein 14
PDE6A	phosphodiesterase 6A
ADH1B	alcohol dehydrogenase 1B (class I), beta polypeptide
RIPK4	receptor interacting serine/threonine kinase 4
COL15A1	collagen type XV alpha 1 chain
DHRS2	dehydrogenase/reductase 2
PCP4	Purkinje cell protein 4
KRT14	keratin 14
CHI3L1	chitinase 3 like 1
ABI3	ABI family member 3
GUCY1A2	guanylate cyclase 1 soluble subunit alpha 2
FRMD3	FERM domain containing 3
BMF	Bcl2 modifying factor
MEGF10	multiple EGF like domains 10
TSGA10IP	testis specific 10 interacting protein
NTSR1	neurotensin receptor 1
SAMD11	sterile alpha motif domain containing 11
KISS1	KiSS-1 metastasis suppressor
TMEM244	transmembrane protein 244
HTR7	5-hydroxytryptamine receptor 7
MEST	mesoderm specific transcript

ITGA10	integrin subunit alpha 10
WNT16	Wnt family member 16
CGA	glycoprotein hormones, alpha polypeptide
DRAXIN	dorsal inhibitory axon guidance protein
PAPPA2	pappalysin 2
DLX2	distal-less homeobox 2
C19orf33	chromosome 19 open reading frame 33
ITGB6	integrin subunit beta 6
SNTG1	syntrophin gamma 1
USP44	ubiquitin specific peptidase 44
WNT7B	Wnt family member 7B
ODAPH	odontogenesis associated phosphoprotein
TINCR	TINCR ubiquitin domain containing
ST8SIA5	ST8 alpha-N-acetyl-neuraminide alpha-2,8-sialyltransferase 5
SNAP25	synaptosome associated protein 25
CPA4	carboxypeptidase A4
SOX5	SRY-box transcription factor 5
ISLR2	immunoglobulin superfamily containing leucine rich repeat 2
TNFAIP6	TNF alpha induced protein 6
TMEM132B	transmembrane protein 132B
PLA1A	phospholipase A1 member A
KRT81	keratin 81
PLAAT4	phospholipase A and acyltransferase 4
BAALC	BAALC binder of MAP3K1 and KLF4
LCE1F	late cornified envelope 1F
SALL1	spalt like transcription factor 1
SYT1	synaptotagmin 1
ANKRD33B	ankyrin repeat domain 33B
CHRNA9	cholinergic receptor nicotinic alpha 9 subunit
HMOX1	heme oxygenase 1
UNC5B	unc-5 netrin receptor B
PGF	placental growth factor

PTPRZ1	protein tyrosine phosphatase receptor type Z1
KRTAP4-8	keratin associated protein 4-8
CRHBP	corticotropin releasing hormone binding protein
CCL20	C-C motif chemokine ligand 20
S100B	S100 calcium binding protein B
LYPD1	LY6/PLAUR domain containing 1
CLDN14	claudin 14
APOD	apolipoprotein D
GALNT15	polypeptide N-acetylgalactosaminyltransferase 15
FABP4	fatty acid binding protein 4
CDH20	cadherin 20
GASK1B	golgi associated kinase 1B
VSIR	V-set immunoregulatory receptor
HEY2	hes related family bHLH transcription factor with YRPW motif 2
LRRC4	leucine rich repeat containing 4
AQP1	aquaporin 1 (Colton blood group)
EXPH5	exophilin 5
MSMP	microseminoprotein, prostate associated
HRK	harakiri, BCL2 interacting protein
LRRN1	leucine rich repeat neuronal 1
SERPINB9	serpin family B member 9
HTR2A	5-hydroxytryptamine receptor 2A
SMOC1	SPARC related modular calcium binding 1
ANO1	anoctamin 1
IL18	interleukin 18
APCDD1	APC down-regulated 1
PRELP	proline and arginine rich end leucine rich repeat protein
SCG2	secretogranin II
WNT11	Wnt family member 11
HES1	hes family bHLH transcription factor 1
GABRB2	gamma-aminobutyric acid type A receptor subunit beta2
CXCL14	C-X-C motif chemokine ligand 14

SFRP4	secreted frizzled related protein 4
BACH2	BTB domain and CNC homolog 2
DMKN	dermokine
CCK	cholecystokinin
G0S2	G0/G1 switch 2
ANKRD30B	ankyrin repeat domain 30B
ZNF556	zinc finger protein 556
HAPLN1	hyaluronan and proteoglycan link protein 1
FABP3	fatty acid binding protein 3
KCNN2	potassium calcium-activated channel subfamily N member 2
PPL	periplakin
GDF5	growth differentiation factor 5
BEX5	brain expressed X-linked 5
TINAGL1	tubulointerstitial nephritis antigen like 1
STEAP4	STEAP4 metalloreductase
COMP	cartilage oligomeric matrix protein
PTGIS	prostaglandin I2 synthase
CFD	complement factor D
ADAMTSL4	ADAMTS like 4

Appendix Figure 1. ***Plots comparing log2 expression profiles of differential expressed genes between gene knockout groups compared to non-targeting control groups.***
1) ABCA1, 2) ABO, 3) ADAMTS6, 4) AFAP1, 5) ALDH9A1, 6) ANAPC1, 7) ANGPT1, 8) ANGPT2, 9) ANGPTL2, 10) ANKH, 11) ANTXR1, 12) ARHGEF12, 13) ATXN2, 14) BCAS3, 15) CAPZA1, 16) CAV1, 17) CAV2, 18) CDH11, 19) COL24A1, 20) CTTNBP2, 21) CYP1B1, 22) DGKG, 23) EFEMP1, 24) EMCN, 25) EMID1, 26) ETS1, 27) FBXO32, 28) FER, 29) FERMT2, 30) FMNL2, 31) FNDC3B, 32) FOXC1, 33) GAS7, 34) GMDS, 35) GNB1L, 36) KALRN, 37) KREMEN1, 38) LMO7, 39) LMX1B, 40) LTBP2, 41) ME3, 42) MECOM, 43) MYOC, 44) MYOF, 45) PARD3B, 46) PDE7B, 47) PKHD1, 48) PLEKHA7, 49) PRSS23, 50) PTPRJ, 51) RALGPS1, 52) RUNX2, 53) SPTBN1, 54) TEK, 55) TES, 56) TEX41, 57) TIMP3, 58) TMCO1, 59) TNS1, 60) TRIOBP, 61) TXNRD2, 62) ZNF280D

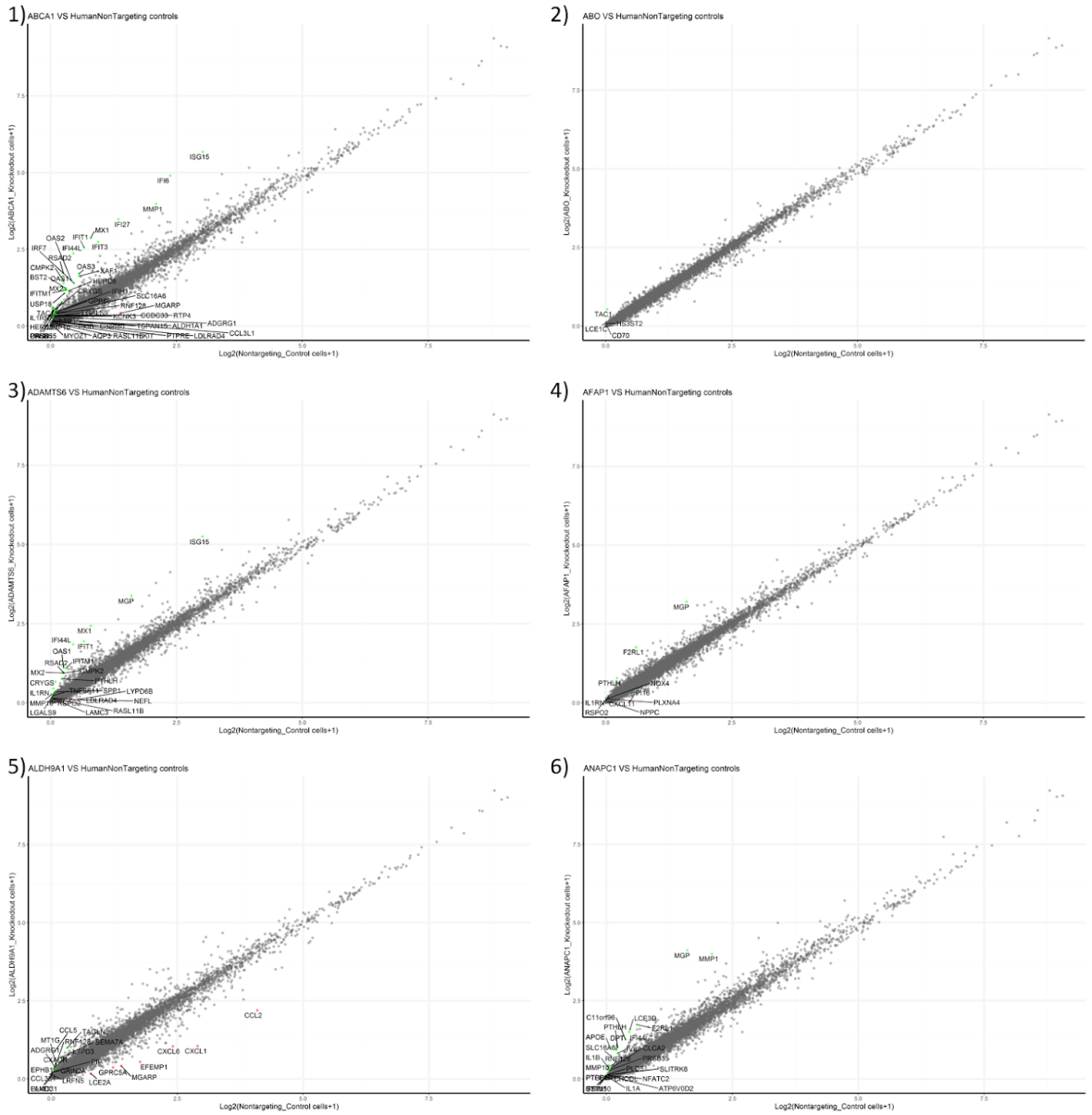
1) ABCA1 VS HumanNonTargeting controls
Log2(ABCA1_Knockdout cells+1)
Log2(Nontargeting_Control cells+1)
ISG15
IFI6
MMP1
IFI27
MX1
OAS2
IFIT1
IRF7
IFI44L
IFIT3
RSAD2
CMPK2
OAS3
KAT2B
BST2
OAS1
HERC5
MX2
IFITM1
CYP26B1
IFI44
SLC16A6
USP18
GDF15
RNF128
MGARP
TAP1
IL1RN
KCNK1
CCDC93
RTP4
HERC6
PSCA
ADGRG1
TSPAN15
ALDH1A1
DHRS3
MYOZ1
ADP3
RASL11B
KIT
PTPRE
LDLRAD4
CCL3L1
2) ABO VS HumanNonTargeting controls
Log2(ABO_Knockdout cells+1)
Log2(Nontargeting_Control cells+1)
TAC1
HS3ST2
LCE1A
CD70
3) ADAMTS6 VS HumanNonTargeting controls
Log2(ADAMTS6_Knockdout cells+1)
Log2(Nontargeting_Control cells+1)
ISG15
MGP
MX1
IFI44L
IFIT1
OAS1
RSAD2
IFITM1
MX2
CRYGS
PTHLH
IL1RN
SPP1
LYPD6B
MMP1
LDLRAD4
NEFL
LGALS9
LAMC3
RASL11B
4) AFAP1 VS HumanNonTargeting controls
Log2(AFAP1_Knockdout cells+1)
Log2(Nontargeting_Control cells+1)
MGP
F2RL1
PTHLH
NDX4
IL1RN
CXCL1
PLXNA4
RSPO2
NPPC
5) ALDH9A1 VS HumanNonTargeting controls
Log2(ALDH9A1_Knockdout cells+1)
Log2(Nontargeting_Control cells+1)
CCL2
CCL5
TAGLN
MT1G
RNF135
SEMA7A
ADGRE5
CXCL6
CXCL1
CYP26B1
EFEMP1
EPHB3
GPRC5A
MGARP
CCL20
LRFN5
LCE2A
6) ANAPC1 VS HumanNonTargeting controls
Log2(ANAPC1_Knockdout cells+1)
Log2(Nontargeting_Control cells+1)
MGP
MMP1
C11orf96
LCE3D
PTHLH
F2RL1
APOE
DPT
IFI44L
SLC16A6
KYNU
CCDC42
IL1B
RN7SL1
PR6835
MMP10
PLCB1
SLITRK6
PTGS2
PHODL
NFATC2
IL1A
ATP6V0D2

7)

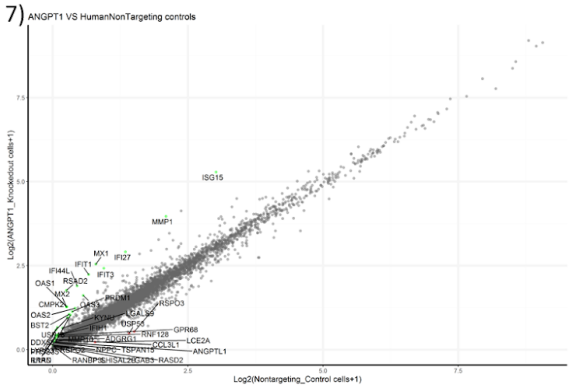
ANGPT1 VS HumanNonTargeting controls
Log2(ANGPT1_Knockdout cells+1)
Log2(Nontargeting_Control cells+1)
ISG15
MMP1
MX1
IFI27
IFIT1
IFI44L
IFIT3
OAS1
RSAD2
MX2
CMPK2
PRKM1
RSPO3
OAS2
LGALS9
BST2
OSF55
GPR68
TNF12B
LCE2A
CCL3L1
ANGPTL1
RASD2

8)

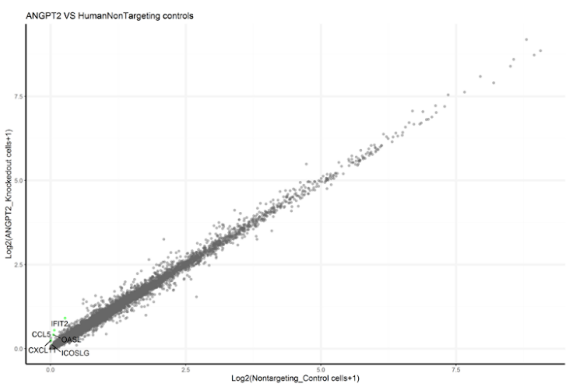
ANGPT2 VS HumanNonTargeting controls
Log2(ANGPT2_Knockdout cells+1)
Log2(Nontargeting_Control cells+1)
IFIT2
CCL5
OASL
CXCL11
ICOSLG

9)

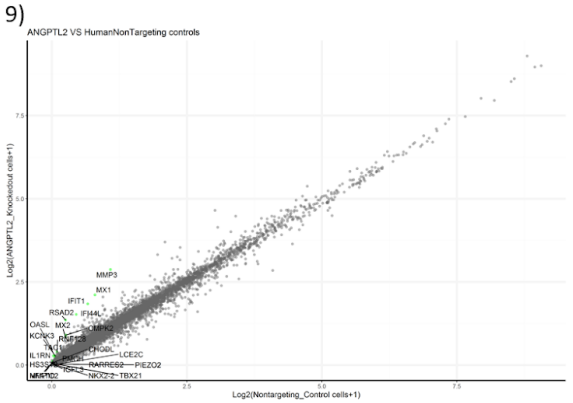
ANGPTL2 VS HumanNonTargeting controls
Log2(ANGPTL2_Knockdout cells+1)
Log2(Nontargeting_Control cells+1)
MMP3
MX1
IFIT1
RSAD2
IFI44L
OASL
MX2
CMPK2
KCNK3
IL1RN
LCE2C
HS3ST1
RARRES3
PIEZO2
NKX2-2
TBX21

10)

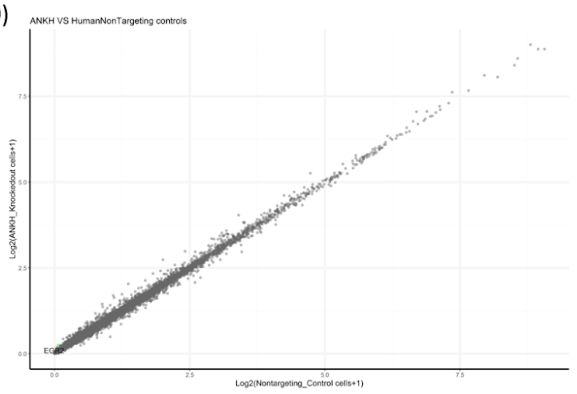
ANKH VS HumanNonTargeting controls
Log2(ANKH_Knockdout cells+1)
Log2(Nontargeting_Control cells+1)
ECM1

11)

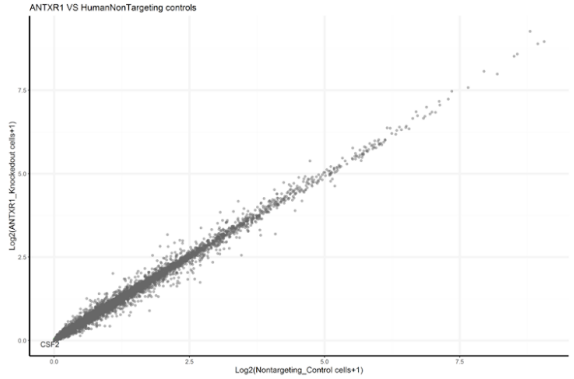
ANTXR1 VS HumanNonTargeting controls
Log2(ANTXR1_Knockdout cells+1)
Log2(Nontargeting_Control cells+1)
CSF2

12)

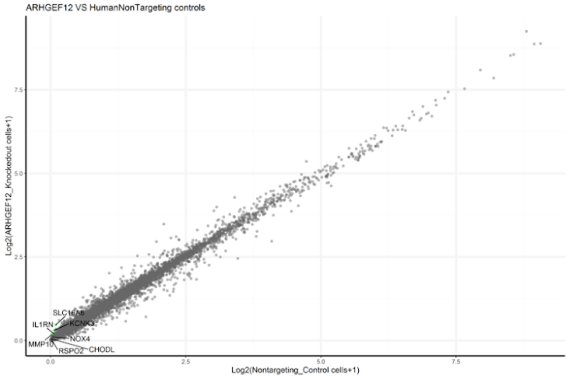
ARHGEF12 VS HumanNonTargeting controls
Log2(ARHGEF12_Knockdout cells+1)
Log2(Nontargeting_Control cells+1)
SLC16A6
IL1RN
KCNK3
NOX4
MMP10
RSPO2
CHODL

13)

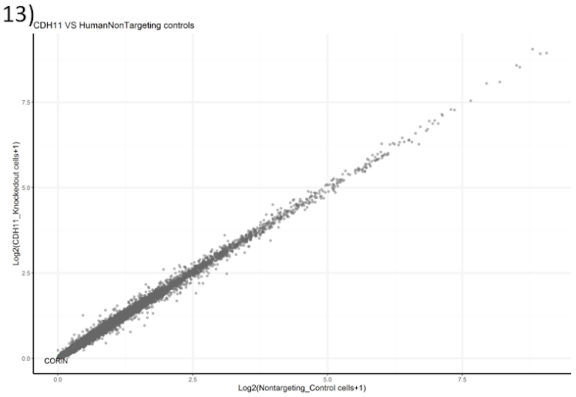

14)

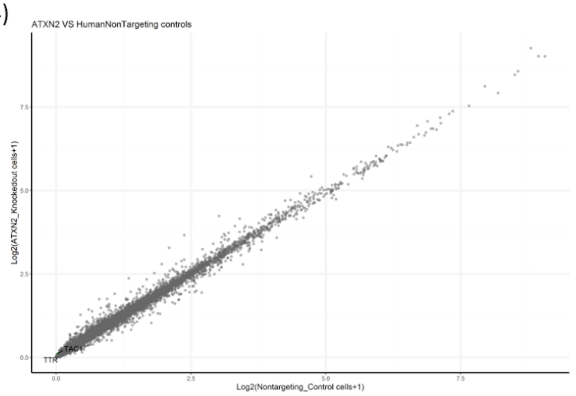

15)

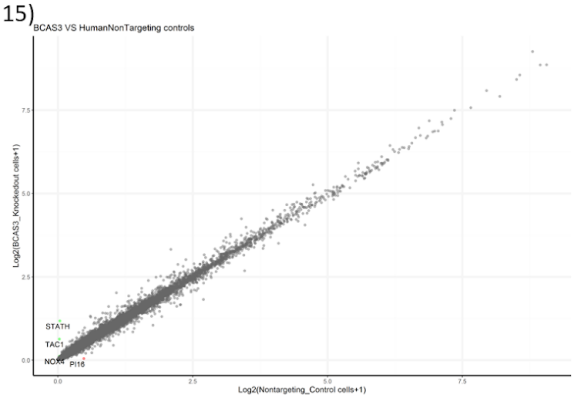

16)

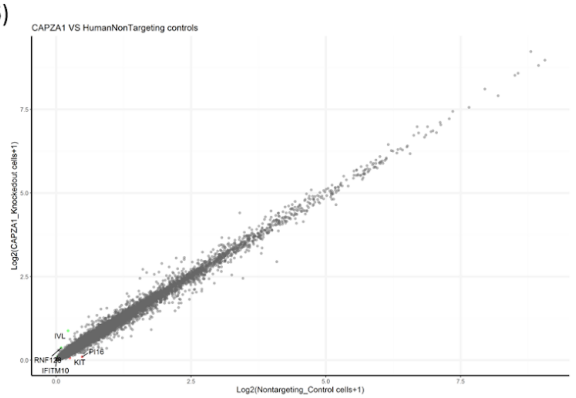

17)

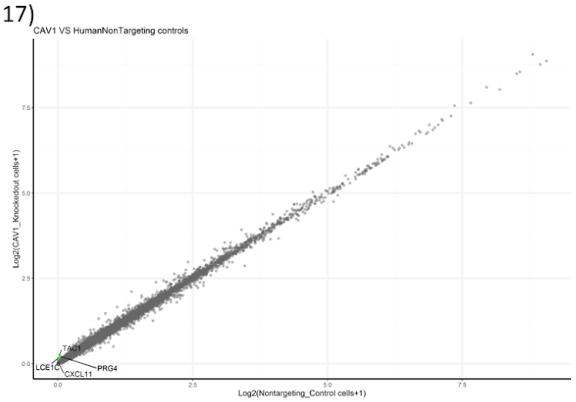

18)

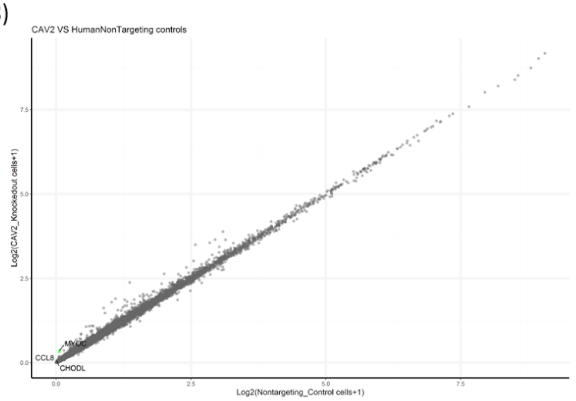

19)

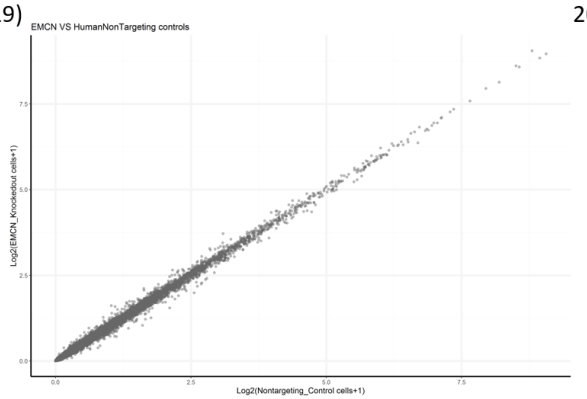

20)

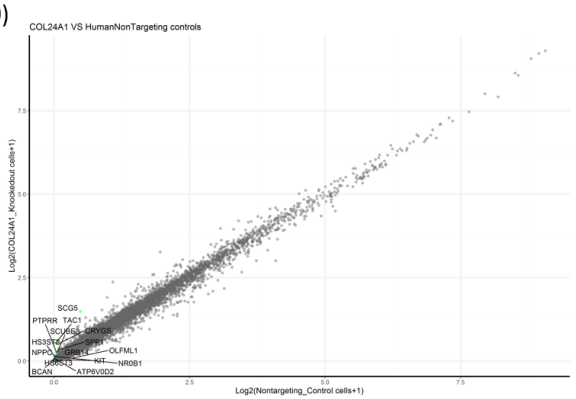

21)

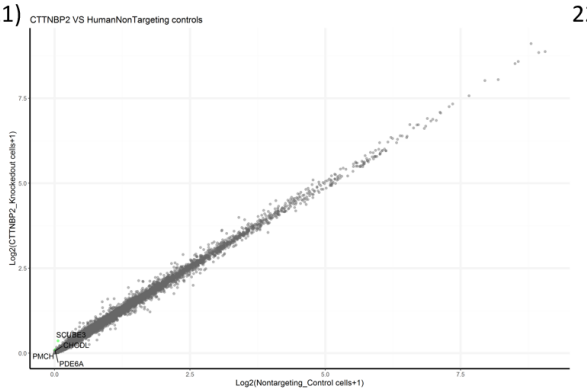

22)

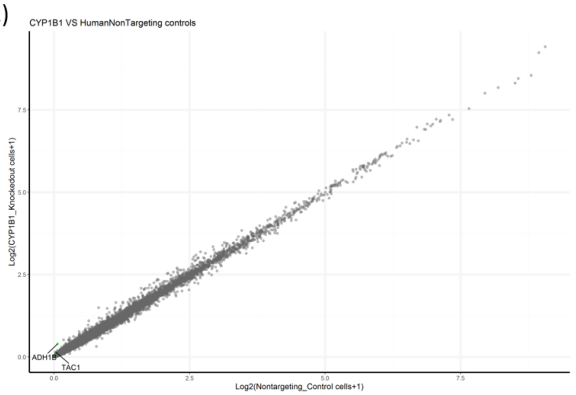

23)

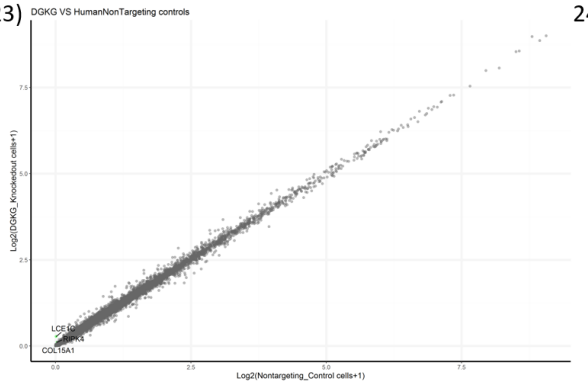

24)

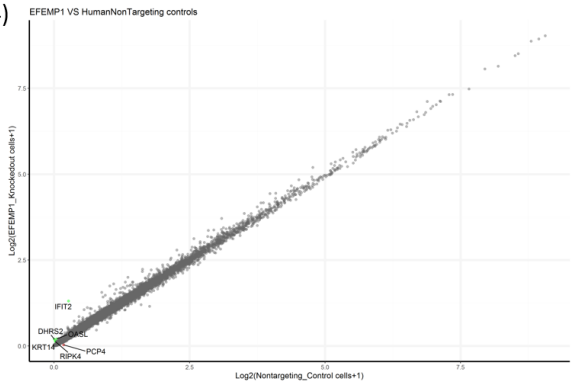

25)

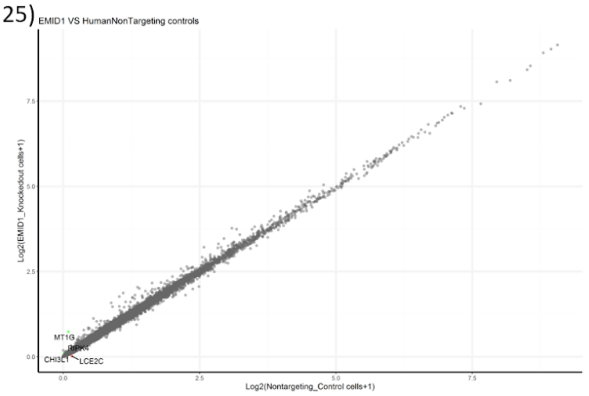

26)

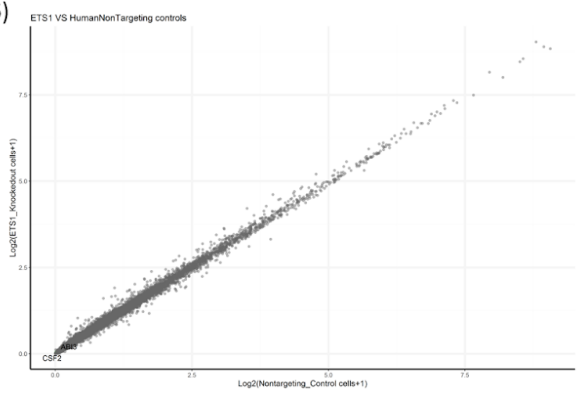

27)

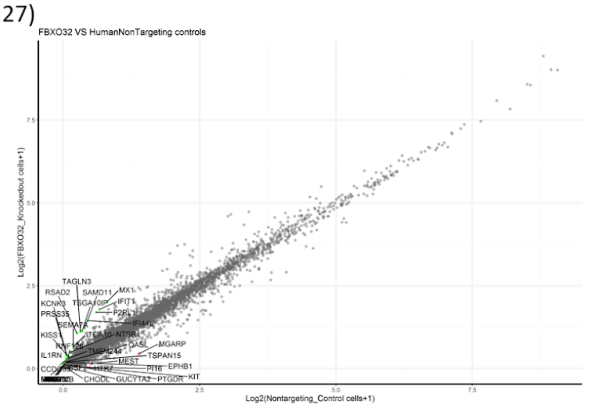

28)

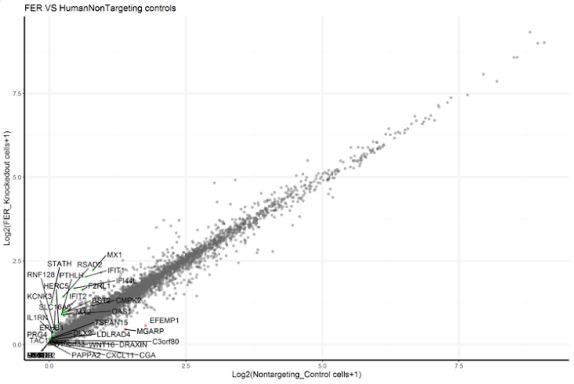

29)

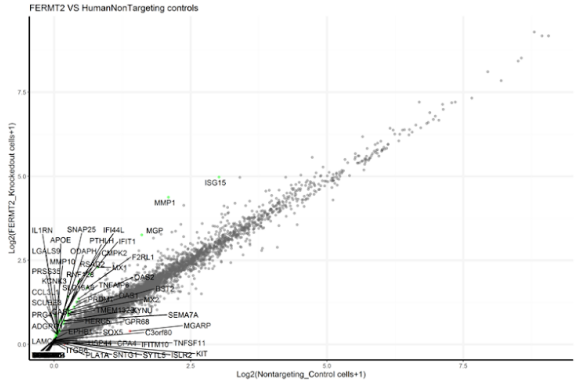

30)

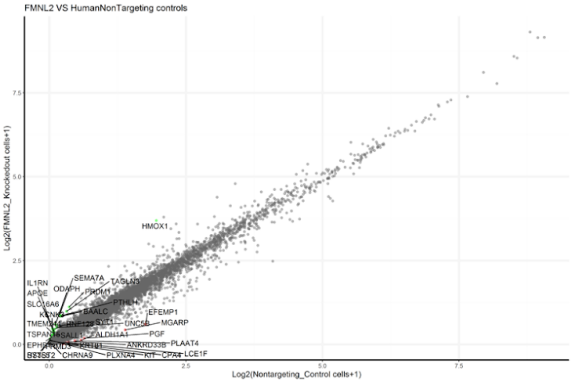

31)

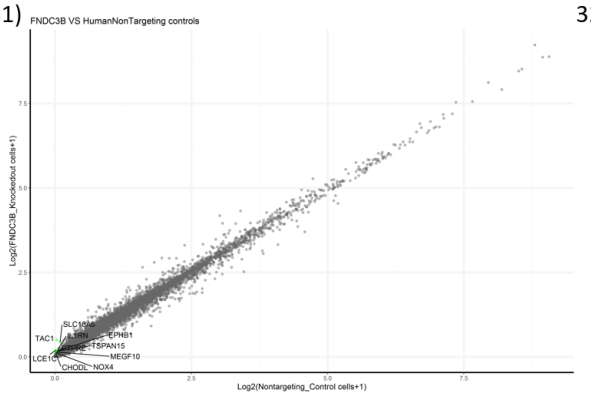

32)

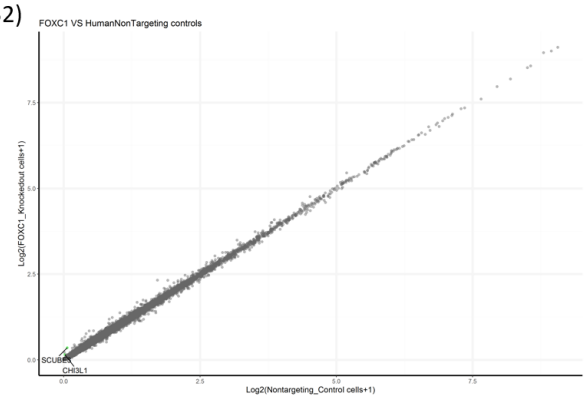

33)

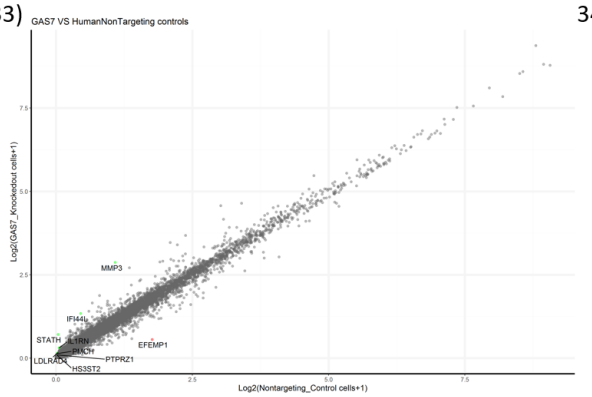

34)

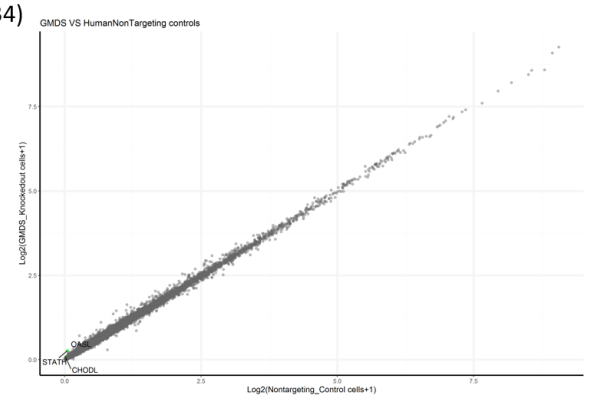

35)

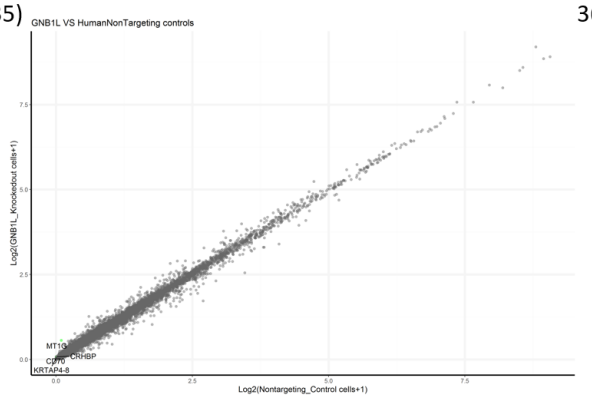

36)

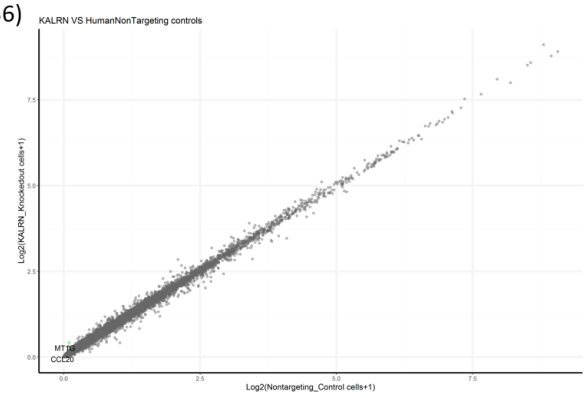

37)

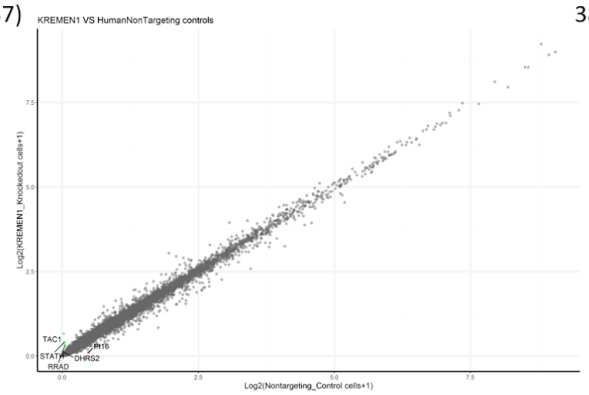

38)

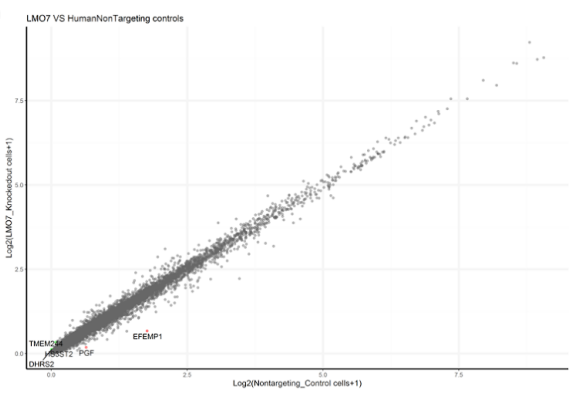

39)

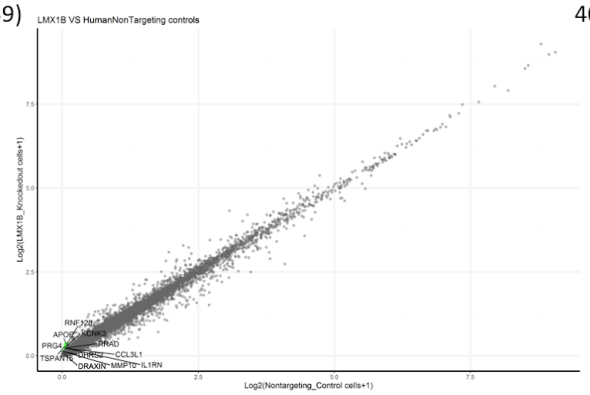

40)

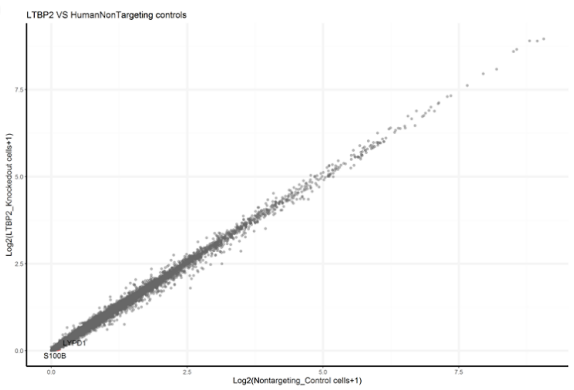

41)

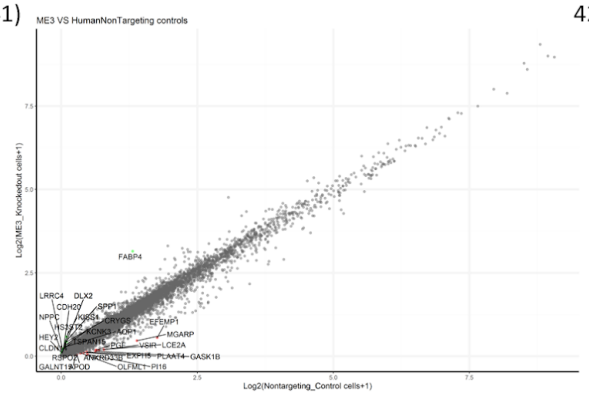

42)

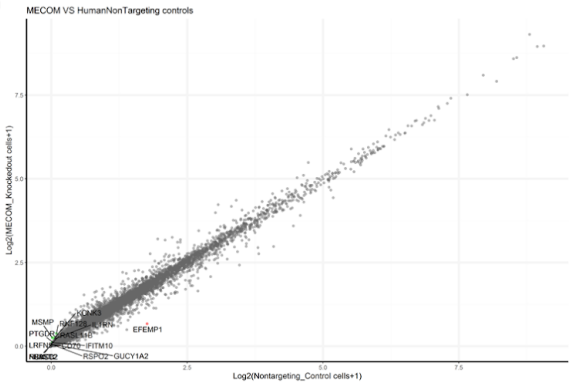

43) PLEKHA7 VS HumanNonTargeting controls

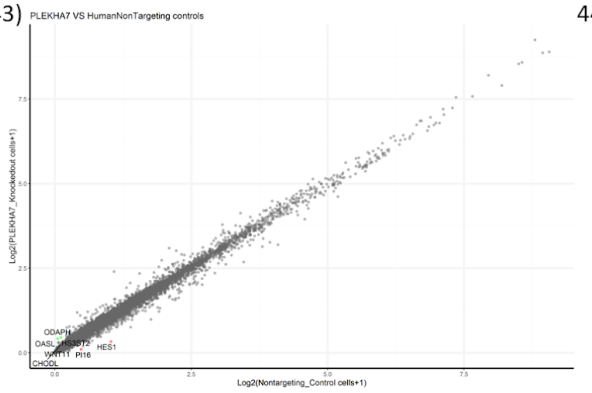

44) MYOC VS HumanNonTargeting controls

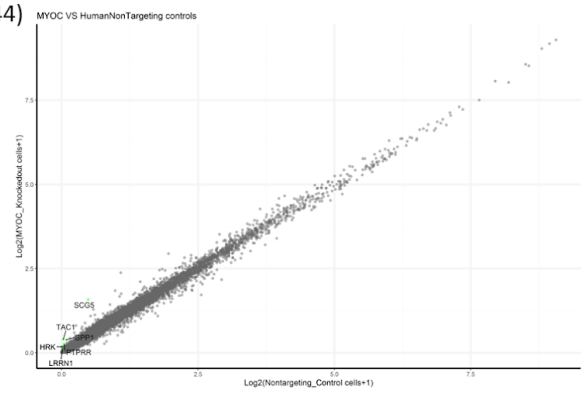

45) MYOF VS HumanNonTargeting controls

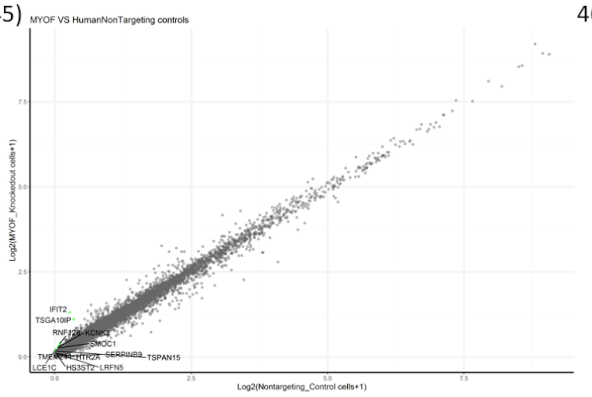

46) PARD3B VS HumanNonTargeting controls

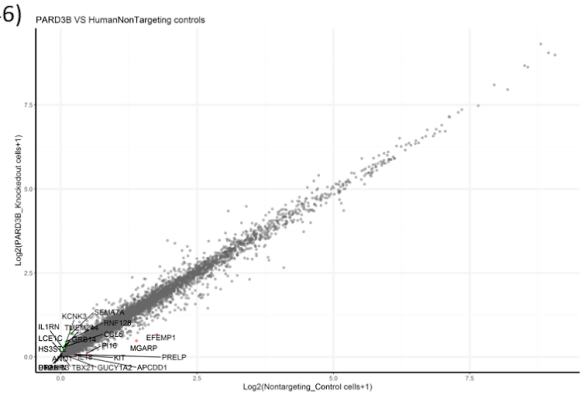

47) PDE7B VS HumanNonTargeting controls

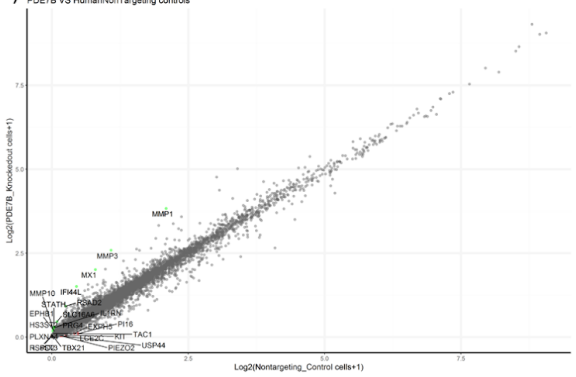

48) PKHD1 VS HumanNonTargeting controls

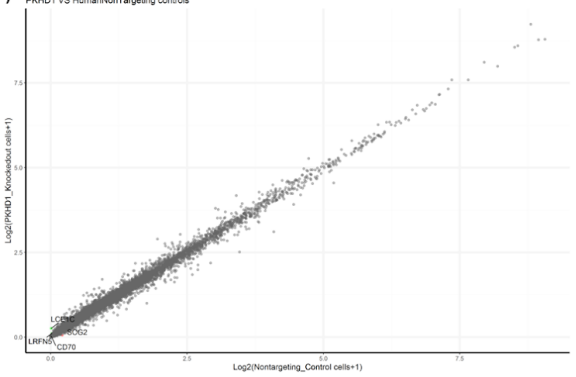

49) PRSS23 VS HumanNonTargeting controls

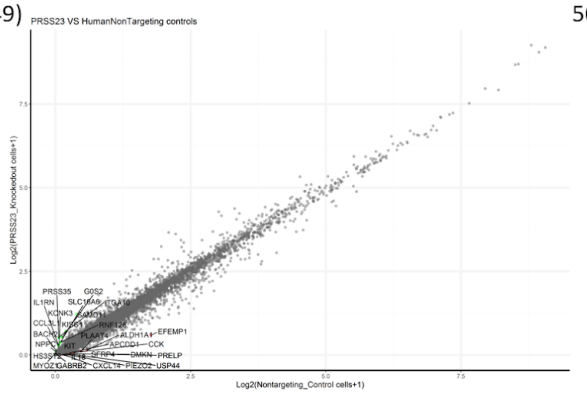

50) PTPRJ VS HumanNonTargeting controls

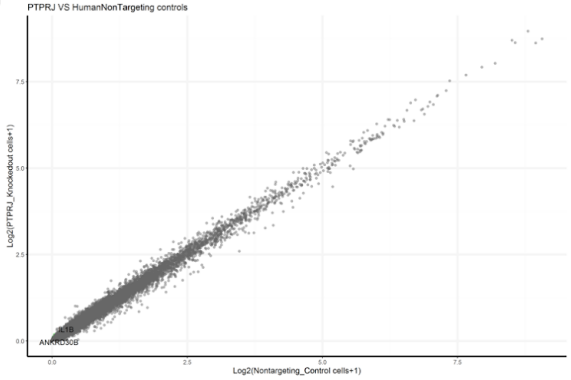

51) RALGPS1 VS HumanNonTargeting controls

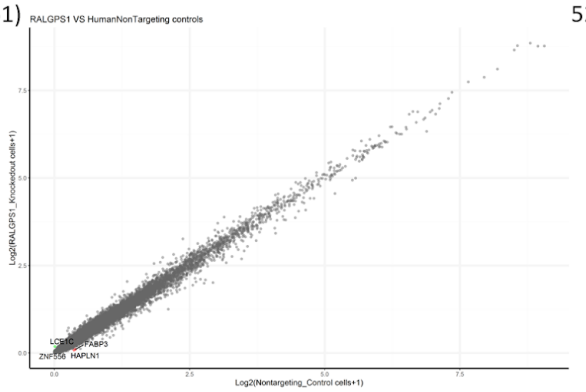

52) RUNX2 VS HumanNonTargeting controls

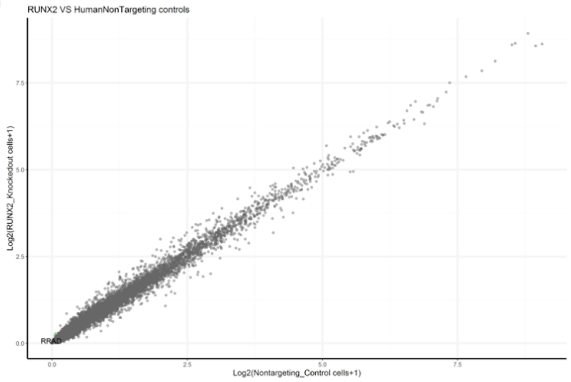

53) SPTBN1 VS HumanNonTargeting controls

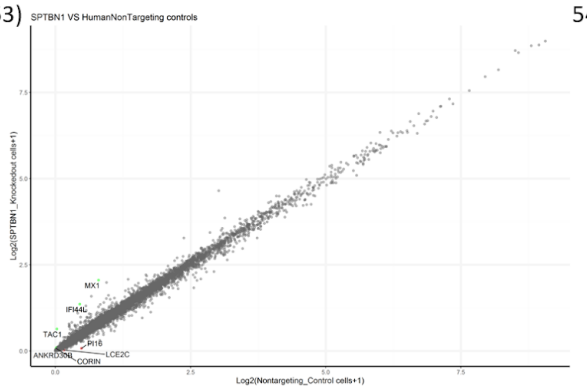

54) TEK VS HumanNonTargeting controls

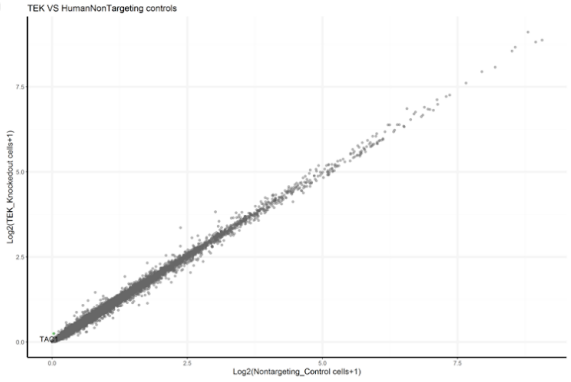

55) TIMP3 VS HumanNonTargeting controls

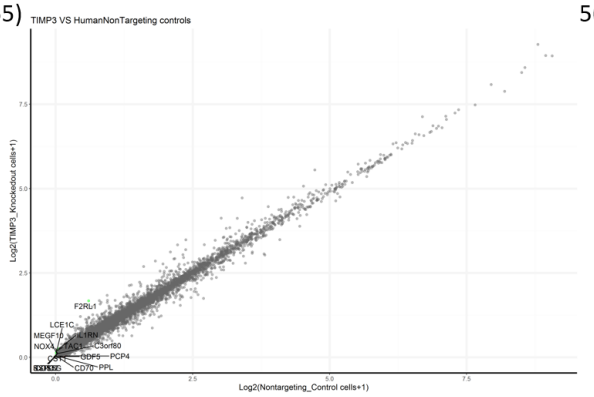

56) TMCO1 VS HumanNonTargeting controls

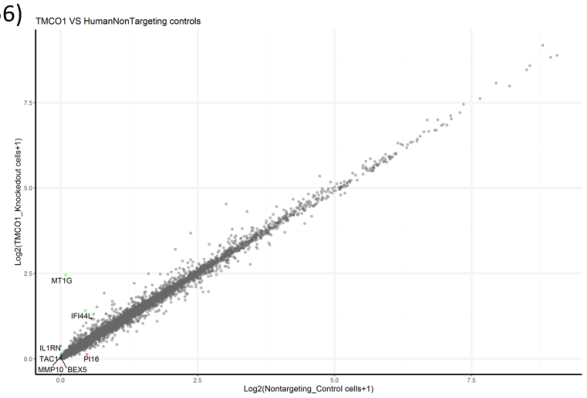

57) TNS1 VS HumanNonTargeting controls

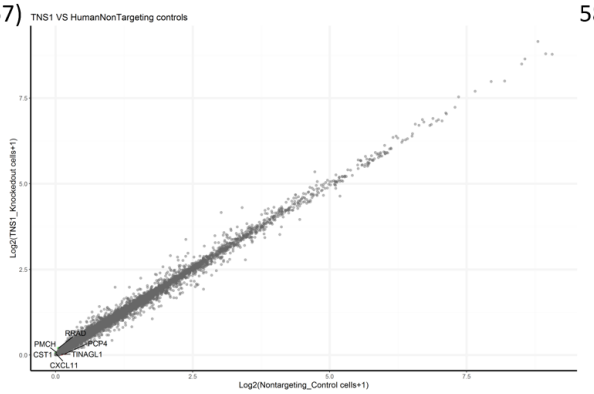

58) TRIOBP VS HumanNonTargeting controls

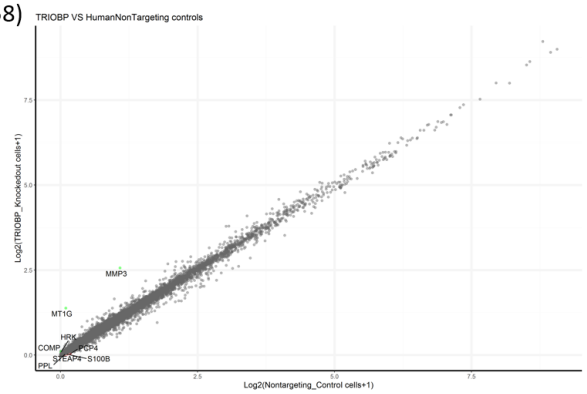

59) TES VS HumanNonTargeting controls

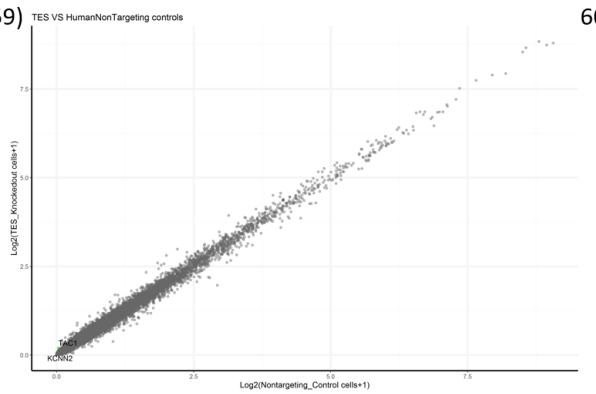

60) TEX41 VS HumanNonTargeting controls

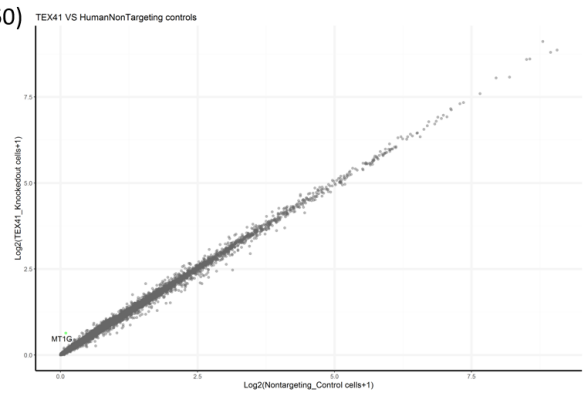

61)

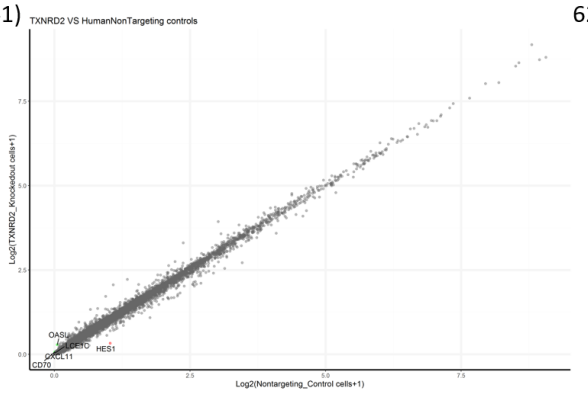
TXNRD2 VS HumanNonTargeting controls
Log2(TXNRD2_Knockedout cells+1)
Log2(Nontargeting_Control cells+1)
0.0
2.5
5.0
7.5
OASL
HES1
CD70

62)

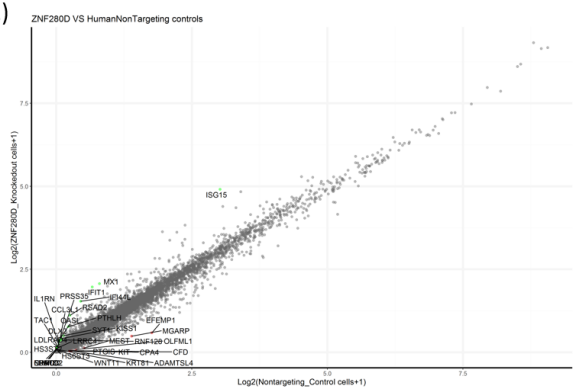
ZNF280D VS HumanNonTargeting controls
Log2(ZNF280D_Knockedout cells+1)
Log2(Nontargeting_Control cells+1)
0.0
2.5
5.0
7.5
ISG15
MX1
IFIT1
IL1RN
PRSS33
TAC1
EFEMP1
MGARP
OLFML1
CFD
ADAMTSL4